ORGANIC CHEMISTRY ON FUNCTIONAL MATERIALS

FOR SUSTAINABLE PROCESS ENGINEERING

A thesis submitted to attain the degree of

DOCTOR OF SCIENCES of ETH Zurich

(Dr. sc. ETH Zurich)

presented by

ELIA MICHAEL SCHNEIDER

MSc ETH Chemistry

born on 14.07.1988
citizen of Arni (BE)
Switzerland

accepted on the recommendation of

Prof. Dr. Wendelin J. Stark, examiner

Prof. Dr. Maksym Kovalenko, co-examiner

2017

We are made from chemicals, but what holds us together is much more than that.

Tigers Jaw, Chemicals

Acknowledgments

During the time at the Functional Materials Laboratory, I had the pleasure to meet many amazing and unique people who I will never forget. Thank you all for accompanying me on this great journey.

I would like to express my deepest gratitude to Prof. Wendelin Stark for giving me the opportunity to start, continue and finish this exciting PhD thesis in his group. There are many great professors at ETH Zurich but Wendelin Stark stands out: I first heard his name from a colleague at work before even studying. He was then one of the youngest professors at ETH and had a quite different approach to science. Wendelin's creativity and approach to solve seemingly unsolvable problems impressed me greatly and inspired me to think further. Furthermore, I have learned a lot about chemical engineering, problem solving, and entrepreneurship from him, preparing me proficiently for my future outside the FML.

Also, special thanks go to my co-examiner Prof. Maksym Kovalenko for his interest in my work and for investing his precious time to co-examine this thesis.

Furthermore, I am very thankful to Dr. Robert Grass who impressed me greatly with his vast scientific knowledge. Also, I had the pleasure to help him with the process control lecture, which was an intense and very interesting out-of-my-field experience.

Moreover, this work would not have been possible without the help of all my laboratory colleagues all around the world. Many big thanks go out to: Tino, for always sharing with me his elaborate insights on magnetic nanoparticle chemistry and Falkenbeer. Sam, for being the best Japan travel mate and sports coach. Corinne, for proofreading my thesis and being my sister in chemistry. Mario, for being an open and social office buddy. Mirjam, for being the good soul of the group and the support for magnificent skiing days. Michi, for printing ping pong medals when they were needed most. Carlos, for his centrist yet social political opinion and singing skills of radio songs. Michela, for good times in Liverpool and the muscle pump sessions. Dirk, for introducing me to the California reaper. Vlad, for intense ping pong sessions and support during Balkan beats lab cleanings. Lukas, for his excellent whiskey taste. Antoine, for interesting discussions about social enterprises and proficient cell growing skills. Konstantin, for being the first group biologist focusing on organic chemistry. Xavier, for help printing the BS2000. Nicholas, for Christmas songs

Table of Contents

Zusammenfassung

In dieser Doktorarbeit wird die Herstellung von funktionellen Materialien durch Kombinationen von organischen und anorganischen Bauteilen beschrieben. Ziel ist die Erforschung und Entwicklung nachhaltiger Prozesse. Mittels Funktionalisierung von organischen oder anorganischen Oberflächen können komplexe Systeme hergestellt werden, welche in der chemischen Industrie Anwendung finden, um beispielsweise chemischen Abfall oder Kohlenstoffdioxidemissionen zu vermindern.

Kapitel 1 fasst die Entwicklung der organisch-anorganischen Hybriden in den letzten Jahrzehnten zusammen. Es werden verschiedene chemische Möglichkeiten, Hybrid-Materialien zu synthetisieren, untersucht. Das Hauptaugenmerk liegt auf dem gezielten Modifizieren von Materialen für nachhaltige Prozesse. Als spezifisches Beispiel wird die magnetische Separation diskutiert und es wird gezeigt, wie diese Technik genutzt werden kann, um industrielle Aufarbeitungsprozesse nachhaltiger zu gestalten.

In **Kapitel 2** wird ein magnetischer Nanokatalysator für die Knoevenagel-Kondensation eingeführt, welcher die chemische Aufbereitung − eine zeit- und lösungmittelintensive Prozedur in der organischen Chemie − vereinfachen soll. Vor allem Reaktionen, welche organische Basen benötigen, profitieren stark von einer vereinfachten Separation, da sie schwierig vom Produkt zu trennen sind. Darum wurde ein Derivat des superbasischen Protonenschwamms synthethisiert und kovalent mit den stärksten kommerziell erhältlichen magnetischen Nanopartikeln verbunden, welche auf Kohlenstoff-beschichteten Kobalt-Metall-Nanopartikeln basieren. Die immobilisierte magnetische Superbase wurde in der Knoevenagel- und der Claisen-Schmidt-Kondensation getestet und zeigte eine hohe Aktivität. Auch hohe Ausbeuten (bis zu 97 %) vom isolierten Produkt konnten erreicht werden, da für ein reines Produkt nur einmal rekristallisiert werden musste und keine Säulenchromatographie nötig war.

Kapitel 3 beschreibt einen neuen Katalysator für die Knoevenagel-Kondensation: Kupfer. Preisgünstiges Kupferpulver wurde verwendet, um eine breite Palette von verschiedenen Knoevenagel-Produkten zu synthetisieren. Dabei konnte das Kupferpulver, wie bei der heterogenen Katalyse üblich, einfach mit einem Filter abgetrennt werden und womit die Separation stark vereinfacht und Lösungmittel konnte eingespart werden. Um eine mögliche Anwendung in der Industrie zu zeigen, wurde ein grosser Ansatz von Benzaldehyd und Cyanessigsäureethylester

mit Kupfer reagiert, was in dem gewünschten Katalyse-Produkt resultierte. Eine grosstechnische Anwendung kann somit möglich sein.

In **Kapitel 4** wird ein in Wasser dispergierbares, auf magnetischen Nanopartikeln basierendes «Klick und Spalt»-System präsentiert. Der spaltbare Linker wurde mit einem spannungs-getriggerten, kupferfreien Klick-Reagenz kombiniert, um eine spezifische Verbindung zu erschaffen. Gleichzeitig wurde eine Silaneinheit eingebaut, die mittels Fluorid unter milden Bedinungen gekappt werden kann. Organische Moleküle, azid-funktionalisierte Farben und funktionalisierte Enzyme können so an die magnetischen Partikel gebunden und bioorthogonal wieder gelöst werden.

In **Kapitel 5** wird die erste erfolgreiche Silika-Beschichtung von Polymilchsäure-Nanopartikeln beschrieben, welche zu vollständig Glas-(Silika)-beschichteten Polymilchsäure-Nanopartikeln führt. Die nachfolgende Auflösungsprozedur in Dichlormethan löste das Polymilchsäuretemplat heraus, was zu hohlen Silika-Kugeln führte. Die gelöste Polymilchsäure konnte danach direkt rezykliert und wieder zu Nanopartikeln verarbeitet werden, um einen neuen Ansatz von hohlen Silika-Kugeln zu synthetisieren. Somit wurde ein nachhaltiger Prozess entwickelt, welcher im Vergleich zur Standardprozedur viel weniger Kohlendioxidemissionen zur Folge hat. Hohle Silika-Kugeln sind von grossem Interesse in der Industrie, sowohl für die nächste Generation von Isoliermaterialien, als auch als leichtes Füllmaterial in Polymeren für Treibstoff-effiziente Mobilität.

Zum Schluss wird in **Kapitel 6** eine Zusammenfassung aller präsentierten nachhaltigen Reagenzen, Katalysatoren und Prozesse präsentiert. Ausserdem werden zukünftige, mögliche Anwendungen für die Industrie aufgelistet und die potenziellen Probleme diskutiert.

Summary

It is described how the combination of the advantageous properties of organic and inorganic building blocks leads to functional materials applicable in sustainable chemical engineering. The chemical functionalization of surfaces of organic or inorganic origin leads to complex yet functional structures and reagents that can be applied to reduce waste or carbon dioxide emission in chemical industry.

Chapter 1 summarizes the development of organic and inorganic hybrids over the last decades. Different chemical approaches to synthesize hybrids are examined and reviewed. A special emphasis is placed on the engineering of materials suitable for sustainable processes. Magnetic separation is discussed as a specific example of how to make separation procedures more sustainable.

In **chapter 2**, a magnetic nano-catalyst for the Knoevenagel condensation is introduced to facilitate work-up in organic synthesis, which can be quite solvent and time intensive. In this respect, reactions involving organic bases would strongly profit from a tremendously simplified separation. Therefore, a derivative of the superbasic proton sponge was synthesized and covalently linked to the strongest currently available nanomagnets based on carbon-coated cobalt metal nanoparticles. The immobilized magnetic superbase reagent was tested in Knoevenagel and Claisen-Schmidt type condensations and showed conversions up to 99%. High yields up to 97% of isolated product could be obtained by a simple recrystallization without using column chromatography.

Chapter 3 describes the catalysis of the Knoevenagel condensation using heterogeneous copper materials. Inexpensive, widely available copper powder was used to catalyze the Knoevenagel condensation of ethyl cyanoacetate and benzaldehyde under mild conditions, resulting in quantitative yield after 30 minutes. Separation could be done by using a simple filtration protocol, thus reducing considerably the amount of solvent needed. To ensure general applicability, a wide variety of different substrates was successfully reacted and a scale up to a 100 g batch was accomplished.

In **chapter 4**, a water dispersible, magnetic nanoparticle supported "click and release" system is presented. The cleavable linker was synthesized by using a strain-promoted copper-free "click" reagent to establish the specific link and a fluoride cleavable silane moiety for mild cleavage. Small

organic molecules, dyes and enzymes, which were functionalized with azide groups, were bound to the magnetic particle and released in a bioorthogonal way.

In **chapter 5**, the first successful silica coating of polylactic acid nanoparticles, resulting in fully coated polylactic acid-silica core-shell nanoparticles, is introduced. Subsequent dissolution treatment efficiently dissolved the polylactic acid core template and yielded exclusively hollow silica spheres. The collected polylactic acid could then be recycled directly from the template removal solution and re-used to synthesize polylactic acid nanoparticles for a next batch of hollow silica nanospheres. Such hollow particles are of interest in next generation insulation materials and as light weight fillers in polymers for fuel efficient mobility.

To conclude, **chapter 6** includes a summary of all presented sustainable reagents, catalysts and processes. Possible applications in industry are listed and the potential pitfalls are discussed.

1 Towards organic-inorganic hybrid materials for sustainable process engineering

1.1 Sustainable process engineering using hybrid functional materials

The main task of process engineering is to develop the best industrial production possible. However, if we look at chemical processes or desired properties of functional materials over the last decades, we find that the focus has shifted from inexpensive production cost, efficiency or synthesis time to sustainability. During the industrialization, which started in the eighteenth century in England, sustainability as well as energy efficiency were mostly irrelevant.[1] Charcoal and later atomic energy made energy readily available and, thus, there was no incentive to save energy. The same is true for fossil-fuel derived base chemicals (*i.e.* from non-renewable resources), which were the starting point for most industrial chemistry processes. Additionally, there was little awareness of the environmental and toxicological damages that chemical industries generate.

Today, this has changed remarkably. Never in history has there been a time when the impact of the human race on this planet was more substantial than now, never has the earth been that densely populated (see **Table 1-1**). More people need more industrial products − which translates to an increased demand of resources in general.

Table 1-1. *Population numbers of earth and doubling time thereof (0 AD to 2000 AD)*[2]

Year AD	0	1750	1950	2000
Population (millions)	252	771	2529	6115
Annual growth (%)	0.037	0.064	0.594	1.766
Doubling time of the population (years)[a]	1854	1083	116	40
a. Doubling time is the time it takes for a population to double in size at a constant growth rate.				

This fact demands new and radically innovative concepts of how to preserve and maintain our planet in a functioning state for the future generations. If we truly want to achieve a sustainable process, we have to take into account the source of the reactants (*e.g.* bio-derived), the solvent waste (*e.g.* recycling) and the energy consumption (*e.g.* catalysts, shorter synthesis paths). Furthermore, the optimization of production processes might be achieved by the integration of green technologies (materials management).[3] The idea behind it is that waste from one process might be an appropriate resource for another process (*e.g.* biorefineries). These hybrid processes

are a possibility to eliminate waste as such in chemical industry altogether. Therefore, the term *clean technologies* has been coined and defined by the European Commission Directorate-General for Environment.[4] The following nine main points are the core of what a clean technology should consist of:

1. Conservation of raw materials
2. Optimization of production processes
3. Rational use of raw materials
4. Rational use of energy
5. Rational use of water
6. Disposal or recycling of unavoidable waste
7. Accident prevention
8. Risk management to prevent major pollution
9. Restoring sites

These are general requirements that cannot be fulfilled immediately, but they give a good overview on where to start. One way is through process-intensification, a strategy that aims towards dramatic reductions in the size of a chemical plant and, thus, decreasing greenhouse gas emissions and energy consumption. Other possible methods include hybrid separations, integration of reaction and separation, techniques using alternative energy sources and new process-control methods.[5]

Hybrid materials, combining sustainable features of organic and inorganic chemistry, play a big role in achieving these goals. With all the knowledge gathered in these fields over the past century, many problems can now be tackled using this hybrid approach. Exciting examples for thriving research in this area are hybrid membranes used for solvent waste treatment, gas separation, catalysis and fuel cells.[6, 7] Another interesting field that uses hybrid materials for the benefit of sustainable process engineering is catalysis, more specifically nanoparticle-mediated catalysis.[8] Nanoparticles enable quasi-homogeneous catalysis while still retaining the advantages of heterogeneous catalysis, such as simple separation from the reaction mixture. The field is rapidly evolving, but the most interesting compounds remain functionalized Pd, Pt, Au and Rh nanoparticles.[9] Although much research has been done, implementation into industry remains challenging, as nanomaterials demand proper risk and toxicology assessment and the handling is more difficult. Therefore, the design of such catalysis system has to be analyzed thoroughly and optimized until it fits the industrial needs.

1.2 Design and engineering of hybrid functional materials

Generally, the design of any functional material always starts with a desired application in mind, as depicted in **Figure 1-1**.[10] The application (*e.g.* water filter) demands that certain functions and properties are present in the material, nanoparticle or molecule, which fulfill the task (*e.g.* removal of bacteria). If the desired properties are determined (step 1), the material can be designed (step 2). This involves deeper knowledge of reactivity and structure of the desired compounds, which is usually obtained from literature. After deciding on materials and experimental conditions, synthesis (step 3) is carried out and the resulting product is characterized (step 4). Finally, the obtained properties are analyzed (step 5) and compared to the desired properties. If the discrepancy is too large, the whole process is repeated and thus, the obtained properties are optimized until they match the desired properties.
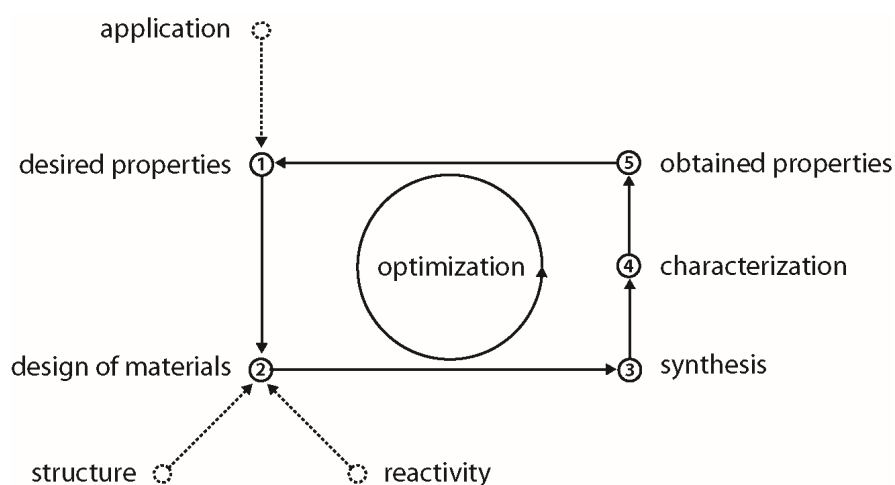
Figure 1-1. *Modus operandi in molecular engineering, adapted from Hitzky et al.*[10]

This general approach can also be applied to engineer functional hybrid materials, especially if the desired properties cannot be achieved with pure inorganic or organic compounds. Obviously, the design of materials will then also include many additional steps, such as design of the nanohybrid

structures or advanced engineering of the surface of the matrix structure in order to achieve the desired properties. Additionally, special attention has to be paid to the product characterization, which might involve analytical methods from both fields, organic and inorganic chemistry.

There are two main bottom-up strategies for the design of hybrid functional materials that are currently investigated: molecular assembly and blocks assembly.[11] The molecular assembly approach describes the use of monomers (*e.g.* small molecules) and subsequent polymerization. This is usually done using a Sol-Gel approach, which is discussed in chapter 1.6. On the other hand, the blocks assembly approach is used when a surface or a nanoparticle is combined with another block or functionality (*e.g.* through surface functionalization, intercalation or grafting). This approach is described in more detail in chapter 1.5.

The design of hybrid functional materials has gained considerable attention in the last decade. Once a relatively small field, it has evolved into a massive multidisciplinary research area, including topics such as metal-organic framework membranes,[7] hybrid membranes for fuel cells[12] and hybrid materials for optics and photonics.[13] This research effort resulted in a *plethora* of functional materials used in industry, for example smart coatings for the protection of buildings and monuments or hybrid-based photovoltaic cells.[14]

Organic compounds	Mixed / composite compounds	Inorganic compounds
- Consist mainly of C,H - Low melting points (-100 to 200 °C) - Low boiling points - Flammable - Covalent bonds - Modifiable - Functional - Low density (0.9 - 1.2 kg m^{-3})	?	- Consist of all elements - High melting points (>200 °C) - High boiling points - Nonflammable - Ionic bonds - Mostly inexpensive - Robust - High density (2.0 - 4.0 kg m^{-3})

Figure 1-2*. General properties of organic and inorganic compounds.[15]*

1.3   Properties of organic and inorganic materials

In inorganic chemistry, the radicals are simple; in organic chemistry, they are compounds − that is the sole difference.

Jean Baptiste André Dumas, 1837

The differentiation of organic and inorganic chemistry is not as clear as the technical terms suggest. Whereas organic chemistry originally was described as the chemistry of the building blocks of life, it is now mainly referred to as the chemistry of hydrocarbons and their derivatives.[16] On the other hand, inorganic chemistry is the chemistry of all remaining chemical elements, such as metals, oxides and minerals. However, this binary classification does not include a large class of compounds, namely materials that consist of both, organic and inorganic, elements. If we only look at organic compounds, there are physical and chemical properties that are inherent to most of them, for example low melting points, low boiling points, high flammability and the covalent nature of the chemical bond (**Figure 1-2**). As for inorganic compounds, properties such as high melting points, high boiling points, low flammability and ionic bonding nature were described.[17] In **Figure 1-2**, these properties have been summarized. However, the interesting question is what the properties of mixed or composite compounds are going to be. There is a variety of applications that demand very specific properties, which need to be tailored by combining organic and inorganic chemistry. Therefore, research at the interface of organic and inorganic chemistry has gained a lot of attention in the last decades, especially since the birth of mild inorganic processes ("Chimie Douce").[18]

1.4   Exploring the interface of organic and inorganic chemistry

Since there are about 120 properly characterized chemical elements, there are countless approaches to combine organic and inorganic compounds. It is therefore difficult to categorize the different hybrid molecules and materials in a methodical way. However, **Figure 1-3** depicts an overview of some representative examples, giving an insight into the vast variety of possible combinations. The bidimensional structure (organic-inorganic) of this graph implies a classification according to the predominant phase. This usually defines the nature of the host (*i.e.* matrix) material.

Organic   **Inorganic**

10^1 Å

10^2 Å

10^3 Å

Molecular species

- Donor-acceptor complexes
- Intergrown O-I perovskites

- Active inorganic molecules doped into conducting polymers

- Sol-Gel silica modified with organic molecules

Nanosized

- Polymer-supported inorganic clusters or nanoparticles

- Organically modified Mesoporous materials
- Mixed O-I polymers

- Active organic molecules intercalated into layered silicates, chalcogenides, oxides

- Biomineral type composites
- Silica-embedded bioactive species

- Organically substituted polysiloxanes
- Silica + organic polymer

Extended structures

Polymer-coated inorganic nano-particles

Figure 1-3. *Overview of organic-inorganic hybrid materials of molecular, supramolecular, nano-sized and extended structures. Adapted from Functional Hybrid Materials.[19]*

For example for *Sol-Gel silica modified with organic molecules* (top right, **Figure 1-3**), the matrix is a silica structure and the functional part is the organic modification. However, this classification has its limitations, because in certain cases, there is no proper distinction between organic and

inorganic phases (*e.g.* organometallic complexes) or the distribution of the phases is irrelevant. Often, the nature of the interaction between the organic and inorganic phase is more important, since it provides information about the interface and function. Therefore, a classification based on the nature of the interface has been established dividing the organic-inorganic hybrids into two main classes. In class I, there is no covalent or ionic bond interaction between the two phases. This means that in these compounds weak interactions, such as hydrogen bridges or Van der Waals interactions, are present. On the other hand, class II refers to hybrids that are linked *via* strong chemical bonds of either covalent or ionic nature.[19] Depending on the application, either class I (*e.g.* drug delivery vesicles) or class II hybrids (*e.g.* catalyst immobilization) are desired.

Additionally, there is the obvious classification of hybrids according to their application (*e.g.* catalyst, membrane, dispersion) or properties (*e.g.* magnetic, biocompatible, stable under harsh conditions). However, a full review of all these applications and properties lies beyond the scope of this manuscript. The focus of this manuscript is on a subset of important possibilities to generate, modify and use organic-inorganic interfaces.

There are, as mentioned before, two general strategies for the synthesis of hybrid materials (*i.e.* molecular assembly and blocks assembly). In the molecular assembly approach, Sol-Gel synthesis is definitely one of the most prominent strategies resulting in nanocomposite hybrids or molecular hybrids.[20] Important are mild conditions that do not harm the organic moiety.

The block assembly approach provides a much wider variety of strategies to design hybrid materials: one strategy is the self-assembly approach, where templates are used as structure directing agents. Furthermore, hybrid materials can be synthesized by assembly of nano building blocks (NBB), resulting in mesostructured NBB-based hybrids.[15] Another strategy is post-synthesis modification by surface functionalization. By modifying the surface of a bulk material or nanoparticles, functionality can be introduced, mostly by organic moieties. However, it has to be considered that depending on the nature of the interface (class I or II) and the nature of the material, these strategies may not apply for every desired material and have to be adapted. In the next chapters, we will discuss the various specific chemical approaches to introduce organic molecules into inorganic material, as well as building inorganic moieties on organic matter.

1.5   Organic chemistry on inorganic materials

Properties of inorganic materials and especially inorganic nanoparticles often need to be engineered in a specific way in order to be truly functional (*e.g.* band gap engineering in semiconductors, dispersion stabilization and surface charge optimization). There are four different chemical methods for introducing organic molecules into inorganic materials, namely post-synthesis modification, liquid phase modification, addition of non-reactive compounds to precursors and the use of organic-inorganic co-precursors.[19] However, since our focus lies on the functionalization of the interface, we will mainly discuss various possibilities of post-synthesis modification of
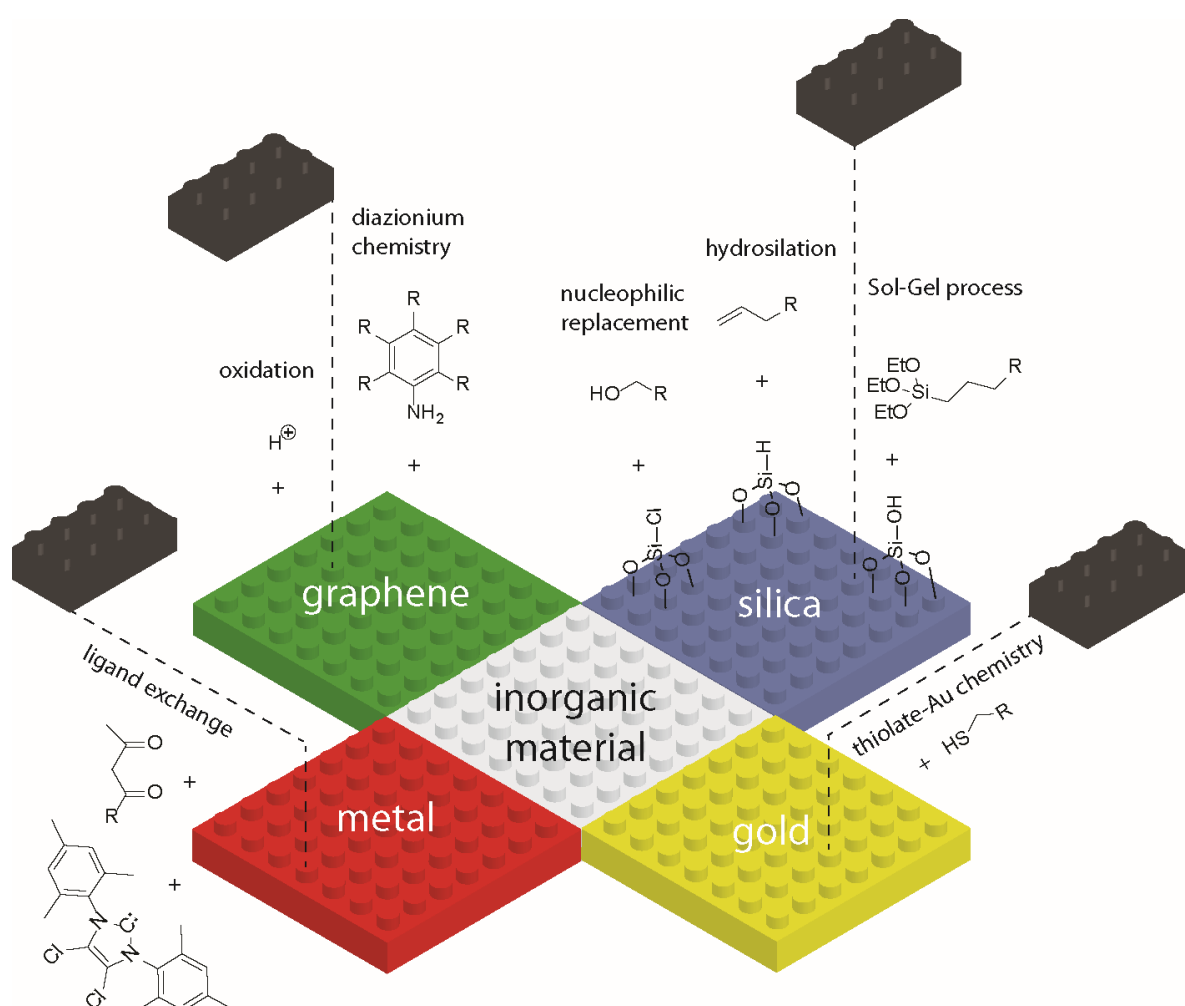

Figure 1-4*. A selection of well-established methods for the surface modification of inorganic materials. Graphene, silica and gold were chosen as specific examples since they are widely used in research.*

inorganic materials with organic moieties as depicted in **Figure 1-4**. Graphene, silica and gold were chosen as examples because of a *plethora* of interesting examples in current literature. Metals, such as palladium, platinum or silver, are equally important, and can be functionalized using a wide variety of organic ligands. Additionally, there are of course many other inorganic materials (*e.g.* metal oxides) which can be modified using a similar approach.

1.5.1   Surface modification on graphene

The most common method to functionalize graphene and graphene-like surfaces is *via* oxidative acid treatment. This is usually done using harsh oxidative conditions (*e.g.* 98% H_2SO_4, $KMnO_4$ and $NaNO_3$ for 48 h at 100 °C), and results in functional groups such as carboxylic acids, aldehydes and alcohols on the graphene surface.[21] A disadvantage of this method is that it disrupts the extended π-conjugation of the pristine graphene and that it creates unwanted defects. Another popular approach to functionalize the graphene layer with organic moieties is *via* diazonium chemistry. By using sodium nitrite and acid, a primary arylamine (see **Figure 1-4**, top left) can be converted into a diazonium salt, which can exhibit a highly reactive free radical upon release of nitrogen. This radical can interact with the sp^2-hybridized carbon atoms of graphene and thus form a stable, covalent C-C bond.[21] Naturally, the hybridization of the graphene carbon atom changes to sp^3, resulting in lower but controllable conductivity, which is useful for semiconductor materials.[22] A convenient feature of this method is the short reaction time: after 30 minutes the reaction is usually finished. Additionally, the broad scope of commercially available aniline derivatives (see **Scheme 1-1**) facilitates the synthesis of tailored products without the use of multistep, elaborate chemical procedures. It should be noted that further, more sophisticated organic chemistry can then be carried out after a successful attachment of the aniline derivative *via* diazonium chemistry.

(4-aminophenyl)methanol   4-(aminomethyl)aniline   4-nitroaniline   2-(4-aminophenyl)acetic acid
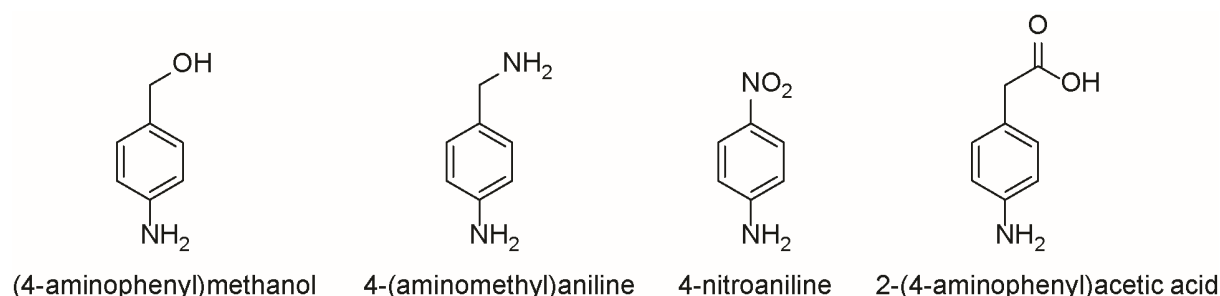
Scheme 1-1. *A selection of commonly used aniline derivatives for graphene functionalization.*

A prominent example is the surface initiated atom transfer radical polymerization (siATRP),[23, 24] enabling the controlled polymerization of any acrylate monomer from the immobilized radical initiator on the graphene surface.[25]

1.5.2 Surface modification on silica

One of the most promising synthesis paths to functionalize silica surfaces with organic moieties is by mixing silica and a silane molecule, for example (3-aminopropyl)triethoxysilane (APTES), in methanol or ethanol to form siloxane bonds between the surface and the silane reagent.[26] A selection of such reagents is depicted in **Scheme 1-2**.[27] In this reaction, the release of the alkoxy-group and subsequent attack of the surface silanol-nucleophile can be catalyzed by a base, similar as in the Sol-Gel process. There are countless commercially available silanes with all kinds of functional groups (*e.g.* amine, allyl, aryl, epoxides, thiols), resulting in a broad scope of possible anchor points for further, more sophisticated organic modifications.[28]

Another possibility is to convert the surface silanol into a surface hydride using $SOCl_2$ and $LiAlH_4$.[29] The hydride can be further reacted catalytically (*e.g.* with H_2PtCl_6) with substituted alkenes (hydrosilation) to generate a stable Si-C bond.[20, 30] Alternatively, if no reducing agent is used, the silanol can be converted into a surface chloride.[31] The chloride can simply be substituted by nucleophiles, most commonly by an organic molecule containing an alcohol group.

3-(triethoxysilyl)propan-1-amine   vinyltriethoxysilane   chloropropyltriethoxysilane

methacryloxypropyltriethoxysilane   3-glycidyloxypropyltrimethoxysilane
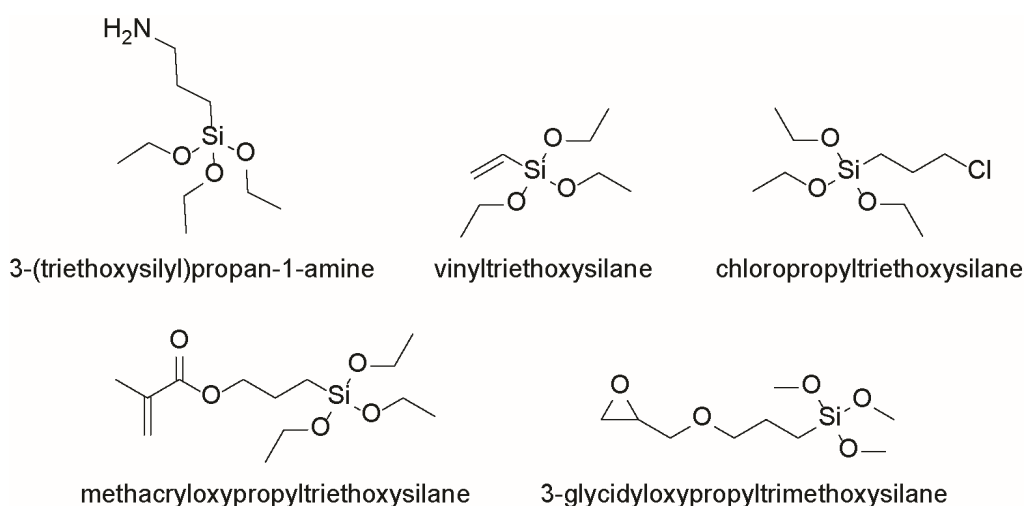
Scheme 1-2. *A selection of well-known silane reagents used in the surface modification of silica.*

1.5.3 Surface modification on gold

The by far best-known modification of gold surfaces or nanoparticles is *via* thiol-functionalized organic molecules. Gold surface and thiols can form the strong S-Au bond under relatively mild conditions in solution or gas phase.[32] Furthermore, this bond is stable under ambient conditions and mostly indifferent to the specific organic rest (*e.g.* anionic and cationic species, polymers, catalysts). This enables the use of gold nanostructures for a wide array of applications, such as biolabelling, drug delivery and photo thermal therapy.[33]

1.5.4 Surface modification of metals using organic ligands

The surface of most metals or metal nanoparticles can be functionalized by using chelating organic ligands. Besides thiols, the most important functional groups for ligand design are amines (amino-acids, hexadecylamine), carboxylic acids (*e.g.* oleic acid, stearic acid) and phosphines (*e.g.* triphenylphosphine).[34] These functional groups usually form strong bonds with the metal surface and form a functional monolayer. The ligand itself can then be designed to exhibit bulky groups (steric stabilization) or charged moieties (electrostatic stabilization).[35] Often, the ligand is designed in such a way that it can be further modified chemically, for example by addition of orthogonal functional groups (*e.g.* azide, alkyne, alcohol). Additionally, it is possible to graft polymers onto metal surfaces using this technique. For example, mono- or bifunctional poly(ethylene glycol) (PEG) molecules can be attached to metal surfaces (PEGylation), in order to create an inert hydrophilic surface that repels proteins and other molecules by steric effects.[36]

1.5.5 Adsorption and heterogeneous catalysis on inorganic surfaces

The interaction of an organic molecule with an inorganic surface to form a new molecule (heterogeneous catalysis) is also an interaction of organic moieties with inorganic material. However, it clearly differs from the chapters before in the sense that the created interface is only short-lived, since in heterogeneous catalysis adsorption and subsequent rapid desorption of the organic molecule are crucial. Therefore, we cannot speak of "surface functionalization" but rather of "surface activation" (*e.g.* with H_2). A description of this interface is not trivial and can be tackled in various ways, depending on the investigator's curriculum.[37] However, compared to homogeneous catalysis, the reaction mechanisms in heterogeneous catalysis are often not as obvious. Yet, there are many examples of name reactions in organic chemistry (*e.g.* Heck reaction, Suzuki reaction, Sonogoshira reaction) including heterogeneous catalysts, which have been studied

thoroughly, also in their mechanistic details.[38, 39] These findings led to a deeper understanding of interfaces and surface chemistry.

1.6   Inorganic chemistry on organic materials

Generally, it is technically more straightforward to functionalize inorganic material with organic moieties than *vice versa*, as for the synthesis of inorganic compounds usually high temperatures are needed (>300 °C). This limits the inorganic compound onto organic material synthesis (hybrid formation process), because the organic material is not stable at these elevated temperatures. However, with the development of the Sol-Gel process, this disadvantage could be avoided by using mild reaction conditions.[40] In general, this process can be described as the inorganic polymerization of dispersed metallo-organic precursors (salts or alkoxides) at ambient temperature. Metal alkoxides ($M(OR)_n$, where OR is an alkoxy group OC_xH_{2x+1} and M= Si, Sn, Ti, Zr, Al, Mo, etc.) are polymerized through hydrolysis and condensation reactions leading to metal-oxo polymers.[15] When the concentration of polymer is high enough, a gel is formed entrapping solvent and monomers. The gel is not necessarily the final form or desired product; possible are xerogels
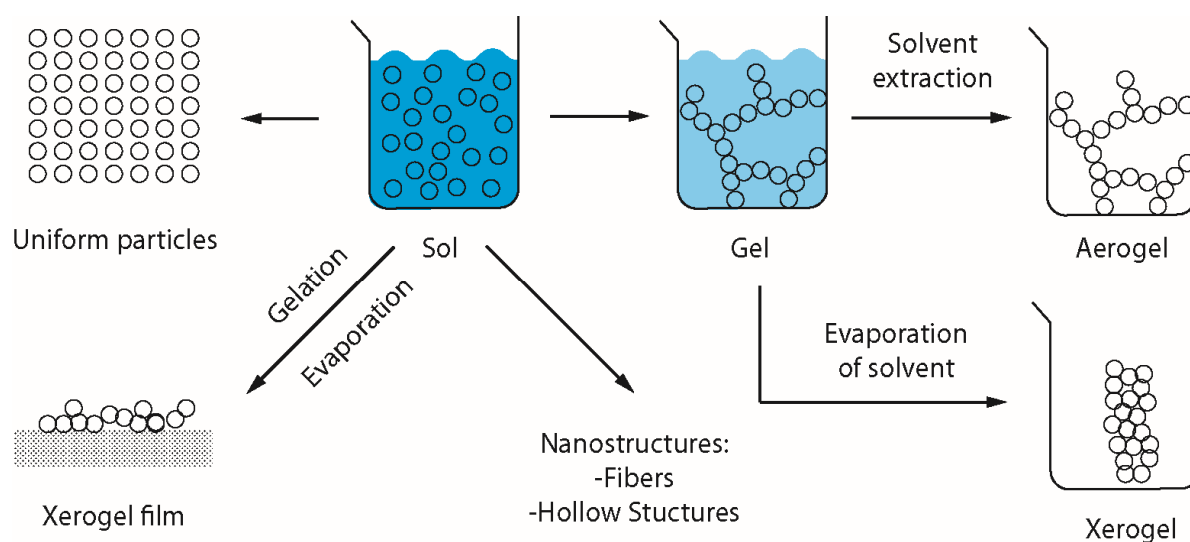

Figure 1-5. Overview of the Sol-Gel process. The mild process opens the door to many different morphologies and nanostructures.[40]

(if the liquid phase of the gel is evaporated quickly), colloidal dispersions (if the polymerization is stopped at an early point) or precipitates (if the formed particles are not stable in the solvent). Additionally, a wide array of nano-structures (*e.g.* hollow spheres, fibers, monodisperse nanoparticles)[41-44] can be obtained with the Sol-Gel process using different techniques, such as hard-templating or surfactant-controlled polymerization.[45] For an overview of possible morphological outcomes of the Sol-Gel process see **Figure 1-5**. The Sol-Gel approach is a key method to combine inorganic compounds with an organic matrix, above all, because the mild synthesis conditions (in solution, ambient temperature, catalyst) are compatible with most organic materials. The most straightforward hybrid synthesis is by simply mixing the organic matrix (*e.g.* polymer or nanoparticle) with the metal alkoxides and a catalyst (*e.g.* ammonia).[44] Using this technique, the morphology of the hybrid material can be engineered (*e.g.* for hollow structures).

However, this approach generally creates class I hybrids (weak interactions at the interface), which might not be stable enough for certain applications. To generate class II hybrids, there has to be either a covalent bond or an ionic interaction. The former can be achieved by adding an anchor to the organic matrix (for example *via* N-trimethoxylsilylpropyl-N,N,N-trimethylammonium chloride),[46] while for the latter the surface charge (ζ-potential) has to be designed using oppositely charged ions in order to create ionic bonds.[45] Finally, if only single inorganic atoms (*e.g.* Rh, Ru, Pt) are needed (mostly as metal centers for catalysts), they can be incorporated into organic structures bearing the fitting ligands, such as N-heterocyclic carbene (NHC) functionalized polymers or polymers containing metallocene derivatives.[47]

A specific example of an application of organic-inorganic hybrids used for sustainable engineering is magnetic separation, which will be discussed in the next chapter.

1.7 Magnetic nanoparticle separation

Historically, magnetic separation was one of the first applications of magnetic nanoparticles. The working principle is that the magnetic particle is able to specifically separate the desired product from a complex reaction solution *via* magnetic dipole-dipole interaction.[48] This method reduces the amount of required resources (solvent, energy, space) considerably, because many common working-up techniques, such as column chromatography, distillation and phase separation, can be avoided. There are three ways how this principle can be applied in the laboratory: as a

straightforward separation of the product, by using magnetic catalysts or as a "quasi-homogeneous" system where the catalyst can be attached and released from the magnetic carrier.[49, 50] These three possibilities are depicted in **Figure 1-6**. The build-up of such a magnetic nanoparticle is usually a magnetic core surrounded by a protection shell. Generally, the core can be any ferromagnetic metal (*e.g.* Fe, Co, Ni) or metal oxide (*e.g.* Fe_3O_4), while the shell can be either organic (*e.g.* surfactants, polymers) or inorganic (*e.g.* silica, graphene).[51, 52] Surface functionalization is often required, since specific molecules have to be extracted (*e.g.* proteins, heavy metal ions) or distinct catalysts have to be attached. Surface functionalization can be done in the same way as discussed in chapter 1.5. For functional magnetic particles to be truly useful in industry, there are certain requirements that need to be fulfilled: (1) Stability in the corresponding solvent and reactions conditions.
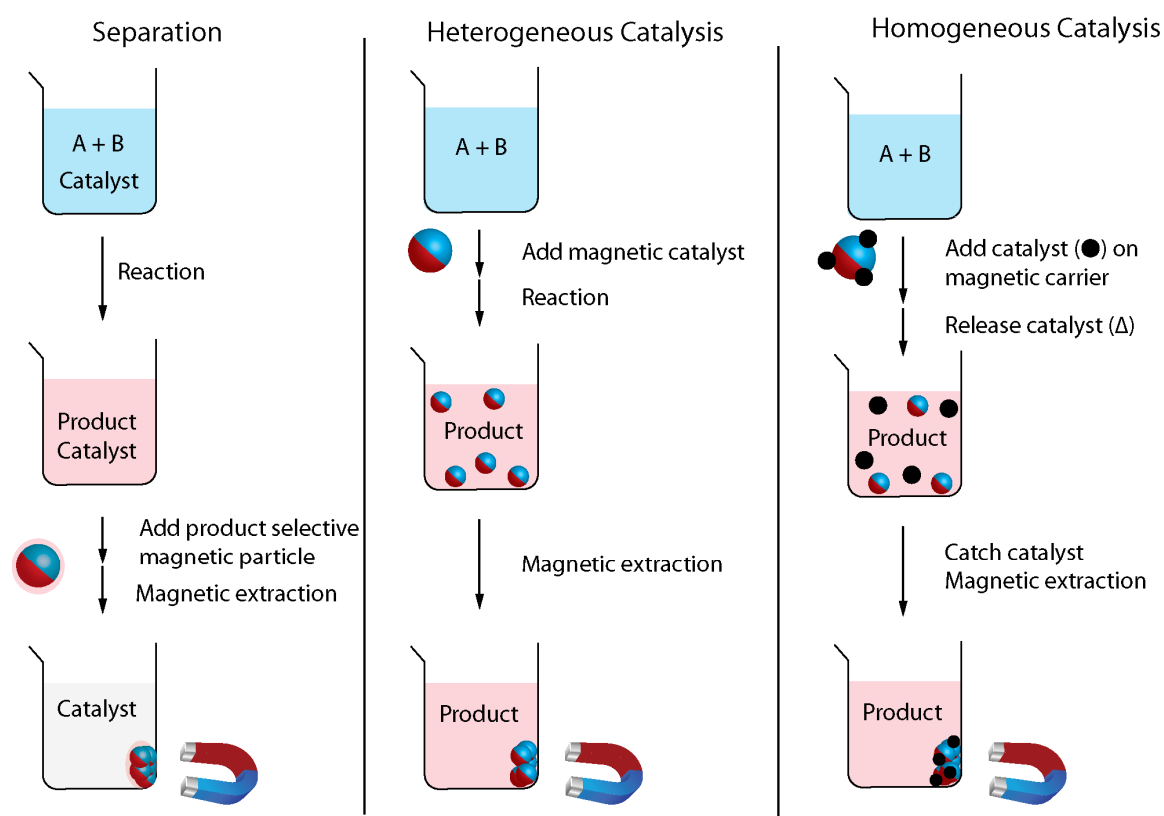
Figure 1-6. *Schematic principle of separation and catalysis with magnetic nanoparticles.*

(2) High saturation magnetization for efficient recovery. (3) Low leaching rate. (4) Low inherent toxicity. If these requirements are met, then the next goal would be to establish a large scale process which can be translated to industry.

Hence, the development of new magnetic nanoparticles, elaborate functionalization thereof and translation to a potential application for industrial processes are the next challenges for scientists and engineers in this area.

1.8   Conclusion

In the first chapter, the development of hybrid materials, combining features of organic and inorganic materials for sustainable process engineering, is discussed. The need for new, sustainable processes is evident. However, to date there are not many satisfying solutions for problems concerning sustainability in the chemical industry. Therefore, new processes and materials have to be developed and investigated. Functional hybrids offer a huge amount of possibilities to solve the upcoming problems of our generation, such as finding substitutes for fuel-derived chemicals, efficient energy storage and a substantial reduction of carbon dioxide emissions.

In the next four chapters, specific examples of functional hybrids used for sustainable applications will be presented and discussed, starting with functionalized magnetic nanoparticles for catalysis.

2 Magnetic superbasic proton sponges are readily removed and permit direct product isolation

2.1   Introduction

Organosuperbases, such as the classic proton sponge 1,8-bis(dimethylamino)naphthalene (DMAN),[53] Verkade's base (proazaphosphatranes) and 1,8-bis(tetramethylguanidino)naph-thalene (TMGN) have become very important reagents in organic chemistry over the past years.[54] Their exceptional basicity is associated with high kinetic activity in proton exchange reactions. These properties are often manifested through low nucleophilicity, making this kind of compound interesting for a wide scope of reactions.[55-58] Furthermore, even heterogeneous organosuperbases are known.[59, 60] However, the work-up of such reactions at laboratory level can be difficult, time consuming and expensive. Similarly, in industry, a broad variety of condensation reactions is applied. At present, mostly free bases, such as sodium hydroxide, potassium hydroxide and various organic bases are used and often lead to corrosion, significant waste production and difficult work-up. Thus, a chemically stable magnetic base with rapid capability for quantitative separation would be most interesting for industrial application and entail significant solvent savings, reduce time, expensive equipment and permit reagent reusability. Moreover, a ready-to-separate reagent is interesting for high-quality products, where impurity carryover defines product performance. Magnetic nanoparticles have fascinated scientists for several decades and were used in a *plethora* of applications,[61] such as drug delivery,[62] in cancer treatment[63] and as contrast agents for magnetic resonance imaging.[64] In chemical synthesis, magnetic nanoparticles have recently gained attention in the field of catalysis[65] since they combine high surface area with simple separation. However, many magnetic reagents and surface linkers for reagent attachment are unstable in acidic, basic or organic solvent containing reaction media. The exceptional chemical stability of carbon coated metal nanoparticles[66] is based on a crystalline graphene-like carbon surface effectively preventing core oxidation. The all-carbon surface further allows covalent particle surface functionalization in a very convenient way using commercially available aryl diazonium salts.[52] At present, a number of promising recyclable, stable, metal-based magnetic catalysts have been proposed.[58, 67-76] Most recently, alkene hydrogenation palladium catalysts[77, 78] or so called "catch and release" systems[49] have been developed. In this work, we present an organic superbase, coupled to magnetic nanoparticles, with stability amenable for use in such challenging reaction conditions. We further show that such an easy-to-separate reagent is useful in a number of condensation reactions, and simplifies work-up and product isolation.

2.2   Experimental

Carbon-coated cobalt nanoparticles[52] were suspended by the use of an ultrasonic bath and subjected to various reactions (see below). After a reaction or a pre-treatment step, nanoparticles were recovered from the reaction mixture with the aid of a conventional magnet (neodymium based magnet, N48, W-12-N, Webcraft GmbH, side length 12 mm). Silica coated magnetite nanoparticles (sicastar®-M plain 350 nm) were purchased from Micromod. Commercially available reagents were used as received. All air-sensitive reactions were carried out under argon atmosphere. The nanoparticles were analyzed by FTIR spectroscopy (5% in KBr) and elemental microanalysis. To determine the conversion of the catalytic reactions, HPLC measurements on a Waters Symmetry® C18 5 μm 2.1 x 150mm column where performed. GC/MS measurements were performed (capillary HP 5 MS 30 m x 250 μm x 0.5 μm) with split injection (at 250 °C and a ratio 50 : 1, injection volume 1 μl) and temperature program (80 °C for 2 min, 20 °C min^{-1} heating until 250 °C). The cobalt concentration present in solution was measured by inductively coupled plasma atomic emission spectroscopy on a HORIBA Ultra 2.

2.2.1   Synthesis of the magnetic proton sponge analogue

Synthesis of C/Co@amine **3**

Carbon-coated cobalt nanoparticles **1** were purchased from Turbobeads™. The functionalization of the particles was done according to reported procedures, *i.e.* 3 g of **1** where suspended in 20 mL H$_2$O and 4-aminobenzylamine **2** (0.7 mL, 5.3 mmol) was added. Then sodium nitrite (0.8 g, 11.5 mmol) was added to the slurry. The vessel was put into the sonication bath and 2 mL concentrated HCl were slowly added dropwise. Upon completion of the reaction (30 min) the nanoparticles were recovered from the reaction mixture with a magnet and washed with toluene (2x10 mL), EtOH (1x10 mL), acetone (2x10 mL) and dried 24 h at 50 °C *in vacuo*. FT-IR: 1603 cm^{-1}, 1503 cm^{-1}, 1015 cm^{-1}, 831 cm^{-1}.

Synthesis of C/Co@hexamethyleneisocyanate **5**

C/Co@amine **3** (2 g) was degassed 3 times in a Schlenk-flask. 50 mL dry DMF, hexamethylendiisocyanate (6 mL, 37 mmol, 97 equiv., 98%, Fluka) and triethylamine (NEt$_3$, 0.01 mL, 99%, Acros) were added under argon atmosphere. Then the solution was dispersed in a sonication bath for 5 minutes. The dispersion was heated to 70 °C and stirred for 6 hours. Upon completion of the reaction the nanobeads were recovered from the reaction mixture with a magnet,

and washed with anhydrous DMF (2x). FT-IR: 2927 cm^{-1}, 2857 cm^{-1}, 1689 cm^{-1}, 1553 cm^{-1}, 1018 cm^{-1}.

Synthesis of C/Co@DMAN 7

Freshly synthesized C/Co@hexamethyleneisocyanate **5** (2 g) was used directly in a 250 mL Schlenk-flask under argon atmosphere. 40 mL dry DMF and triethylamine (NEt$_3$, 0.01 mL, 99%, Acros) were added. The solution was dispersed in a sonication bath for 5 minutes. DMAN-NH$_2$ **6** (1 g, 4.3 mmol) was degassed 3 times in a Schlenk-flask and then dissolved in 10 mL of anhydrous DMF and finally added dropwise to the C/Co-HMDI solution. The dispersion was heated to 35 °C and stirred overnight (16 h). Upon completion of the reaction the nanoparticles were recovered from the reaction mixture with a magnet and washed with DMF (2x10 mL), EtOH (1x10 mL), acetone (2x10 mL) and dried 24 h at 50 °C *in vacuo.* FT-IR: 2931 cm^{-1}, 2857 cm^{-1}, 2783 cm^{-1}, 1676 cm^{-1}, 1532 cm^{-1}, 1249 cm^{-1}.

*Synthesis of polystyrene-supported DMAN **S2***

Chloromethyl polystyrene (1 g, 2% DVB, 100-200 mesh, 0.9-1.5 mmol/g, ABCR) was used in a 50 mL Schlenk-flask. 20 mL anhydrous DMF and triethylamine (NEt3, 0.01 mL, 99%, Acros) were added under argon atmosphere. DMAN-NH2 (0.6 g, 2.58 mmol) was degassed 3 times in a Schlenk-flask and then dissolved in 5 mL of anhydrous DMF and finally added dropwise to the polystyrene slurry. The dispersion was heated to 40 °C and stirred overnight (20 h). Upon completion of the reaction the functionalized polymer was filtrated and intensively washed with acetone, 0.1 M NaOH, H20, EtOH, acetone and dried 24 h at 50 °C *in vacuo.* FT-IR: 3030 cm^{-1}, 2927 cm^{-1}, 2775 cm^{-1}, 1944 cm^{-1}, 1874 cm^{-1}, 1726 cm^{-1}, 1602 cm^{-1}.

*Synthesis of silica-amine **S4***

Silica gel 230-400 mesh (Merck, 1g) was placed in a 50 mL Schlenk-flask and degassed 3 times. 20 mL anhydrous toluene was added and the slurry was heated to 60 °C. N1-(2-aminoethyl)-N2-(3-(trimethoxysilyl)propyl)ethane-1,2-diamine (0.3 mL, 11.6 mmol) was added dropwise to the solution, which was then stirred for 24 h. The resulting solid was filtered with 50 ml toluene, 100 mL DCM and 20 mL Et2O and dried 24 h at 50 °C *in vacuo.* FT-IR: 3289 cm^{-1}, 2940 cm^{-1}, 2828 cm^{-1}, 1863 cm^{-1}, 1474 cm^{-1}, 1109 cm^{-1}.

2.2.2 General procedures for catalysis, catalyst recovery and linker stability

General procedure for Knoevenagel condensation reactions

A mixture of solvent (5 mL) and C/Co@DMAN **7** (0.1 g, 0.01 mmol) was sonicated in an ultra-sonication bath for 5 min in a Schlenk-flask and then stirred at RT. Benzaldehyde (0.5 mmol) and malononitrile (0.5 mmol) were added and the progress of the reaction was monitored by HPLC (MS for ensuring product identity, UV at 280 nm for quantification) or GC-FID using the commercially available product as reference.

Benzylidenemalononitrile (10) *The isolated product was obtained by recrystallization in hot EtOH and hexane, followed by filtration.* ^{1}*H NMR (CDCl$_3$, 200 MHz, 25°C): δ 7.86 – 7.82 (m, 2H), 7.71 (s, 1H), 7.57 – 7.43 (m, 3H).* ***α-Cyanocinnamic acid ethyl ester*** *The pure isolated product was obtained by evaporation at 40 °C.* ^{1}*H NMR (CDCl$_3$, 200 MHz, 25°C): δ 8.19 (s, 1H), 7.9 (m, 2H), 7.47 – 7.43 (m, 3H), 4.37 – 4.27 (q, 2H), 1.37 – 1.30 (t, 3H).* ***2-(4-methoxybenzylidene)malononitrile*** *The pure isolated product was obtained by evaporation at 40 °C.* ^{1}*H NMR (CDCl$_3$, 200 MHz, 25°C): δ 7.86 – 7.75 (m, 2H), 7.58 (s, 1H), 6.96 – 6.92 (m, 2H), 3.84 (s, 3H).* ***2-(4-nitrobenzylidene)malononitrile*** *The isolated product was obtained by evaporation of the solvent, followed by recrystallization in DCM/Hexane.* ^{1}*H NMR (CDCl$_3$, 200 MHz, 25°C): δ 8.73 (s, 1H), 8.45 - 8.42 (m, 2H), 6.96 – 6.92 (m, 2H).*

General procedure for Claisen-Schmidt condensations

A solvent free mixture of acetophenone (2 mL) and C/Co@DMAN **7** (0.1 g, 0.01 mmol) was sonicated in an ultra-sonication bath for 5 min and then stirred at 130 °C under nitrogen atmosphere. Benzaldehyde (0.1 mmol) was added and the progress of the reaction was monitored by HPLC (MS for ensuring product identity, UV at 280 nm for quantification) using the commercially available product as reference. ***1,3-Diphenyl-2-propen-1-one (13)*** *The isolated product was obtained by evaporation in high vacuum at 65 °C.* ^{1}*H NMR (CDCl$_3$, 200 MHz, 25°C): δ 7.93 – 7.97 (m, 2H), 7.18 - 7.71 (m, 10H).*

General washing/drying procedure for catalyst recovery

The used catalyst was washed by sonication (5 min) with the reaction solvent of the catalytic reaction and acetone (2x) and dried 4 h at 50 °C *in vacuo*.

General procedure for linker stability tests

A sample (30 mg) was placed in 10 mL round-bottom flask and solvent (10 mL) was added. The solution was dispersed *via* ultra-sonication bath and then shaken overnight. The solid sample was washed by either sonication (magnetic samples) or filtration (silica samples) with EtOH, H_2O and finally acetone and further on dried 4 h at 50 °C *in vacuo*.
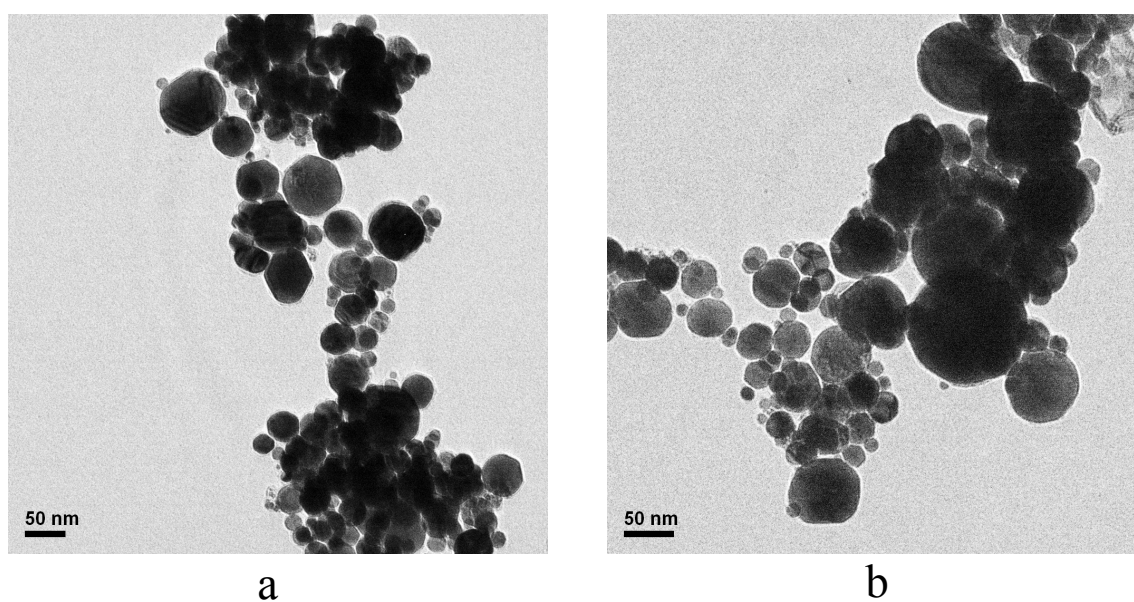

a   b

Figure 2-1*. Transmission electron microscopy micrographs of the magnetic superbase **7** before (a) and after (b) catalysis.*

2.3 Results and discussion

2.3.1 Preparation and characterization of the magnetic base

The magnetic, nano-sized DMAN was prepared from chemically modified magnetic nanoparticles, a linker and a derivative of DMAN: for covalent attachment of the base to the magnetic particle **1**, a bifunctional linker (*i.e.* hexamethylene diisocyanate **4**) was first reacted with the primary amine functionality of 4'-benzylamine-derivatized graphene-coated metal nanoparticles (abbreviated as C/Co@amine) **3** to yield C/Co@hexamethyleneisocyanate **5.** This intermediate contains a stable N-alkylurea bond and an active isocyanate moiety. Subsequently, C/Co@hexamethyleneisocyanate **5** was reacted *in situ* with 4-amino-1,8-bis(dimethylamino)naphthalene **6,** which was prepared according to literature.[79] This afforded a magnetic, covalently bound DMAN C/Co@DMAN **7** in proper yield with a base capacity of 0.11 ± 0.01 mmol g^{-1}. For illustration of the synthesis see **Scheme 2-1**. The chemical identity of the here synthesized reagent C/Co@DMAN **7** was proven by diffuse reflectance infrared Fourier-transform spectroscopy (DRIFTS) and elemental microanalysis (see **Figure A1-1** and **Table 2-1**). The fairly strong urea stretching vibration at 1690 cm^{-1} clearly confirms urea formation in the case of C/Co@hexamethyleneisocyanate **5**. The successful attachment of DMAN to the isocyanate linker of C/Co@hexamethyleneisocyanate **5** was investigated with IR spectroscopy and elemental microanalysis (**Table 2-1**). A substantial increase in nitrogen content ($\Delta N = 0.82\%$), as well as an increased carbon content ($\Delta C = 3.43\%$) are in line with a successful functionalization. Vibrating sample magnetometry (VSM) measurements (at room temperature) resulted in an overall magnetization of 139.6 emu g^{-1}, which is in good agreement with the expected values, namely a little lower than the saturation magnetization of non-functionalized C/Co (lower content of organics or carbon; 158 emu g^{-1}).[25] It is notable that the saturation magnetization of this material is still much higher than even the strongest, conventional magnetite-silica nanoparticles (30-50 emu g^{-1}).[51] The high saturation magnetization is of relevance as it permits rapid and easy separation.[80] In order to confirm the chemical stability and robustness of C/Co@DMAN **7**, transmission electron microscopy (TEM) images of the nanocarrier system **7** were recorded before and after reaction runs. Particles remained spherical and of uniformly sized shape in the diameter range of 20 to 60 nm (**Figure 2-1**). The reactivity of the here proposed magnetic C/Co@DMAN **7** was compared to reactions using similar
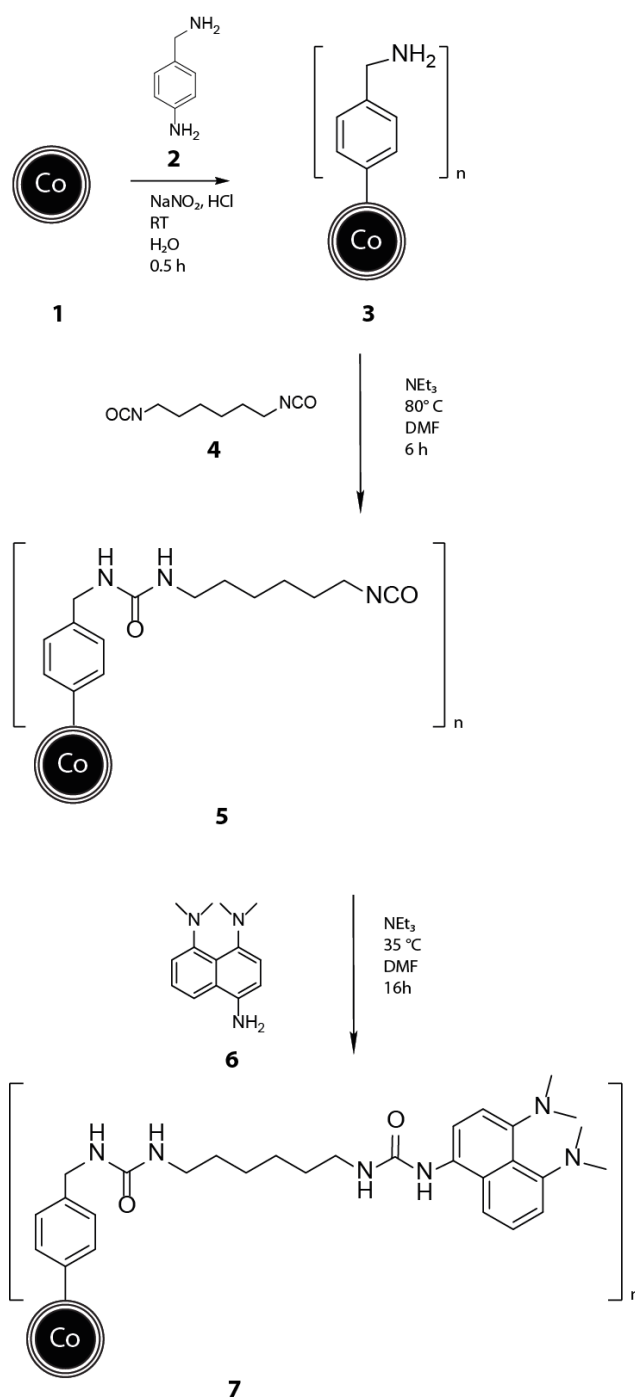
Scheme 2-1. *Synthesis of the magnetic immobilized superbase 7. C/Co 1 was coupled to 4-aminobenzylamine 2 via diazonium-chemistry to yield C/Co@amine 3, which was further reacted with hexamethylendiisocyanate 4 resulting in C/Co@hexamethyleneisocyanate 5. Bearing an active isocyanate moiety, C/Co@hexamethyleneisocyanate 5 was coupled with 4-amino-1,8- bis(dimethylamino) naphthalene 6 to yield C/Co@DMAN 7.*

Table 2-1. *Elemental microanalysis of the functionalized magnetic nanoparticles*

Entry	Name	Magnetic core material	C (%)	N (%)	Calculated degree of functionalization (mmol g⁻¹)
1	C/Co HC	High Carbon[a]	11.41	0.02	-
2	**3**	"	13.33	0.29	0.19[75]
3	**5**	"	14.25	0.62	0.14[c]
4	**7**	"	14.68	0.91	0.11[c]
5	C/Co LC	Low Carbon[b]	2.97	0.01	-
6	**3**	"	5.28	0.51	0.28[c]
7	**5**	"	6.26	0.75	0.19[d]
8	**7**	"	6.55	0.83	0.10[d]
9	Testreaction A	"	11.55	0.66	0.01[c]
10	Testreaction B	"	11.5	0.63	0.01[c]
11	Testreaction C	"	11.75	0.63	0.03[c]

[a] Purchased from NanoAmor, size 23.7 ± 17.1 nm. [b] Purchased from Turbobeads, size 41.1 ± 22.7 nm. [c] Referring to the increase in N. [d] Referring to the increase in C.

Table 2-2. *Elemental microanalysis of analysis of* **S2**

Entry	Name	C (%)	N (%)	Cl (%)	Calculated degree of functionalization (mmol/g)
1	Merrifield polymer resin S**1**	86.88	0.02	5.86	-
2	**S2**	85.99	0.43	5.11	0.1[a]

[a] Referring to the increase in N.
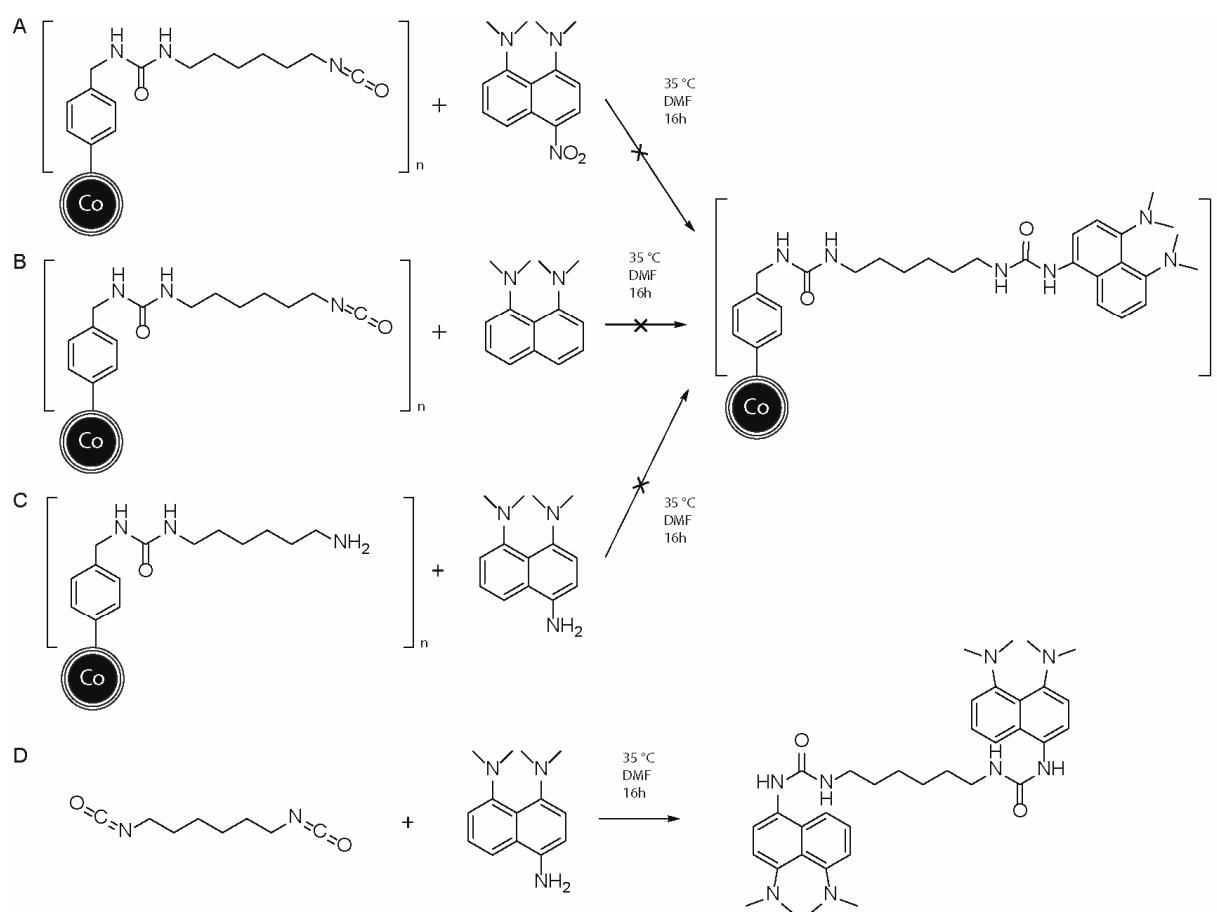
Scheme 2-2. *Test reactions A, B, C and D to prove covalent bonding of DMAN in 7.*

catalysts known from literature. Another reference material, polystyrene-based resin supported DMAN **S2**, was synthesized (**Scheme A1-1**), fully analyzed and characterized (**Figure A1-2** and **Table 2-2**) and used for comparison. Recycling and reliable reagent separation requires a robust confirmation of covalent attachment.

Therefore, we used several test reactions (see **Scheme 2-2**) to prove the covalent nature of DMAN binding to the nanomagnets. As a first control experiment, C/Co@hexamethyleneisocyanate **5**, bearing one free active isocyanate moiety, was reacted with pure (not aminated) DMAN. The lack of a free amine group in DMAN does not allow covalent attachment. Using the same synthesis and purification/washing procedure as for the here proposed reagents, product analysis revealed no nitrogen incorporation and absence of physisorption effects. As a separate control experiment, C/Co@hexamethylene-isocyanate **5** was first quenched with water leading to a primary amine, *i.e.* the linker was deliberately rendered non-functional. Exposure to the functionalized, amine bearing

DMAN derivative **6** and product analysis after applying the same purification/washing procedure as in the preparation of the functional magnetic base, again confirmed absence of reactivity (**Table 2-1,** entries 9-11). These two experiments show that for covalent binding of a DMAN moiety both the linker and the amination of the DMAN are necessary. The experiments further show the absence of base physisorption, a potential experimental error in such reagent anchoring studies.

2.3.2   Knoevenagel and Claisen-Schmidt condensation

Literature states that DMAN indeed has catalytic activity in the Knoevenagel condensation[81] and after identity confirmation, the catalytic activity of C/Co@DMAN **7** for Knoevenagel reaction of benzaldehyde **8** with malononitrile **9** was evaluated in different solvents at RT (**Table 2-3**, entries 1-3). If toluene was used as a solvent, only 61% yield could be obtained. However, in water quantitative conversion was achieved after 7.5 h. Still, the catalyst had to be washed once with toluene to release the product from the carbene surface. Therefore, methanol was tested as a solvent with promising results (**Table 2-3**, entries 3-5). Use of ultrasonication during catalysis is known to ensure good reagent dispersion and consistently leads to excellent yields in shorter contact time. Indeed, when the reaction was conducted in an ultrasonication bath, a higher yield (*i.e.* 91%) was obtained in a shorter time span (**Table 2-3,** entry 4). If the catalyst loading was decreased tenfold, similar yields were detected, but longer reaction time was necessary (**Table 2-3,** entry 5). In comparison, running the same reaction using free DMAN (**Table 2-3,** entry 6), when product work-up and purification was not considered, quantitative conversion was obtained after 6 h. However, column chromatography had to be used to separate the catalyst residues from the product which led to a significant drop in isolated yield. The magnetic base C/Co@DMAN **7,** on the other hand, was separated within seconds and recrystallization of the product was achieved within minutes leading to the pure product.

It is remarkable that even in the absence of any catalysts for the chosen reaction a low conversion (30 %) was detected after 5.5 h (**Table 2-3,** entry 8). More surprisingly, the chosen reaction showed enhanced conversion (90%) in presence of non-modified (*i.e.* naked carbon surface) nanoparticles.

Table 2-3. *Knoevenagel condensation of benzaldehyde and malononitrile under different reaction conditions*
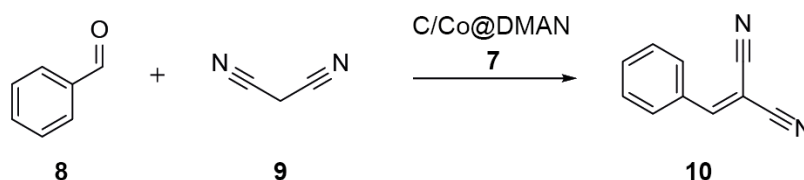
Entry	Catalyst	Catalytic Amount	Solvent	Time (h)	Conversion (%)[a]	Isolated Yield (%)[b]
1	**7**	2 mmol%	Toluene	7.5	63	61 (99)[c]
2	**7**	2 mmol%	H_2O	7.5	99 (2)[c]	97 (94)
3	**7**	2 mmol%	MeOH	7	93 (85)	89 (95)
4	**7**	2 mmol%	MeOH[d]	4.5	98 (95)	91 (96)
5	**7**	0.2 mmol%	MeOH[d]	6	92 (90)	91 (92)
6	DMAN[e]	2 mmol%	MeOH	6	99	63 (96)[f]
7	**S2**	2 mmol%	Toluene	6	99	97 (98)
8	-	-	MeOH	5.5	30	-[g]
9	C/Co	100 mg	MeOH	7.5	90	77 (86)
10	$CoCl_2$	5 mg	MeOH	6	33	-[g]

[a] Conversion determined *via* HPLC with the reference product as standard. Ratio benzaldehyde to malononitrile 1:1 [b] Isolated yield after recrystallization [c] In parentheses (%) conversion without washing the particles once with 3 mL toluene. [d] Reaction done using an ultra-sound bath. [e] Experiment done using the same amount of the free base, *i.e.* 2 mmol%. [f] Isolated yield after column chromatography (DCM : MeOH 20:1). [g] No direct product isolation possible without column chromatography.

Table 2-4. *Knoevenagel condensation with various substrates catalyzed by C/Co@DMAN 7*

Entry [a]	Basic Substrate	Aldehyde / Ketone	Product	Temp. (°C)	Convers. (%)[b]	Isolated Yield (%)
1	NC‒CH₂‒CO‒O‒Et	**8**	(phenyl)CH=C(CN)CO‒O‒Et	40	96[c]	95 (99) [d]
2	CH₃CO‒CH₂‒CO‒O‒Et	**8**	(phenyl)CH=C(COCH₃)CO‒O‒Et	40	7	–[e]
3	**9**	4-MeO‒C₆H₄‒CHO	4-MeO‒C₆H₄‒CH=C(CN)₂	40	99	96 (91) [d]
4	**9**	4-O₂N‒C₆H₄‒CHO	4-O₂N‒C₆H₄‒CH=C(CN)₂	40	83	73 (96) [f]
5	**9**	4-HO‒C₆H₄‒CHO	4-HO‒C₆H₄‒CH=C(CN)₂	40	8	–[e]
6	**9**	(CH₃)₂CH‒CH₂‒CHO	(CH₃)₂CH‒CH₂‒CH=C(CN)₂	RT	81	–[e]
7	**9**	cyclohexanone	cyclohexylidene‒C(CN)₂	40	37	–[e]

[a] Catalyst loading 2 mmol%, basic substrate 0.4 mmol, aldehyde or ketone 0.4 mmol, MeOH 5 mL, 16 h. [b] GC conversion [c] After 3 consecutive cycles still 95% conversion. [d] Isolated yield after solvent evaporation with purity detected by NMR in parentheses. [e] No direct product isolation possible without column chromatography. [f] Isolated yield after recrystallization (DCM/hexane) with purity detected by NMR in parentheses.

To study further this unexpected finding, we included additional experiments. One probable hypothesis is based on leached cobalt ions as a source of activity (hypothesis 1). Also plausible is that the carbon surface itself acts as an active catalyst (hypothesis 2). To exclude the first hypothesis, the reaction was proceeded with deliberate addition of cobalt(II)chloride (CoCl₂;

Table 2-3, entry 10), *i.e.* the species, which is supposed to leach from the particles.[82] The addition of cobalt salts did not significantly affect the conversion (*i.e.* conversion = 33%), hence we do not assign significant activity of ionic cobalt in this kind of reactions.

With regards to the second hypothesis, however, it is known that carbon-based surfaces (graphene, carbon nanotubes (CNT), carbon nanorods (CNR) etc.) indeed have been reported to support catalytic reactions (so called carbo-catalysis).[83, 84] Thus, our finding is in line with such similar carbon surface's activity and is subject to further extended studies by our group. In a second part of the investigation, we tested different substrates (**Table 2-4,** entries 1-7). Ethyl cyanoacetate (**Table 2-4,** entry 1) reacted smoothly with benzaldehyde and the product ethyl α-cyanocinnamate was detected in high yield and purity (*i.e.* 96%, 99% respectively) after 16 h at 40 °C, even after 3 consecutive cycles conversion was similarly high (*i.e.* 95%).
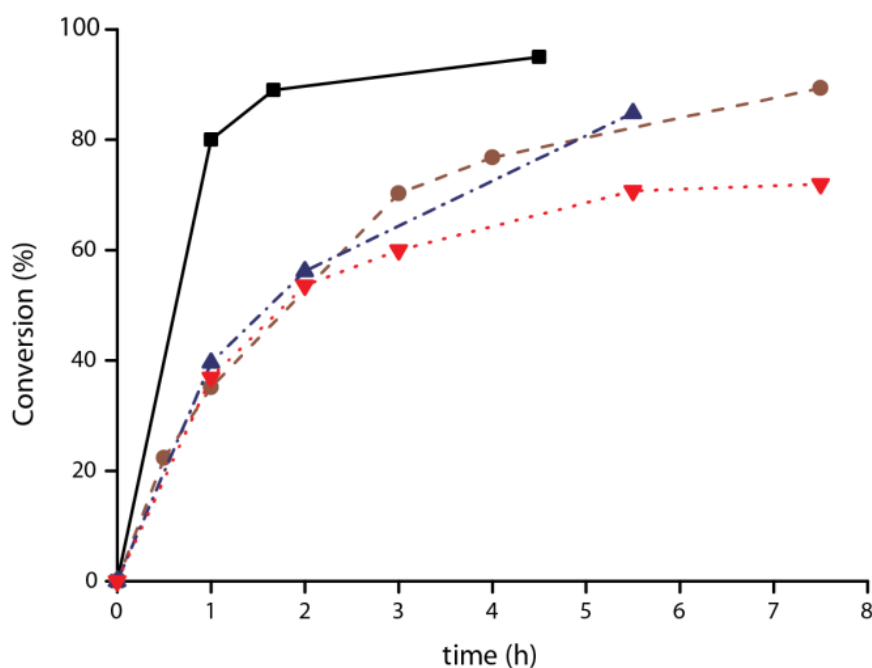

Figure 2-2. *Kinetic plot for the Knoevenagel condensation of benzaldehyde (1.5 eq.) with malononitrile (1 eq.). Plot depicting the reaction using 2.5 mmol% catalyst 7 and different solvents and conditions: ■ methanol and ultrasonication, ● toluene and stirring, ▲ methanol and stirring, ▼ C/Co instead of 7 in methanol and stirring.*
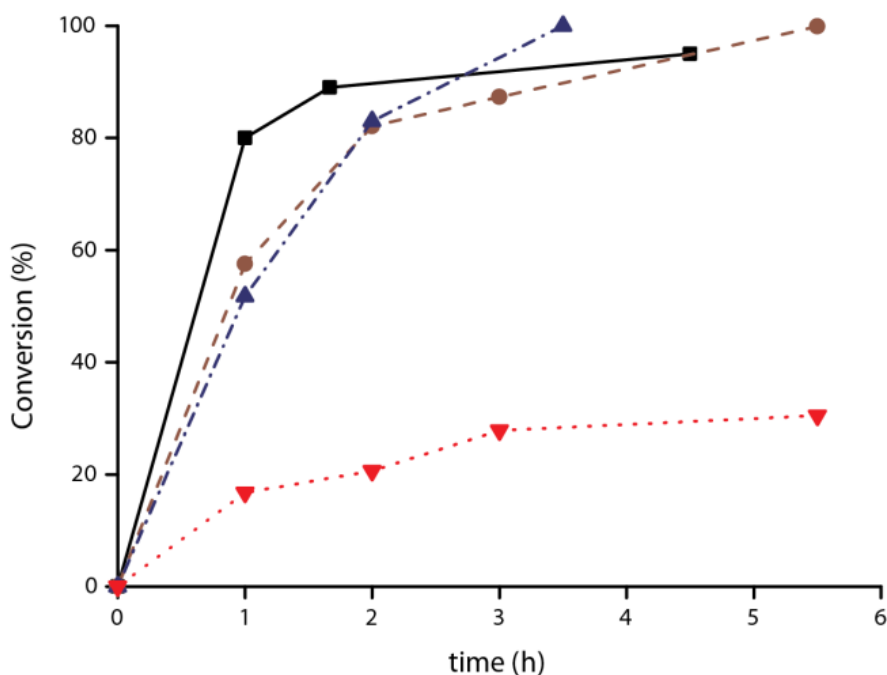
Figure 2-3: *Comparison of reactions with different catalysts (2.5 mmol%) under optimal conditions for each catalyst: ■ 7 in methanol, using ultrasonication, ● free DMAN in methanol, ▲ polymer-bound DMAN* **S2** *in toluene, ▼ without catalyst in methanol.*

The less acidic and thus more demanding substrate ethyl acetoacetate (**Table 2-4,** entry 2) was not very active and only low yields could be obtained. Also, different aldehydes and ketones were reacted with malononitrile. 4-methoxy benzaldehyde performed very well (**Table 2-4**, entry 3), while the electron-poor nitro substrate was slightly less active (**Table 2-4**, entry 4). Surprisingly, 4-methoxy benzaldehyde reacted fast, while 4-hydroxy benzaldehyde showed only low conversion (**Table 2-4,** entry 5). An explanation can be the formation of hydrogen bonds with the solvent and thus one can imagine a shell of solvent molecules shielding the substrate from the catalyst. Non-aromatic substrates such as isobutyraldehyde and cyclohexanone were tested as well (**Table 2-4,** entries 6 and 7). Isobutyraldehyde performed better due to steric reasons (*i.e.* hindrance of nucleophilic attack onto ketones).

Kinetic plots (**Figures 2-2** and **2-3**) confirmed the different reaction rates of C/Co@DMAN **7** when different solvents and mixing conditions (stirring vs. sonication) were used. As expected, the reaction rate increased when the superbase was better mixed with the reactants (degree of mixing).

Table 2-5. *Claisen-Schmidt condensation of acetophenone and benzaldehyde*
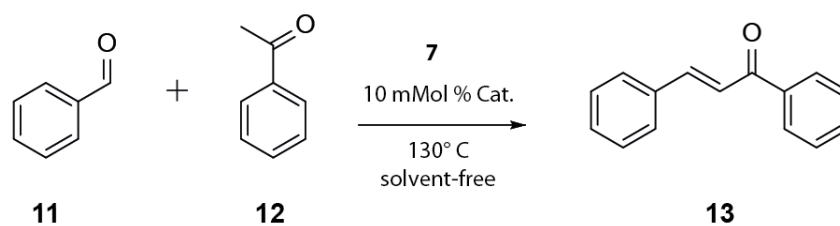
Entry	Catalyst	Run	Conversion (%)[a]	Isolated (%)[b]	Yield	Time (h)	Co (ppm)[c]
1	**7**	1	66	62 (97.6)		16	19
2	``	2	78	_[d]		20	16
3	``	3	71	_[d]		18	5
4	``	4	68	_[d]		18	44
5	``	5	76	75 (98.6)		20	64
6	DMAN	1	<1	_[e]		20	n.a.
7	Co/C	1	58	_[e]		21	42
8	-	1	<1	_[e]		21	n.a.
9	**S2**	1	<1	_[e]		20	n.a.

[a] Conversion determined *via* HPLC with the reference product as standard. [b] Isolated yield after evaporation with purity in parentheses detected by NMR with internal standard. [c] ICP-OES detection limit for Co: 0.2 ppb. [d] No product isolation has been done. [e] No direct product isolation possible without column chromatography.

In order to put the performance of C/Co@DMAN **7** in an appropriate context and provide a fair comparison, reaction kinetics for free DMAN (no mass transfer limitation expected) and polystyrene bound superbase **S2** (under optimal conditions in toluene) were measured (**Figure 2-3**).

C/Co@DMAN **7** initially catalyzes the chosen reaction at least as good as free DMAN, which leads to comparable or even slightly higher efficiency after one hour of reaction time. The conversions converge with time leading to high final conversion for all catalysts. The magnetically immobilized C/Co@DMAN **7** can therefore be considered directly competitive to existing or alternative catalytic systems. The minor changes in activity (rapid first part) may be a result of the altered electronic structure (note that the DMAN was derivatized on position 4 to anchor the nanoparticle). To better figure out the relevance and illustrate a broad applicability of such magnetic organic bases, such as C/Co@DMAN **7**, another condensation reaction (Claisen-Schmidt) between acetophenone and benzaldehyde was tested (**Table 2-5**). This well-known reaction yields *trans*-chalcones, an important precursor for flavonoids, which are widely used in medicine as anti-inflammatory,[85] anti-viral[86] and anti-cancer agents.[87] The magnetic base C/Co@DMAN **7** catalyzed the reaction with yields up to 75% and high purity.

Additionally, the same catalyst was reused in five iterative runs with constant yield. The harsh temperature (130 °C) permits the conclusion that C/Co@DMAN **7** indeed remains stable using covalent linker systems (**Table 2-5,** entries 1-5). Surprisingly, free DMAN does not catalyze the above condensation reaction (**Table 2-5,** entry 6; yield = 1%). This behavior is explainable considering the pKa-values. Because acetophenone has a higher pKa-value (pKa = 25)[88] than does DMAN (pKa = 12.1),[60] it can be concluded that the basicity of DMAN is not the key factor governing this catalysis. Furthermore, this result is in line with earlier work in the literature. Corma *et al*. experimentally investigated a similar case and reported that heterogeneous base catalysts work considerably better than free bases.[89]

2.3.3   Comparison to known solid support catalytic base reagents

In the recent literature a number of excellent examples describe immobilized base catalysts.[59, 60, 89-92] Magnetic supports have been realized using modified magnetite and cobalt ferrite with good yields (**Table 2-6**, entries 6-7). In comparison to metal-based C/Co@DMAN **7** the oxidic supports exhibit a much lower saturation magnetization (133 emu/g for C/Co@DMAN **7**, ca. 70 emu/g for magnetite[93]). This is a direct result of the inherently lower magnetization of most oxides. This value is important as it correlates directly with separation efficiency/speed and has recently enabled

***Table 2-6**. Comparison to different solid support base reagents*

Entry	Catalyst / Base	Saturation magnetization (emu g^{-1})	Reaction	Loading (mmol %)	Time [h]	Convers. (%)	Conversion after 3 Cycles (%)
1	**7**	139	Knoevenagel	2	16	96	95
2	PS-MCM-41-DMAN[59]	-	"	0.5	7	99	85
3	DMAN/SiO$_2$-0.5[60]	-	"	1	6	90	85
4	TMGN/SiO$_2$-0.5[60]	-	"	1	6	100	97
5	**7**	139	"	2	4.5	98	96
6	CoFe$_2$O$_4$@Si-N1-propylethane-1,2-diamine[94]	30[95]	"	2.5	0.33	100	100
7	Fe$_2$O$_3$@HAP@SiImidazoliumsalt[92]	55[96]	"	-	1	98	97
8	**7**	139	Claisen-Schmidt	10	20	78	71
9	DMAN/SiO$_2$-0.5[60]	-	"	1	24	95	n.a.
10	TMGN/SiO$_2$-0.5[60]	-	"	1	14	98	n.a.
11	Fe$_3$O$_4$-DABCO[91]	<60	Morita–Baylis–Hillman	20	5	88	88

magnetic metal nanoparticles to purify water at a ton per hour scale.[97] In a typical laboratory setting, the improved magnetization facilitates work-up, as demonstrated using commercially available silica/iron oxide particles and the herein described metal reagent (**Figure 2-4**). The high magnetization of the carbon-coated cobalt allows clean, quantitative separation of the organic base within seconds. Established immobilized catalyst supports (non-magnetic) are frequently based on zeolites and silica beads. The active site/moiety is mostly attached over a siloxane-type linker.[98, 99] These catalytic systems usually show excellent performance and reusability (**Table 2-6**, entries 2-4 and 9-10). In the case of harsh reaction conditions (*e.g.* strong base), the weakest links of these otherwise well performing materials are the siloxane-type moieties. It is well known that extreme acidic or basic environment (pH < 4, pH > 9) hydrolyze silane-linkers.
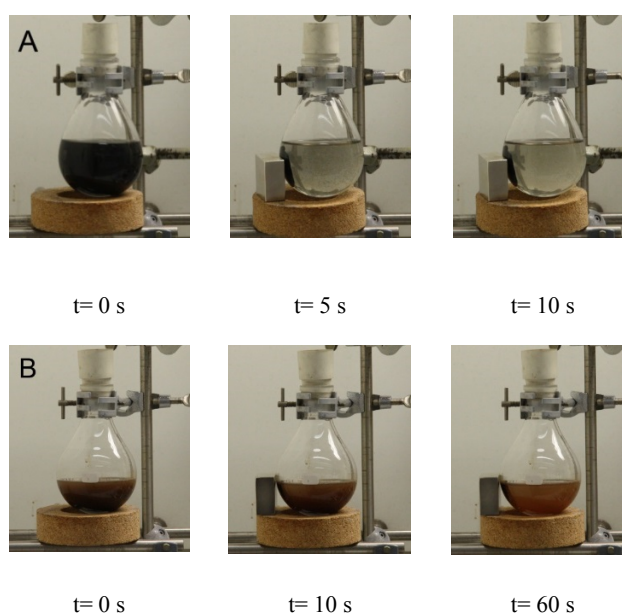
t= 0 s	t= 5 s	t= 10 s
t= 0 s	t= 10 s	t= 60 s

Figure 2-4. Recovery of organic base bound to magnetic nanoparticles using a low cost external magnet (model system in H₂O; same particle concentration as used in all experiments, i.e. *0.7 mg mL⁻¹). A: metal based reagents derived from Co/C. B: Silica coated Fe₃O₄. Note the different times above and below.*

In contrast to this, the here presented dialkyl urea moiety shows higher stability over a broad range of pH. In order to further experimentally confirm this statement, siloxane linkers were directly compared to the here used C/Co@DMAN **7** in a number of representative acidic and basic environments. After 24 hours at RT, at pH = 4 more than 20% of the siloxane linker but less than 5% of the urea type linkers were cleaved (see **Figure 2-5** and **Scheme 2-3**). At pH = 9.5 the dialkyl urea linkers afford less stability (about 10% cleaved), but it is notable that at this conditions more than three-fourth of the siloxane linkers were cleaved (>75%). Furthermore, the stability at elevated temperatures in different solvents (toluene and water) was tested: the dialkyl urea linkers perform superiorly under these conditions than their silane-based pendants (**Figure 2-5**). The intrinsic stability of the particles in acidic or basic media has already been investigated[66] and has also been proven to be superior to silica-coated magnetite.
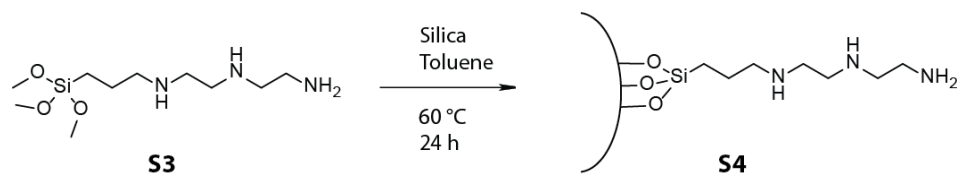
Scheme 2-3. *Synthesis of the silica-linked amine moiety for the linker-stability tests.*
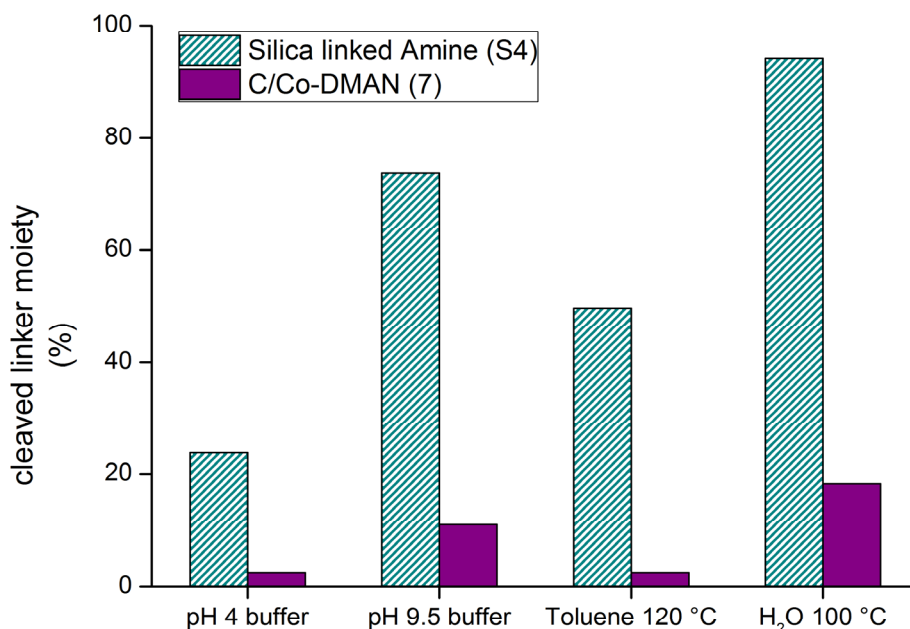

 Figure 2-5. *Immobilization linker-stability tests (overnight) under harsh reaction conditions. The amount of cleaved linker was determined* via *the nitrogen content of the materials before and after exposure using quantitative elemental microanalysis. Buffers used: pH 4 = 0.1 M potassium hydrogen phthalate w/ HCl, pH 9.5 = 0.1 M carbonate-bicarbonate.*

2.4　Conclusion

We have described the preparation of a covalently bound, chemically stable magnetic nanoparticle immobilized organic superbase and its extensive characterization using quantitative elemental microanalysis, infrared spectroscopy, vibrating sample magnetometry and transmission electron microscopy. A number of control reactions were conducted to prove that the reagent was indeed chemically linked to the nanoparticles and this confirmed the importance of linker type and reliability under relevant, harsh reaction conditions. We further demonstrated the experimental advantages of magnetic bases in a number of Knoevenagel condensations reporting quantitative conversion and rapid product isolation in minutes. The demanding Claisen-Schmidt condensation afforded conversions of around 70% at 130 °C. The base catalyst was separated from the reaction mixtures in less than one minute and could be recycled at least during 5 iterative runs. A quantitative comparison between siloxane linkers used in many immobilization studies and the here described carbon shell-based chemistry revealed the important role of linker stability when designing reliable reagents for rough everyday laboratory use.

3   Base-free Knoevenagel condensation catalyzed by copper metal surfaces
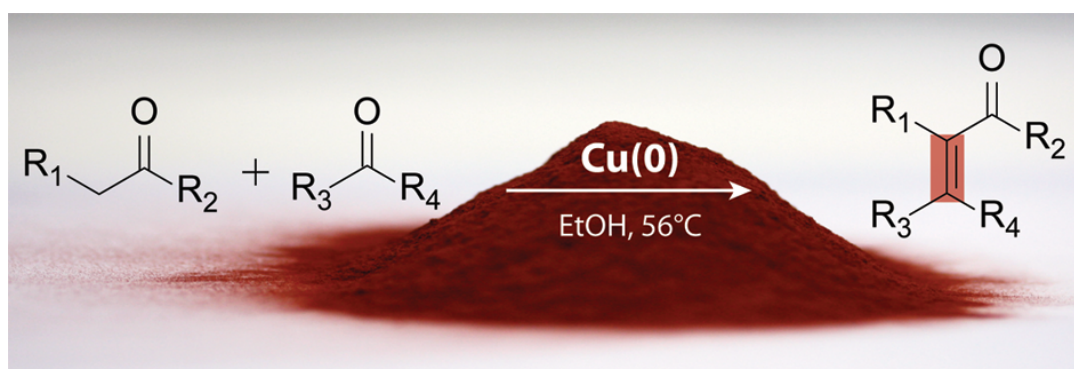
published in parts as:

Elia M. Schneider, Martin Zeltner, Niklaus Kränzlin, Robert N. Grass, Wendelin J. Stark

Author contribution:
E.M.S. and W.J.S. elaborated the concept. E.M.S. performed the experiments with support of M.Z. N. K provided hollow copper samples. E.M.S., R.N.G. and W.J.S. wrote the manuscript with contributions and review from all authors.

3.1 Introduction

Copper has been a fascinating element in catalysis for decades.[100-106] In the early days of copper catalysis, famous name reactions such as the Ullmann coupling,[107] the Sandmeyer reaction and the Chan-Evans-Lam coupling emerged.[108, 109] Around the millennium, Sharpless and coworkers developed the extremely important "click chemistry", in which the copper catalyzed azide-alkyne Huisgen cycloaddition (CuAAc) plays the most essential role.[110] However, much more expensive noble metals such as platinum, palladium and gold received most attention in the field of catalysis, while the inexpensive yet semi-noble copper has been more or less neglected.[111-113]

The Knoevenagel condensation (**Scheme 3-1**) is a widely used reaction in research and industry and has been of importance for several pharmaceutical products.[114-117] Generally, this reaction is catalyzed by organo-bases, such as pyridine or piperidine. But using these homogeneous base catalysts often leads to time consuming work-up procedures. Additionally, undesired side-reactions, such as oligomerizations can occur, high temperatures are necessary and catalyst recovery is difficult.[118] Thus, numerous accounts on heterogeneous Knoevenagel catalysts, for example modified zeolites, ionic liquids or magnetic base analogues, have been reported.[119-125] This leads to cleaner products, while complex neutralization procedures can be avoided. Moreover, these catalysts can be recovered and regenerated. In one of these studies it was shown that carbon-coated cobalt nanoparticles (C/Co)[52] showed activity in the Knoevenagel condensation compared to the uncatalyzed reaction (entries 1-2, **Table 3-1**).[123]
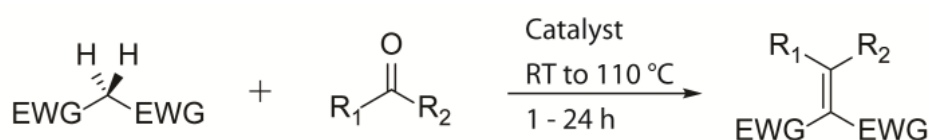

Scheme 3-1. *Knoevenagel condensation of an active methylene compound with an aldehyde or a ketone.*

3.2   Experimental

All air-sensitive reactions were carried out under an argon atmosphere. HPLC measurements were conducted on an AGILENT 1100 (WATERS Column, particle size, 5 μm; column size, 2.1 × 150 mm2) to determine the yield of the catalytic reactions. GC−MS measurements were performed (capillary, 30 m × 250 × 0.5 μm2) with split injection (250 °C; ratio = 10:1; injection volume, 1 μL) and a temperature program (80 °C for 2 min; increase at 20 °C min−1 until 300 °C). The copper concentration present in solution was measured by inductively coupled plasma-atomic emission spectroscopy (ULTIMA ICPOES). ^{1}H NMR (200 MHz) were recorded on a Bruker AMX-200 spectrometer and reported in ppm (δ). NMR spectroscopy abbreviations: br, broad; s, singlet; d, doublet; t, triplet; q, quartet; m, multiplet. XRD measurements were performed on a X'Pert Pro-MPD diffractometer (PANalytical), using Cu-Kα radiation (λ = 1.54060 Å), generally over a range of 70° 2θ with a step size of 0.05°. Scanning electron microscopy (SEM) micrographs were measured on a FEI Nova NanoSEM 450, 5 kV. Brunauer-Emmett-Teller (BET) measurements were done on a Micromeritics TRISTAR surface analyzer.

3.2.1   General procedure for the Cu(0) catalyzed Knoevenagel condensation
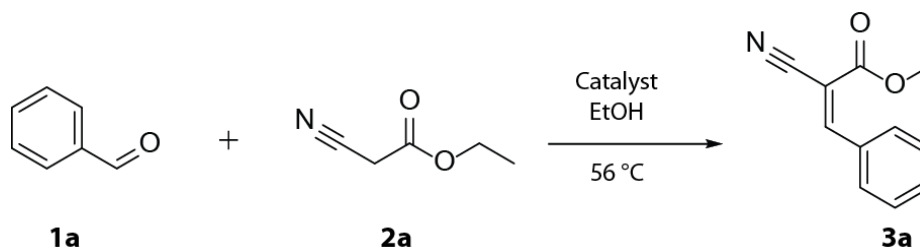
A mixture of solvent (1 mL) and catalyst (4 mg) was prepared in an Eppendorf-tube. Aldehyde or ketone (0.11 mmol) and active methylene compound (0.1 mmol) were added and the whole reaction mixture was shaken at 56 °C for 2 h. The residue was filtrated using a standard frit and 3 g of aluminum oxide (removing solvated Cu(II) ions) and the solvent was removed under reduced pressure. The resulting solid was dissolved in hot EtOH and recrystallized at 8 °C.

3.2.2 Synthesis of various Knoevenagel products via copper catalysis

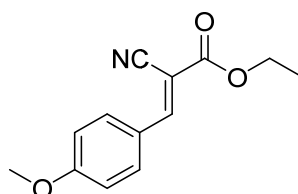*Ethyl (Z)-2-cyano-3-phenylacrylate*
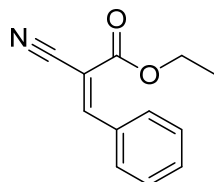
Ethyl (Z)-2-cyano-3-phenylacrylate was prepared from benzaldehyde (0.12 mmol) and cyano 2-ethylacetate (0.1 mmol) following the general procedure and was obtained as a white solid (19.1 mg, 0.095 mmol, 95%). ^{1}H NMR (CDCl₃, 200 MHz, 25°C): δ 8.19 (s, 1H), 7.9 (m, 2H), 7.47 – 7.43 (m, 3H), 4.37 – 4.27 (q, 2H), 1.37 – 1.30 (t, 3H). ESI-MS: [M+H]⁺ 202.08 m/z.

Benzylidenemalononitrile
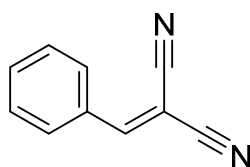
Benzylidenemalononitrile was prepared from benzaldehyde (0.12 mmol) and malononitrile (0.1 mmol) following the general procedure and was obtained as a yellowish solid (15.2 mg, 0.099 mmol, 99%).   ^{1}H NMR (CDCl₃, 200 MHz, 25°C): δ 7.86 – 7.82 (m, 2H), 7.71 (s, 1H), 7.57 – 7.43 (m, 3H). ESI-MS: [M+H]⁺ 155.03 m/z.
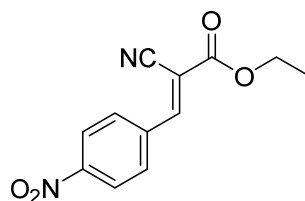
Ethyl 2-cyano-3-(4-methoxyphenyl)acrylate

Ethyl 2-cyano-3-(4-methoxyphenyl)acrylate was prepared from anisaldehyde (0.22 mmol) and ethyl cyanoaceate (0.2 mmol) using 20 mg of Cu powder, stirring 16 h in EtOH at 56 °C and was obtained as a white solid (45.3 mg, 0.196 mmol, 98%). ^{1}H NMR (CDCl₃, 200 MHz, 25°C): δ 8.10

(s, 1H), 7.95 – 7.91 (m, 2H), 6.94 – 6.90 (m, 2H), 4.35 – 4.25 (q, 2H), 3.82 (s, 3H), 1.37 – 1.30 (t, 3H). ESI-MS: [M+H]$^+$ 232.07 m/z.

Ethyl (2-cyano-3-(4-nitrophenyl)acrylate

Ethyl (2-cyano-3-(4-nitrophenyl)acrylate was prepared from 4-nitrobenzaldehyde (0.22 mmol) and ethyl cyanoaceate (0.2 mmol) using 20 mg of Cu powder, stirring 16 h in EtOH at 56 °C and was obtained as a white solid (42.8 mg, 0.174 mmol, 86%). ^{1}H NMR (CDCl$_3$, 200 MHz, 25°C): δ 8.31 (s, 1H), 8.24 (m, 2H), 8.09 – 8.04 (m, 2H), 4.41 – 4.30 (q, 2H), 1.39 – 1.32 (t, 3H). ESI-MS: [M]$^-$ 246.03 m/z.

Ethyl 2-cyano-5-phenylpenta-2,4-dienoate
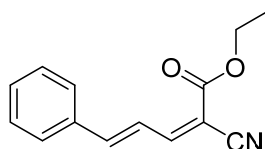
Ethyl 2-cyano-5-phenylpenta-2,4-dienoate was prepared from cinnamic aldehyde (0.22 mmol) and ethyl cyanoaceate (0.2 mmol) using 20 mg of Cu powder, stirring 16 h in EtOH at 56 °C and was obtained as a yellow solid (39.4 mg, 0.174 mmol, 86%). ^{1}H NMR (CDCl$_3$, 200 MHz, 25°C): δ 7.95 (m, 1H), 8.24 (m, 2H), 7.50 (m, 2H), 7.37-7.22 (m, 5H), 4.33 – 4.22 (q, 2H), 1.34 – 1.27 (t, 3H). ESI-MS: [M+Na]$^+$ 250.09 m/z.

Ethyl 3-(anthracen-9-yl)-2-cyanoacrylate

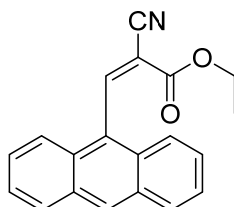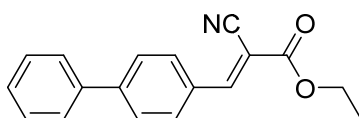Ethyl 3-(anthracen-9-yl)-2-cyanoacrylate was prepared from anthracene aldehyde (0.22 mmol) and ethyl cyanoaceate (0.2 mmol) using 20 mg of Cu powder, stirring 15 h in DMSO at 70 °C and was obtained as a yellow solid (19.3 mg, 0.064 mmol, 32%).

^{1}H NMR (CDCl3, 200 MHz, 25°C): δ 9.24 (s, 1H), 8.51 (s, 1H), 8.02-7.87 (m, 4H), 7.46 (m, H), 4.49 – 4.38 (q, 2H), 1.45 – 1.38 (t, 3H). ESI-MS: [M+Na]+ 324.01 m/z.

Ethyl 3-([1,1'-biphenyl]-4-yl)-2-cyanoacrylate

Ethyl 3-([1,1'-biphenyl]-4-yl)-2-cyanoacrylate was prepared from biphenyl aldehyde (0.22 mmol) and ethyl cyanoaceate (0.2 mmol) using 20 mg of Cu powder, stirring 16 h in EtOH at 56 °C and was obtained as a yellow solid (30.5 mg, 0.11 mmol, 54%). ^{1}H NMR (CDCl3, 200 MHz, 25°C): δ 8.21 (s, 1H), 8.00 (s, 1H), 7.59-7.34 (m, 8H), 4.39 – 4.28 (q, 2H), 1.38 – 1.31 (t, 3H). ESI-MS: [M+H]+ 278.04 m/z.

2-cyano-3-phenylacrylamide

2-cyano-3-phenylacrylamide was prepared from benzaldehyde (0.22 mmol) and cyano acetamide (0.2 mmol) using 20 mg of Cu powder, stirring 16 h in EtOH at 56 °C and was obtained as a yellow solid (29.2 mg, 0.17 mmol, 85%).
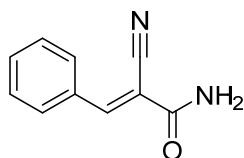
^{1}H NMR (CDCl3, 200 MHz, 25°C): δ 8.25 (s, 1H), 7.88 (m, 2H), 7.47 (m, 3H), 6.29 – 6.05 (br, 2H). ESI-MS: [M+H]+ 173.06 m/z.

Table 3-1. *Activity of different catalysts for the Knoevenagel reaction of benzaldehyde and ethyl cyanoacetate[a]*
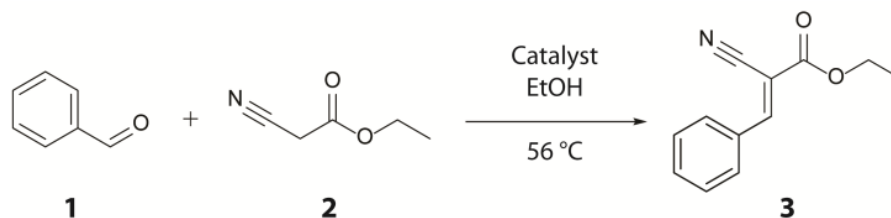
Entry	Catalyst	Time (h)	Yield (%)[b]
1	none	2	3
2	C/Co	2	8
3	Co powder	2	9
4	C/Fe	4	4
5	$FeCl_3$	4	4
6	Fe powder	4	6
7	C/Cu	4	12
8	Cu powder	2	32
9	Brass alloy 260	2	5
10	Ag powder	4	7
11	Au powder	4	6
12	$ZnCl_2$	6	4

[a]Reaction conditions: catalyst (4 mg), benzaldehyde (0.12 mmol) and ethyl cyanoacetate (0.1 mmol) in 1 mL EtOH for 2 h. [b]Only E-isomer detected, yield determined *via* HPLC-UV (MS) using the commercial product **3** as the reference standard.

3.3 Results and discussion

As a consequence of these results (active C/Co), several other carbon-coated nanoparticles were tested; amongst which carbon-coated copper nanoparticles (C/Cu)[126] showed the highest activity. As reference, we compared the nanoparticles with pure metal powders. These experiments afforded the insight that commercially available, dendritic copper powder Cu(D) catalyses the Knoevenagel condensation
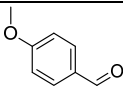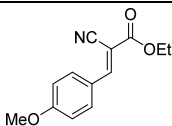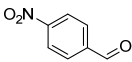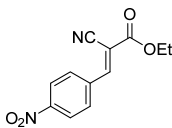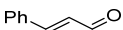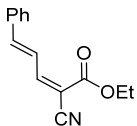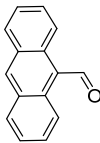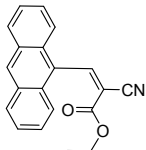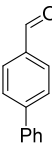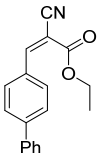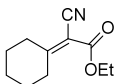
Table 3-2. *Optimization of the reaction conditions[a]*
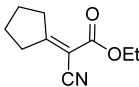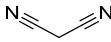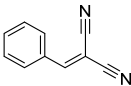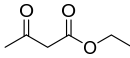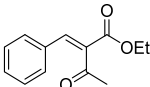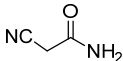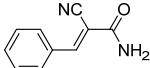
Entry	Solvent	Loading (mg)	t (h)	Cu (ppm)[b]	Yield (%)[c]
1	EtOH	0.4	2	3	6
2	EtOH	2	2	38	14
3	EtOH	4	2	44	32
4	EtOH	10	2	216	96(95)[d]
5	EtOH	40	2	114	99 (85)[d]
6	EtOH	4	6	44	99 (95)[d]
7	Acetone	4	20	18	1
8	Cyclohexane	4	20	32	3
9	Toluene	4	20	30	3
10	DMF	4	6	17	99 (98)[d]
11	DMSO	4	2	241	99
12	MeCN	4	2	230	99 (98)[d]

[a]Reaction conditions: copper (4 mg), benzaldehyde (0.12 mmol) and ethylcyanoacetate (0.1 mmol). [b]Cu leaching measured by ICP-OES. [c]Determined *via* HPLC-UV using the commercial product **3** as the reference standard. [d]Isolated yield.

of benzaldehyde **1** and cyanoacetate **2** in ethanol to **3** (**Table 3-1,** entry 8) with enhanced yields. Compared to other heterogeneous catalysts for the Knoevenagel condensation, the unmodified, commercially available copper does not need any special treatment, synthesis procedure or sophisticated storage and is base stock in many laboratories. It is noteworthy that silver, gold, ZnCl2 and brass showed only low activities compared to elemental copper (entries 9-12). To optimize the reaction conditions, the catalyst loading was varied, and, as expected, higher loading resulted in higher yields (up to 99%; **Table 3-2,** entry 8).

Table 3-3. *Substrate scope of the copper catalyzed condensation[a]*

Entry	Reactant	Reactant	Product	Yield (%)[b]
1[c]	2a			99 (98)[d]
2	2a			99 (87)[d]
3[c]	2a			90 (86)[d]
4[e]	2a			54 (32)[d]
5[c]	2a			64 (55)[d]
6	2a			55

7	2a	(cyclopentanone)	(ethyl 2-cyano-2-cyclopentylideneacetate)	42
8[f]	1a	(malononitrile)	(2-benzylidenemalononitrile)	99 (99)[d]
9[e]	1a	(ethyl acetoacetate)	(ethyl 2-benzylidene-3-oxobutanoate)	23
10[c]	1a	(2-cyanoacetamide)	(2-cyano-3-phenylacrylamide)	87 (85)[d]

[a]Reaction conditions: Cu (20 mg), aldehyde (0.21 mmol) and active methylene (0.2 mmol) for 6 h at 56 °C. [b]Yield determined *via* HPLC-UV or GC-FID. [c]Stirred for 16 h. [d]Isolated yield. [e]Stirred for 15 h in DMSO at 70 °C. [f]Stirred for 1 h at RT.

Table 3-4. *Overview of the copper(0) containing catalysts and their properties*

Entry	Catalyst	Abbreviation	Colour	Size (nm)	Shape	BET SSA ($m^2\ g^{-1}$)
1	copper powder dendritic	Cu(D)	red	500-1000	dendritic	0.2
2	copper nanoparticles A	Cu(NPA)	brown	40-60	spherical	4.2
3	copper nanoparticles B	Cu(NPB)	black	20-50	spherical	15.9
4	carbon-coated-copper nanoparticles	Cu(C)	black	5-50	spherical	61.1
5	copper hollow spheres	Cu(Hol)	black	1000-1500	hollow sphere	2.1

It should be noted that an equivalent amount of copper compared to the reagents is not imperative to result in full conversion (**Table 3-2,** entry 6). Optimization tests with different solvents clearly favored aprotic, polar solvents over non-polar solvents (entries 7-12). These results are in line with general literature on the Knoevenagel condensation, namely with the first step in the reaction

mechanism which is the generation of an anion at the α-position of the carbonyl followed by enolate formation.[118] After optimizing the reaction conditions with the model substrates, a variety of different aldehydes and active methylene compounds were reacted (**Table 3-3**). Substrates resulting in conjugated products (entries 1-5) were quite active, while the sterically demanding ketones only exhibited low activity (entries 6-7). Other active methylene compounds were tested, such as the very reactive malononitrile (99% yield in 1h, entry 8) and the less reactive ethylacetoacetate (26% yield after 15 h, entry 9). The different reactivities of these compounds is well known and correlates with their ability of stabilizing the anion.[118] To gain more detailed insight into the reaction mechanism, further experiments concerning the nature of the copper catalyst have been conducted. A possible first hypothesis was that copper leaching, *i.e.* soluble Cu(I) or Cu(II) species, could be the reason for catalytic activity. Several Cu(I/II) compounds have been tested (**Table 3-5,** entries 1-5) to investigate the activity of copper ions in solution. None of
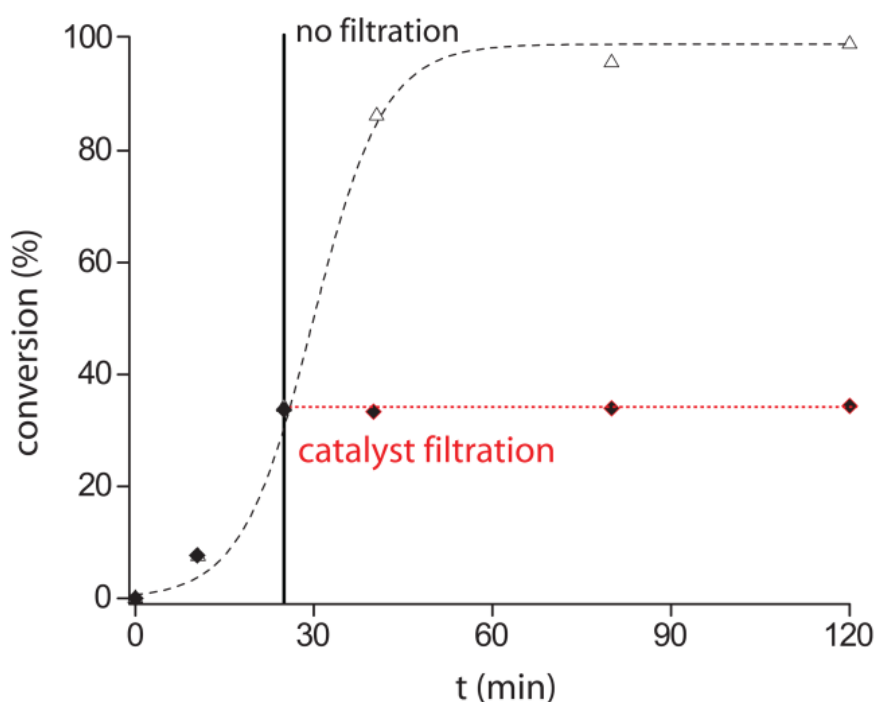
***Figure 3-1**. Knoevenagel condensation of benzaldehyde (0.12 mmol) and ethyl cyanoacetate (0.1 mmol) with copper Cu (D) (4 mg) at 56 °C in DMSO: After 20 minutes half of the reaction volume was extracted and filtrated and further kept at reaction conditions without solid catalyst (black diamonds).*

these copper species showed substantial activity, instead of a high measured solvated Cu amount (entries 2 and 3). Also, there are reports of metal-alkoxide catalysed Knoevenagel condensations, and activity of *in situ* generated CuOMe may also be possible.[127, 128] However, if the solid catalyst is filtrated (**Figure 3-1**), conversion stops immediately. This leads to the conclusions that either there is a very unstable homogeneous reactive species formed on the surface of Cu or leaching is not the reason for catalytic activity. Hence, a second hypothesis can be formulated around Cu surface-based catalysis, where the yield is expected to correlate with the specific surface area (SSA) of the catalyst. Cu (D) has dendritic structures between 0.5 – 1 μm (**Figure 3-2** and **Figure A2-3**) and thus a relatively low BET surface area of 0.2 m^2 g^{-1}.
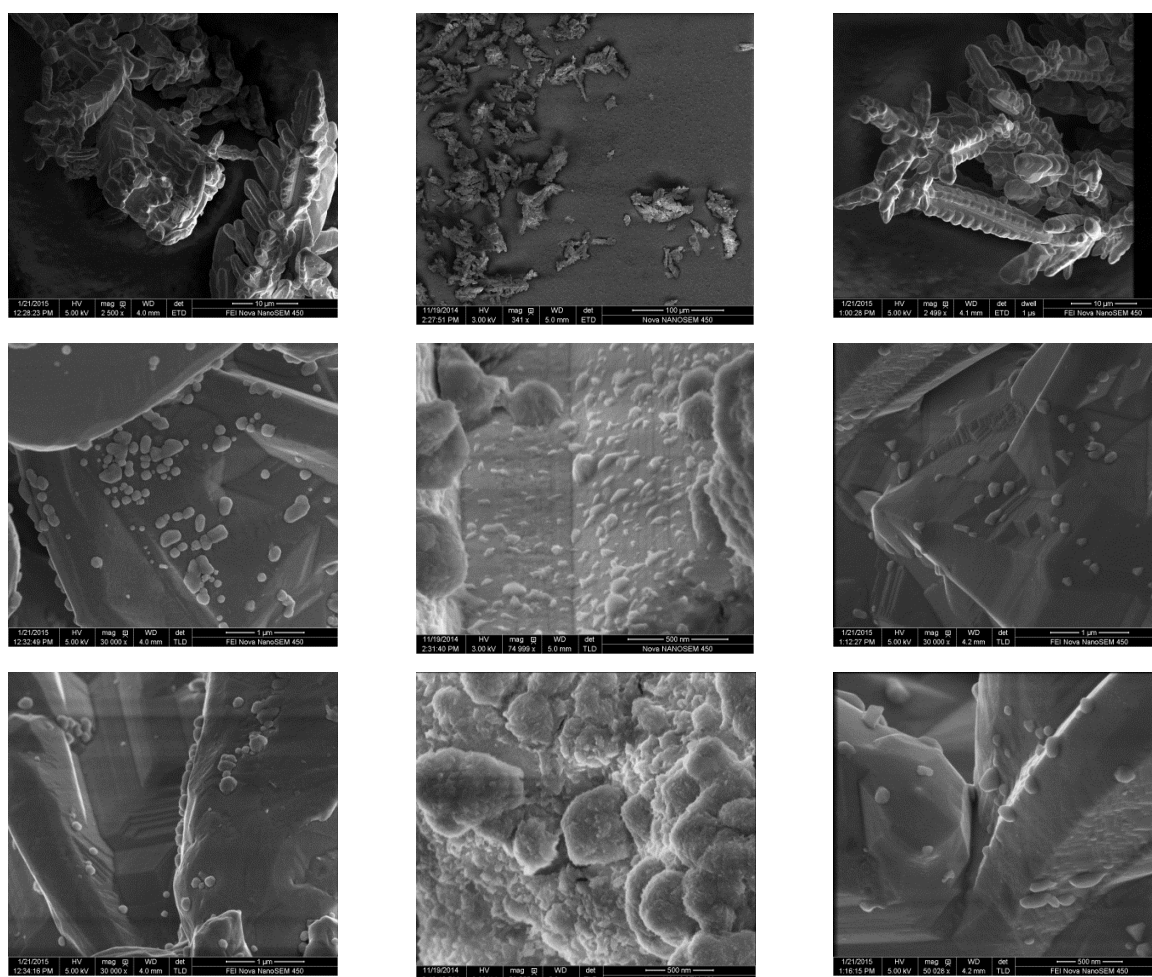
| Untreated Cu(0) powder | Cu(0) after catalysis (washed) | Cu(0) after 16 h at 56 °C in EtOH |

***Figure 3-2.** SEM micrographs showing Cu(0) powder at different stages of the catalysis.*

If a tenfold larger surface area (**Table 3-5,** entries 6-7) was used, the yield increased to 99%. However, the nature of the surface state required for catalytic action was still unknown. Thus, surface activation experiments were done: the copper catalyst was pre-treated under different reducing conditions in order to reduce the copper oxide layer. This resulted in higher yields, most obviously for toluene, where the pre-treated copper yielded 53% product after 20 h, while the untreated copper did not catalyze the reaction at all (**Table 3-6,** entries 4-5).

Table 3-5. *Copper containing reference substances as catalysts for the Knoevenagel condensation[a]*

Entry	Catalyst	Time (h)	SSA ($m^2 \, 10^{-4}$)	Cu (ppm)	Yield (%)[b]
1	$Cu(II)_2(OH)_2CO_3$	2	-	6	2
2	$Cu(II)Cl_2$	16	-	740	1
3	$Cu(I)Cl$	16	-	460	3
4	$Cu(II)O$	20	-	6	4
5	$Cu(I)_2O$	20	-	12	14
6	Cu (D)	2	8	44	32
7[c]	Cu (D)	2	80	114	99
8	Cu (Hol)	2	84	62	65
9	Cu (NPA)	2	168	176	96
10	Cu (NPB)	2	636	197	99

[a]Reaction conditions: catalyst (4 mg), benzaldehyde (0.12 mmol) and ethyl cyanoacetate (0.1 mmol) in EtOH at 56 °C. [b]Yield determined *via* HPLC-UV (MS) using commercial product **3** as the reference standard. [c]40 mg of Cu (D) used.
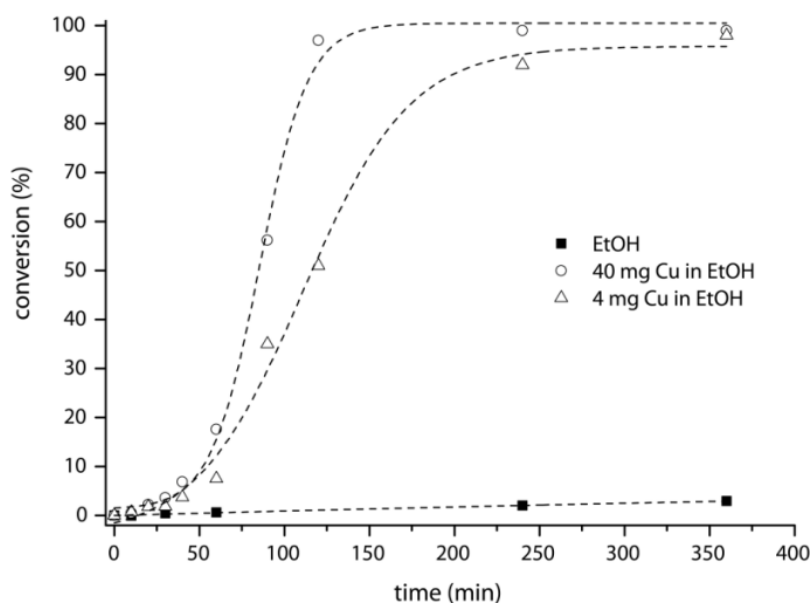
Figure 3-3. Knoevenagel condensation of benzaldehyde (0.2 mmol) and ethyl cyanoacetate (0.1 mmol) with dendritic copper powder at 56 °C: no visible reaction without catalyst was detected.
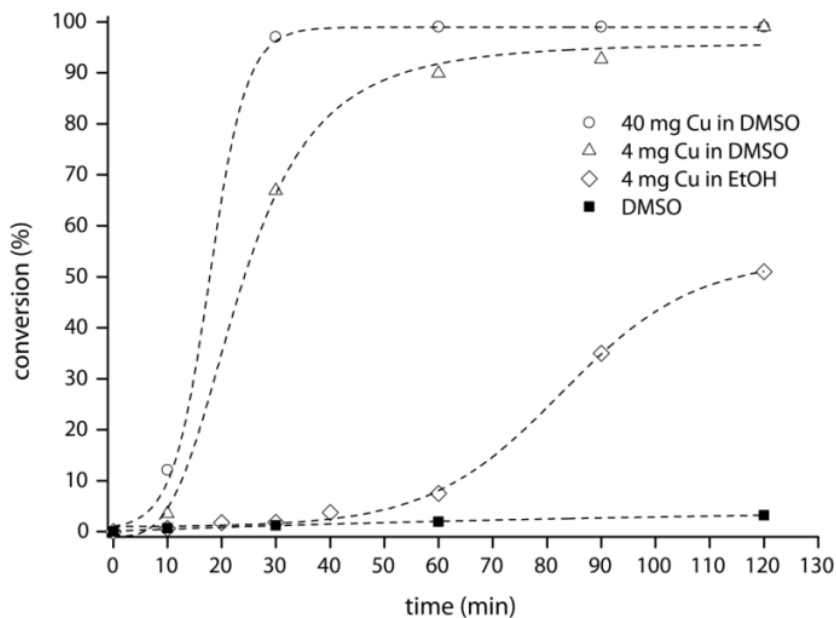
Figure 3-4. Knoevenagel condensation of benzaldehyde (0.2 mmol) and ethyl cyanoacetate (0.1 mmol) with dendritic copper powder at 56 °C. Nearly linear conversion with Ethanol, zero order kinetics fit.

Table 3-6. *Effect of surface activation of Cu(0) on the reaction rate[a]*
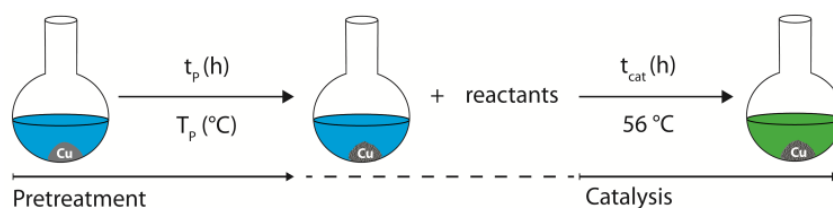
Entry	Pretreatment	t_P (h)	T_P (°C)	t_{cat} (h)	Solvent	Yield (%)[b]
1	-	-	-	2	EtOH	32
2	reduction w/ FA[c]	1	RT	2	EtOH	49
3	reduction w/ H$_2$	2	60	2	EtOH	52
4	-	-	-	20	Toluene	3
5	reduction w/ H$_2$	2	110	20	Toluene	53

[a]Reaction conditions: pre-treated catalyst (4 mg), benzaldehyde (0.21 mmol) and ethyl cyanoacetate (0.2 mmol) at 56 °C. [b]Yield determined *via* HPLC-UV (MS) using commercial product **3** as the reference standard. [c]In 2% formic acid.

This finding leads to the conclusion that a non-oxidized Cu(0) surface reacts with the substrates. Kinetic measurements support the surface catalyzed mechanism, too, as a zero order kinetic model fits well in the beginning of the reaction (See **Figures 3-3** and **3-4**). An initial TOF of 0.88 s^{-1} was calculated using optimal conditions (**Figure 3-1**, 41% yield after 30 min) and the conservative assumption that every Cu(0) atom on the surface is an active site. Further mechanistic studies are subject of ongoing research.

Moreover, similar copper(0) species with different BET surface areas (see **Table 3-5**), such as copper hollow spheres Cu(hol),[129, 130] copper nanoparticles A Cu(NPA) and copper nanoparticles B Cu(NPB) were tested (entries 8-10). A correlation between the surface area and conversion could be confirmed. To illustrate the practical synthetic utility of our method, a 100 gram scale
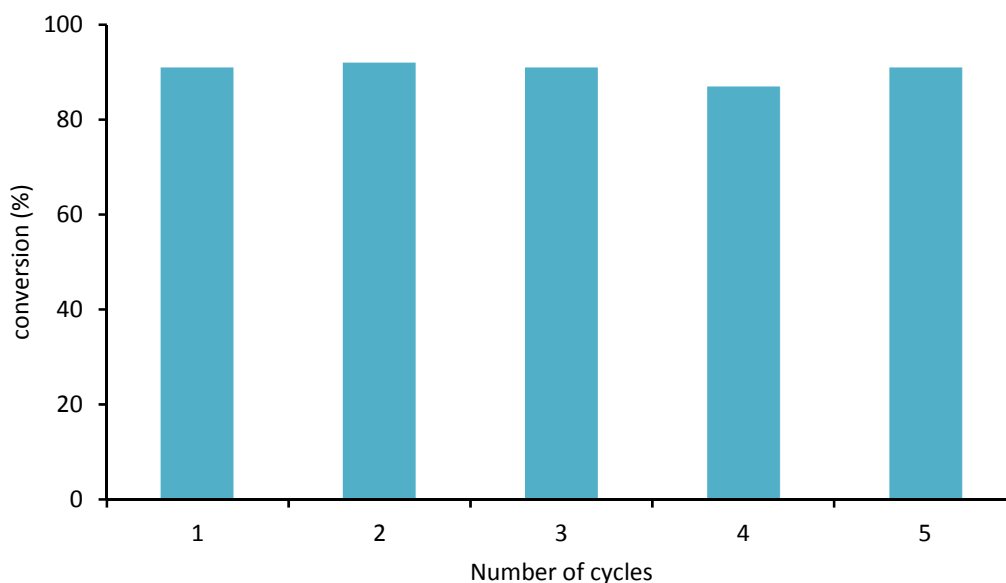
Figure 3-5. *Conversion of the condensation between benzaldehyde (0.1 mmol) and ethyl-cyanoacetate (0.1 mmol) in 1 ml DMSO with 4 mg Cu @56 °C after 1 h. 5 successive cycles using the same catalyst.*

experiment was performed (**Figure A2-1**). Benzaldehyde **1** (81.2 mL, 0.8 mol) was reacted with ethyl cyanoacetate **2** (84.8 mL, 0.8 mol) and 16 g Cu (D) in EtOH at 56 °C for 16 h. After filtration through aluminum oxide and recrystallization, 91% (146 g) pure isolated yield was obtained. This satisfying result highlights the simplicity of both catalyst and work-up and, hence, is of interest for industrial scale Knoevenagel reactions. It should be noted that this kind of upscale experiment is difficult to perform with soluble base catalysts, as large amounts of solvent and neutralization agent have to be used.

Additionally, 5 successive cycles of catalysis were done using the same catalyst batch (**Figure 3-5**). No substantial decrease in conversion was observed, highlighting the reusability of this catalyst. Also, no oxidation of the copper was observed by XRD before and after catalysis (see **Figure A2-3**).

3.4   Conclusion

In summary, we have developed a simple and mild method for the Knoevenagel condensation using commercially available semi-noble copper. In this catalysis, tedious separation procedures are not necessary and no traces of base remain if the catalyst is filtered off with basic aluminium oxide. Further experiments revealed that a Cu(0) surface is necessary to catalyze the condensation and, surprisingly, other noble metals, such as gold and silver, were not active. Moreover, a substantial scale up (>100 g) experiment demonstrated simple applicability. Furthermore, the catalyst remained active after 5 consecutive cycles, highlighting the advantageous reusability properties.

4 Click and release: fluoride cleavable linker for mild bioorthogonal separation
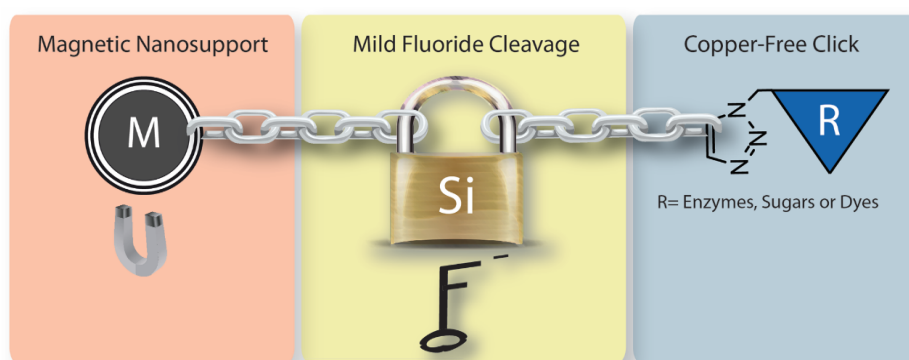
published in parts as:

Elia M. Schneider, Martin Zeltner, Vladimir Zlateski, Robert N. Grass, Wendelin J. Stark

Chem. Commun., **2016**, *52*, 938-941.

Author contribution:
E.M.S. and W.J.S. elaborated the concept. E.M.S. performed the experiments with support of M.Z. and V.Zlateski. E.M.S., R.N.G. and W.J.S. wrote the manuscript with review from all authors.

4.1   Introduction

Bioorthogonal chemistry[131] opened the way for a detailed description and understanding of many biological processes, namely by the possibility to label and track specific biomolecules, such as enzymes, lipids and sugars *in vivo*.[132-134] However, this kind of reactions, such as the Staudinger ligation or the 1,3-dipolar Huisgen cycloaddition of azides and alkynes ("click"),[110, 135] are not reversible und cannot be cleaved in a specific and bio-compatible way (*i.e.* low temperatures, at neutral pH and in water). This would be beneficial for a large set of applications, for example native protein analysis,[136] protein glycosylation analysis[137] and analysis of protein complexes[138] *via* mass spectroscopy. There exist only a few reports of such linker systems;[139, 140] however, the cleaving conditions are often quite harsh or not fully bioorthogonal. Our idea was to implement a cleavable silane moiety, one of the most often used protecting groups for alcohols in organic chemistry.[141, 142] The main advantage of this system is the cleavage *via* fluoride ions, which has already been used in solid peptide synthesis.[143] However, instead of using anhydrous HF we opted for buffered oxide etch (mild buffered fluoride solution) which has been used to uncage DNA and RNA from silica without damaging the biomolecules.[26, 144-147] Our aim was to combine this mature technique to the modern copper-free "click" chemistry. Since the Huisgen-cycloaddition usually needs a high amount of copper catalyst, which hinders proper cell function,[148] a variety of strain-promoted copper-free click reagents has been developed.[149-152] These reagents promote the relatively fast dipolar cycloaddition without the need of any copper catalyst, thus leading to bio-compatible chemistry.

By combining the mature and biorthogonal silane-chemistry with the state-of-the-art copper-free "click" chemistry, the creation of a cleavable "click and release" system is anticipated. Additionally, a suitable way to get in and out of a biological system has to be considered. A promising approach is provided by magnetic nanoparticles, since they can be separated quickly from any solution by using a permanent magnet. Recently, a *plethora* of magnetic nano-sized reagents has been developed,[66, 123, 153, 154] based on magnetic carbon-coated metal nanoparticles. The advantages of these nanoparticles are a higher saturation magnetization and thus faster separation compared to silica coated iron oxide nanoparticles.[123] Furthermore, the graphene layer protects the particle from degradation by buffered oxide etch and it can be functionalized in a covalent and stable manner.[66]
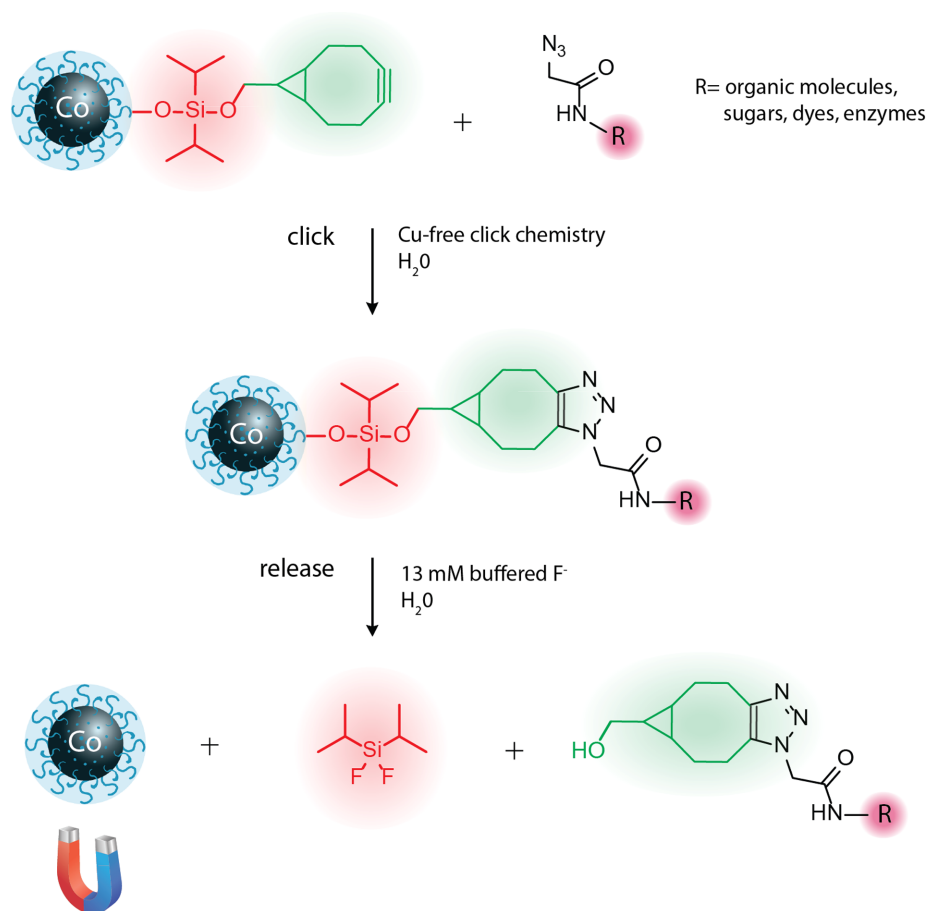
Scheme. 4-1. *Copper-free dipolar cycloaddition (click) on the magnetic nanoparticle followed by the fluorine-mediated release.*

However, one of the main drawbacks of this material is the unspecific protein adsorption ("fouling") on the highly hydrophobic, graphene-like surface. To provide a solution for this problem, defined coatings have been developed, often PEG-chains or analogues.[25, 155] A practical route to coat nanoparticles in an uniform and defined way is surface-initiated atom transfer radical polymerization (SI-ATRP), a "grafting from" approach.[24, 156, 157] Herein, we present the synthesis of a bioorthogonal "click" and release system (**Scheme 4-1**) on a magnetic, PEG-coated support.

4.2   Experimental

Carbon-coated cobalt nanoparticles were suspended by the use of an ultrasonic bath and subjected to various reactions (see below). After a reaction or a pre-treatment step, nanoparticles were recovered from the reaction mixture with the aid of a conventional magnet (neodymium based magnet, N48, W-12-N, Webcraft GmbH, side length 12 mm). The nanoparticles were analyzed by Fourier transform infrared spectroscopy (FT-IR), using 5 wt% nanoparticles in KBr with a Tensor 27 Spectrometer (Bruker Optics) equipped with a diffuse reflectance accessory (DiffuseIR, Pike Technologies) and elemental microanalysis (ELEMENTAR, Elementar Analysensysteme). Transmission electron microscopy (TEM) was measured with a CM12 (Philips, operated at 120 kV). The nanomaterial was further characterized by magnetic hysteresis susceptibility as a powder in a gelatin capsule (vibrating sample magnetometer, VSM, Princeton Measurements Corporation, model 3900).   HPLC measurements were conducted on an AGILENT 1100 (WATERS Column, particle size, 5 μm; column size, 2.1 × 150 mm2). GC−MS measurements were performed (capillary, 30 m × 250 × 0.5 μm2) with split injection (250 °C; ratio = 10:1; injection volume, 1 μL) and a temperature program (80 °C for 2 min; increase at 20 °C min^{-1} until 300 °C). UV Spectroscopy was done using a Thermo Scientific NANODROP 2000c spectrometer.

C/Co@starter **1** was prepared according to literature.[52] It should be noted that only fresh 2-Bromo-2-methylpropionyl bromide should be used to generate an active starter moiety.

FT-IR: 2980 cm^{-1}, 2931 cm^{-1}, 1733 cm^{-1}, 1277 cm^{-1}, 1162 cm^{-1}.

Elemental microanalysis: [C]: 10.7%, [N]: 0.13%, [Br]: 0.62%.

4.2.1 Synthesis of the magnetic click and release reagent

Synthesis of C/Co@PEGMA 2
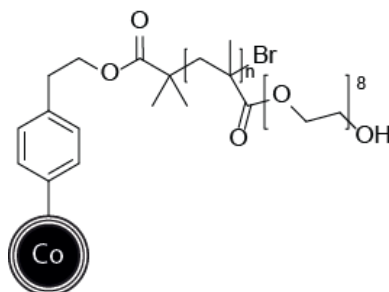
All reaction steps were performed under protective nitrogen atmosphere. Poly(ethylene glycol)methacrylate (PEGMA, M_n 360, 5 mL) was filtered over a basic aluminum oxide column in order to remove the inhibitor (MEHQ), then mixed with 25 mL of solvent (MeOH : H_2O, 4:1) and degassed with nitrogen by bubbling through for 30 min. $CuBr_2$ (10 mg, 0.045 mmol), bipyridine (52 mg, 0.033 mmol) and L-ascorbic acid (60 mg, 0.34 mmol) were added to the mixture and degassed for additional 5 minutes. Meanwhile, C/Co@starter **1** (900 mg) was dispersed in 10 mL of solvent (MeOH : H_2O, 4:1) and degassed with nitrogen for 30 min. Subsequently, the monomer/catalytic system-solution was added to the particles and sonicated at 20 °C overnight. Upon completion of the reaction the polymerized particles were recovered from the reaction mixture with the aid of a permanent magnet and washed with H_2O (4x), EtOH (2x) and acetone (1x). The nanoparticles were dried in a vacuum oven at 50 °C for 16 h.

FT-IR: 2920 cm^{-1}, 2876 cm^{-1}, 1725 cm^{-1}, 1455 cm^{-1}, 1105 cm^{-1}.

Elemental microanalysis: [C]: 35.08%, [N]: 0.04%.

Synthesis of C/Co@PEGMA-Si-Octyne 3
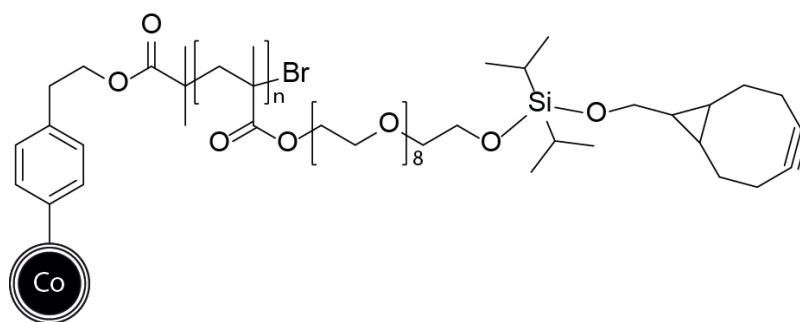
All reaction steps were performed under protective nitrogen atmosphere. (1R,8S,9s)-Bicyclo[6.1.0]non-4-yn-9-ylmethanol (49 mg, 0.32 mmol) and 4-dimethylaminopyridine (27 mg, 0.22 mmol) were degassed 3 times in a 10 mL Schlenk-flask and dissolved in 1 mL dry DMF. The solution was cooled in an ice bath and triethylamine (75 µL, 0.74 mmol) was added. Subsequently, dichlorodiisopropylsilane (69 µL, 0.35 mmol) was added dropwise. After 6 hours, the reaction mixture was allowed to warm to room temperature.

C/Co@PEGMA **2** (200 mg) was washed with dry DMF (3x) and dispersed in 10 mL dry DMF. Subsequently, the *in situ*-generated mono-chlorinated silane solution was added and the resulting dispersion stirred overnight. Upon completion of the reaction, the functionalized particles were recovered from the reaction mixture with the aid of a permanent magnet and washed with DMF (3x), EtOH (3x) and H_2O (2x). For analysis, a fraction of the nanoparticles was dried in a vacuum oven at 40 °C for 24 h.

FT-IR: 2929 cm^{-1}, 2871 cm^{-1}, 1731 cm^{-1}, 1463 cm^{-1}, 1113 cm^{-1}.

Elemental microanalysis: [C]: 40.33%, [N]: 0.00%.

Synthesis of C/Co@PEGMA-Si-Naphthol
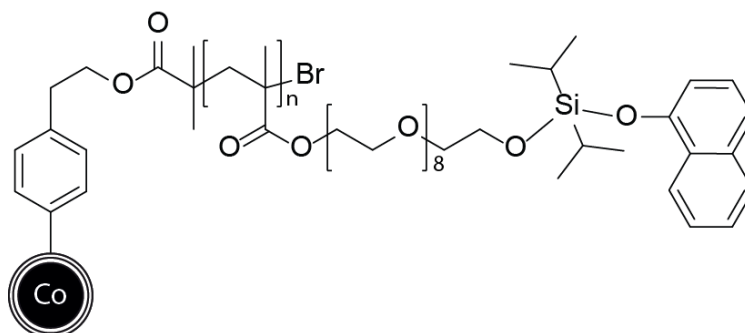
All reaction steps were performed under protective nitrogen atmosphere. 1-naphthol (400 mg, 2.7 mmol), 4-dimethylaminopyridine (180 mg, 1.3 mmol) were degassed 3 times in a 10 mL Schlenk-flask and dissolved in 1 mL dry DMF. The solution was cooled in an ice bath and triethylamine (0.7 mL, 6.9 mmol) was added. Subsequently, dichlorodiisopropylsilane (0.5 mL, 2.7 mmol) was added dropwise. After 8 hours, the reaction was allowed to warm to room temperature. GC-MS found: m/z 292 (monochlorinated adduct)

C/Co@PEGMA **2** (500 mg, different batch, carbon mass content = 20.1%) were washed with dry DMF (2x) and dispersed in 20 mL dry DMF. Subsequently, the *in situ*-generated mono-chlorinated

silane solution was added and the resulting dispersion stirred overnight. Upon completion of the reaction, the functionalized particles were recovered from the reaction mixture with the aid of a permanent magnet and washed with DMF (2x) and EtOH (2x). For analysis, a fraction of the nanoparticles was dried in a vacuum oven at 40 °C for 24 h.

FT-IR: 2868 cm^{-1}, 1731 cm^{-1}, 1643 cm^{-1}, 1460 cm^{-1}.

Elemental microanalysis: [C]: 22.12% (different precursor 20.1% C), [N]: 0.00%.

4.2.2 Standard procedures

Functionalization of α-Chymotrypsin with azide moieties

α-Chymotrypsin (8 mg, 0.3 μmol) was dissolved in 2 mL of 0.2 M NaHCO$_3$ in an Eppendorf tube. Azide-PEG-NHS (5 EQ, 0.57 μL) was added and the solution was shaken (500 RPM) at RT for 16 h. Purification of the protein was done using Amicron-Ultra centrifugal filter units, diluting with Milli-Q water (4 mL, MWCO 10000, 6000 RPM, 20 min, 3 times).

TAMRA-Azide dipolar cycloaddition (click)

C/Co@PEGMA-Si-Octyne **3** (10 mg) was dispersed in 1 mL H$_2$O using a 2 mL Eppendorf tube. TAMRA-azide solution (40 μL, 0.01 mM) was added and the solution was shaken for 3 h. The reaction was monitored by UV-spectroscopy (550 nm). Particles were separated using a permanent magnet.

Enzyme magnetic particle dipolar cycloaddition (click)

C/Co@PEGMA-Si-Octyne **3** (10 mg) was dispersed in 1 mL H$_2$O using a 2 mL Eppendorf tube. α-Chymotrypsin-Azide solution (100 μL, 0.001 mM) was added and the solution was shaken for 16 h (500 RPM). Particles were separated using a permanent magnet.

Enzymatic assay with α-Chymotrypsin

The activity of the protease was determined *via* UV monitoring of the cleavage of N-benzoyl-L-tyrosine p-nitroanilide. Therefore, a standard enzymatic assay was performed based on the enzyme

catalyzed hydrolysis of the peptide and monitored by UV-spectroscopy at 390 nm over a defined amount of time (*i.e.* 10 min). 2 mL of Tris/HCl buffer pH 7.8 was added to a PS-cuvette, followed by 80 μL 2 M CaCl$_2$ solution, 100 μL substrate (1.4 mM, DMSO : H$_2$O, 1:1) and at t = 0 100 μL sample. Measurements were taken each 30 s.

Cleavage reaction using buffered oxide etch

Particles were dispersed in 0.9 mL distilled water using an Eppendorf tube. Subsequently, 0.1 mL buffered oxide etch (0.13 M) was added and the tube was shaken at RT. Detailed preparation and handling of buffered oxide etch can be found in literature.[26]
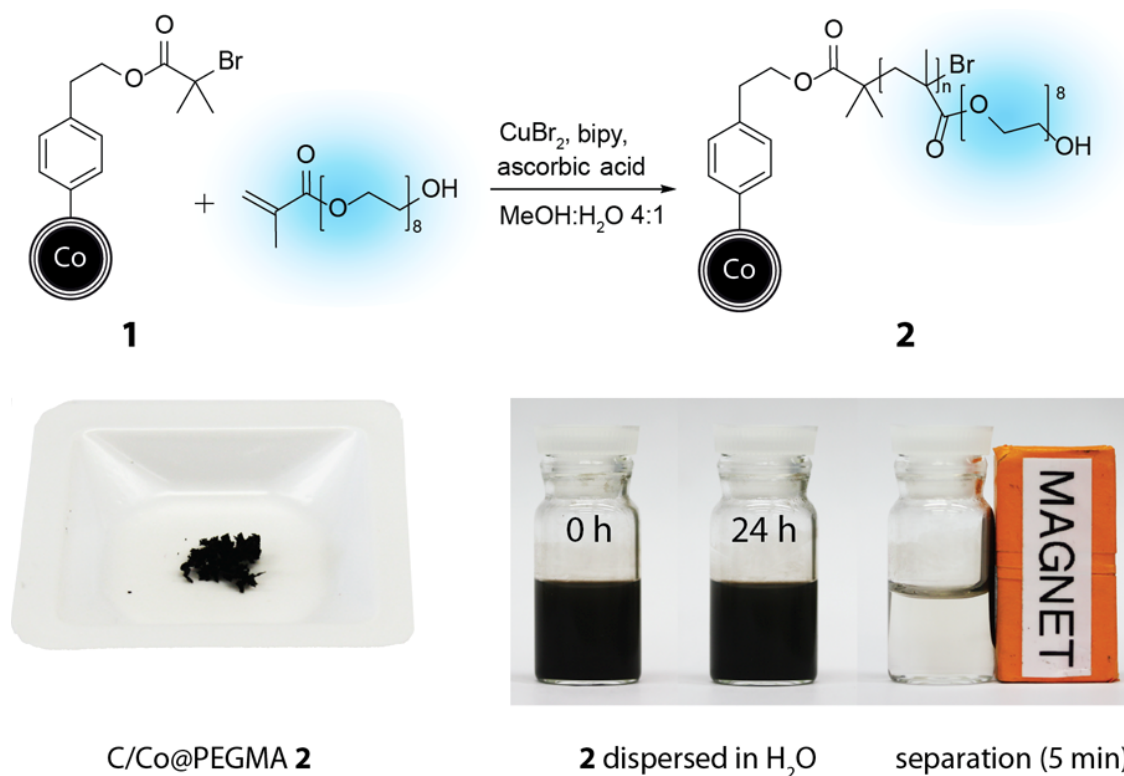
Figure 4-1. *PEG-methacrylate polymerisation* via *SI-ATRP. Sufficient dispersion stability in aqueous media is obtained while magnetic separation is still possible. Amount of solid (left) 150 mg, concentration (right) 10 mg mL^{-1}.*

4.3   Results and discussion

The preparation of the PEG-coated magnetic nanoparticles was conducted *via* standard surface-initiated atom transfer radical polymerization using CuBr$_2$ and bipyridine (bipy) as catalyst and ligand, respectively (**Figure 4-1**). First, the magnetic carbon-coated cobalt nanoparticles (C/Co) were functionalized according to literature,[25] yielding covalently bound starter particles **1**. Subsequently, **1** was polymerized using ascorbic acid to reduce Cu(II) to the active Cu(I) form (known as activator regenerated by electron transfer (ARGET) ATRP),[23] resulting in the novel PEG-coated magnetic nanoparticles C/Co@PEGMA **2**. Compound **2** was characterized *via* elemental microanalysis (ΔC= 24.4%, see **Table 4-1**) and IR (**Figure 4-2**). Using this polymerization technique, control of the polymer length and thus the desired dispersion stability could be obtained.[155] Indeed, the so obtained polymer-coated particles were sufficiently dispersible in an aqueous solution and the formation of a polymer layer around the magnetic particles was confirmed by transmission electron microscopy (**Figure 4-3**). Comparing the unfunctionalized C/Co particles to the polymerized C/Co@PEGMA **2**, the former stack while the latter do not, due to steric repulsion of the transparent polymer layer. Compound **2** was characterized *via* elemental microanalysis (ΔC= 24.4%, see **Table 4-1**) and IR (**Figure 4-2**). Since an extensive polymer layer can significantly lower the saturation magnetization, a vibrating sample magnetometer measurement (VSM) was executed. 151 emu g^{-1} was obtained for non-functionalized carbon-
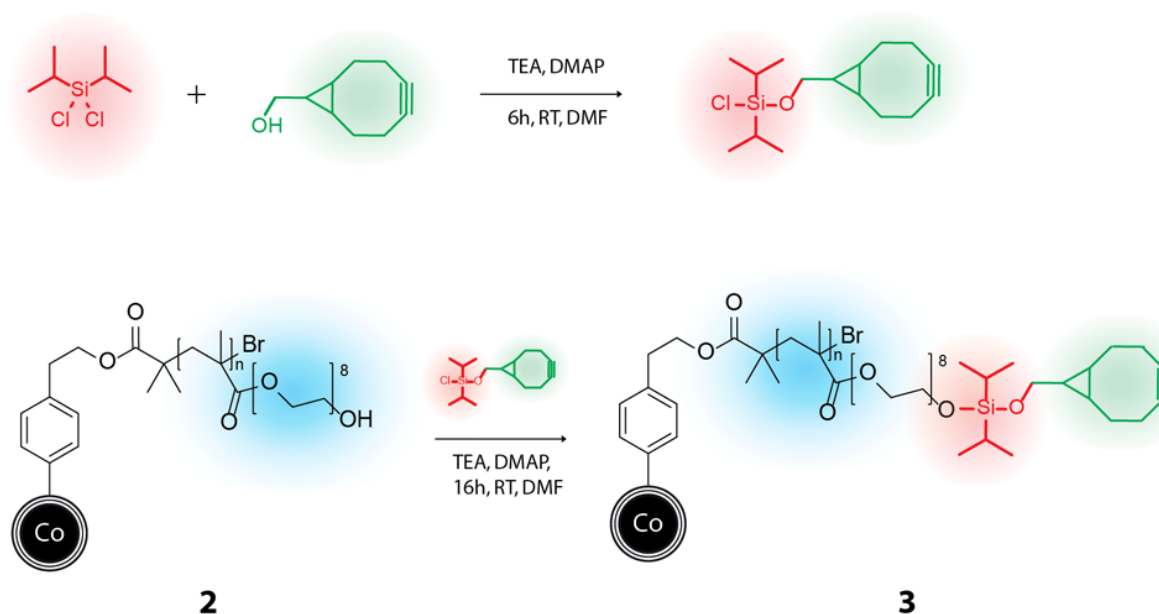
Scheme 4-2. *Synthesis of C/Co@PEGMA-Si-Octyne.*

coated cobalt nanoparticles C/Co, while for **2** 61.1 emu g^{-1} was measured. Despite the lower magnetization and high dispersion stability, fast separation was possible by using a permanent magnet (**Figure 4-1**).

To introduce the cleavable silyl linker, dichloro-diisopropylsilane was reacted with a hydroxyl-bearing moiety for 6 h and subsequently added to well-dispersed C/Co@PEGMA particles **2**, thus affording the fluoride-cleavable linker system (**Scheme 4-2**). In order to verify that the silane linking system was indeed cleavable with dilute F$^-$ solution (buffered oxide etch, BOE) and to determine the ideal cleaving conditions, test reactions were run using fluorescent 1-naphthol as the leaving group (see **Figure A3-1**). The linker system was stable in water, 5 mM HCl solution and pH 4 sodium phosphate buffer (SPB). Notably, 13 mM of BOE pH 4 proved to be an optimal amount of fluoride to cleave the silane bond in quantitative yields. The formation of 1-naphthol and difluoro- iisopropylsilane upon treatment with BOE was confirmed by LC-MS and GC-MS,
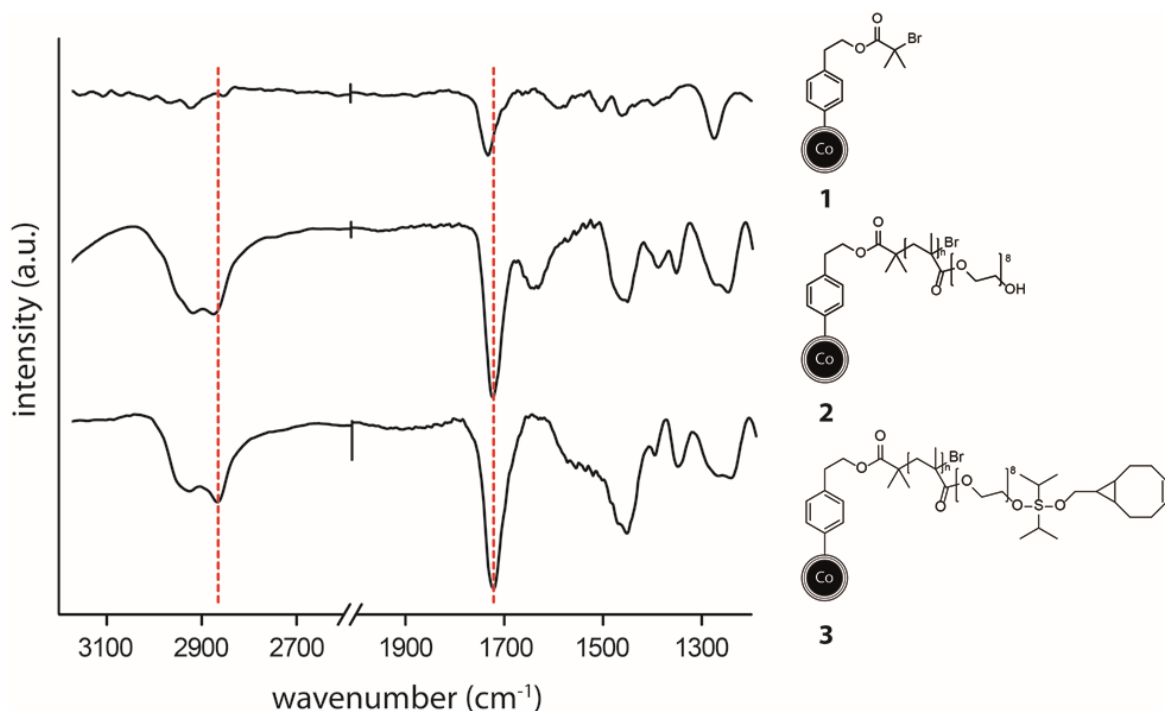
Figure 4-2. *FT-IR spectra of the magnetic compounds 1-3. Red lines highlight the following vibrations: 2876 cm^{-1} C-H stretch, 1725 cm^{-1} C=O stretch.*
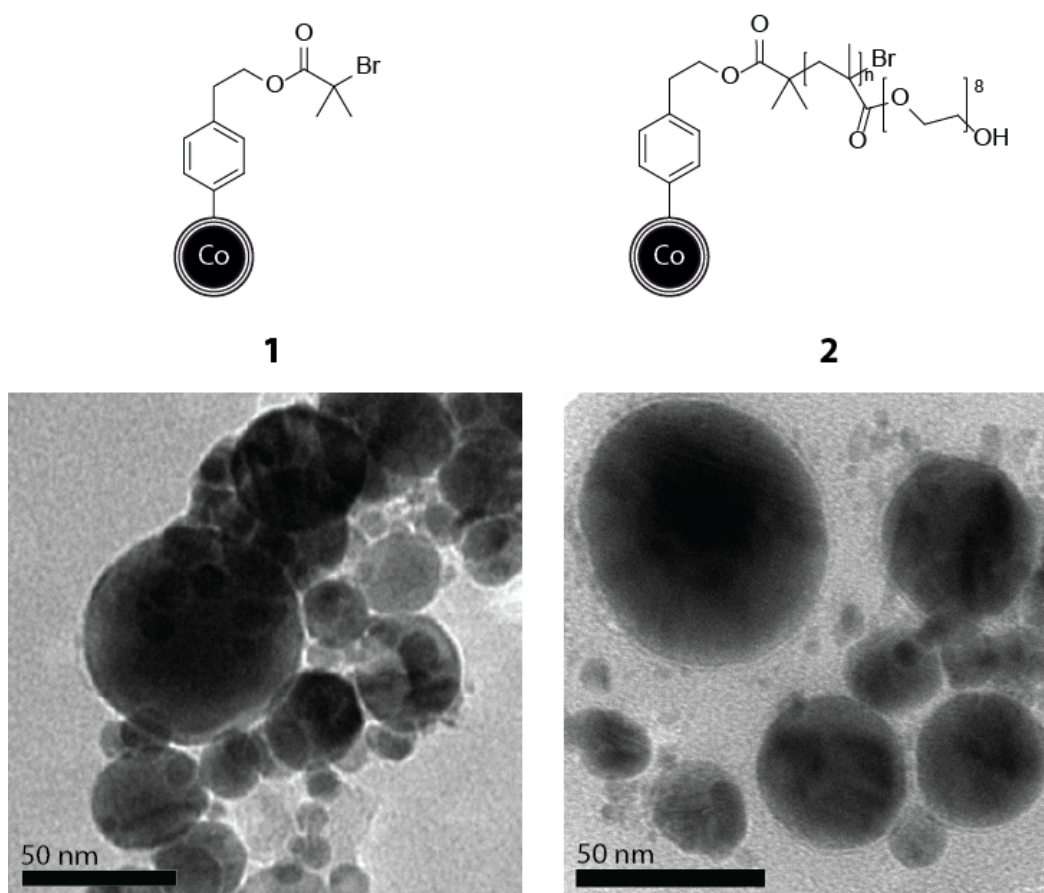
Figure 4-3. *TEM micrographs of the magnetic particles before **1** and after polymerization **2**.*

respectively. Subsequently, the more sophisticated copper free click reagent ((1R,8S,9s)-bicyclo[6.1.0]non-4-yn-9-ylmethanol), which contains an accessible hydroxyl group, was reacted with dichloro-diisopropylsilane and *in situ* added to C/Co@PEGMA **2** to afford a magnetic, cleavable copper-free click reagent C/Co@PEGMA-Si-Octyne **3** (**Scheme 4-2** for IR and **Figure A3-2** for VSM measurement). Characterization *via* elemental microanalysis and IR (esp. C-H stretch at 2876 cm^{-1}) confirmed the establishment of the desired linker system. Additionally, XRD was done to prove the metallic nature of the copper (**Figure A3-3**). The loading was determined by clicking the commercially available azide functionalized dye carboxy-tetramethylrhodamine (TAMRA-Azide) to **3** (**Figure 4-4**). Therefore, the dye and **3** were shaken for 6 h, resulting in a 1,3-Huisgen dipolar cycloaddition. Subsequently, the absorbance of the supernatant was measured at 550 nm, containing the remaining dye species. The particles were washed with water three times for one hour, resulting in no absorbance at 550 nm, *i.e.* no color.

However, if dispersed in 13 mM BOE, a clear peak at 550 nm appeared, also visible as a purple coloring.
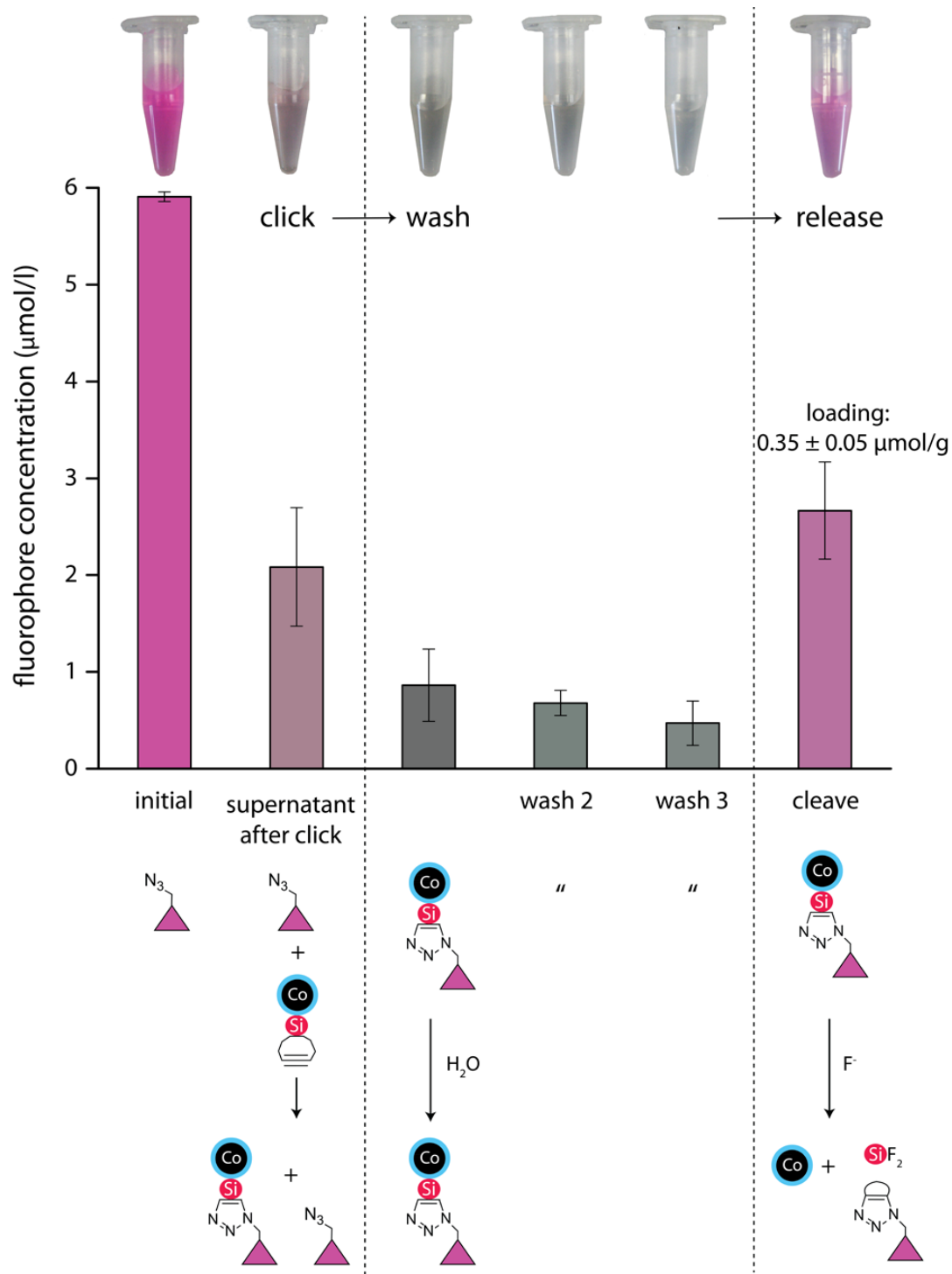
Figure 4-4. *Click and release of an azide-functionalized dye (TAMRA-Azide). Conditions: in water, click for 3 h at RT, wash with water (3x, 1 h), cleave for 16 h using 13 mM BOE.*

It should be noted that 13 mm buffered oxide etch contains a relatively low amount of fluoride (247 ppm), comparable to common toothpaste (1000-1500 ppm).[158]

Table 4-1. *Elemental analysis results*

Entry	Compound	C (%)	N (%)
1	**1**	10.67	0.13
2	**2**	35.08	0.04
3	**3**	38.14	0.00
4	**3** w/ enzyme	37.78	0.14
5	**3** after cleavage	34.88	0.04
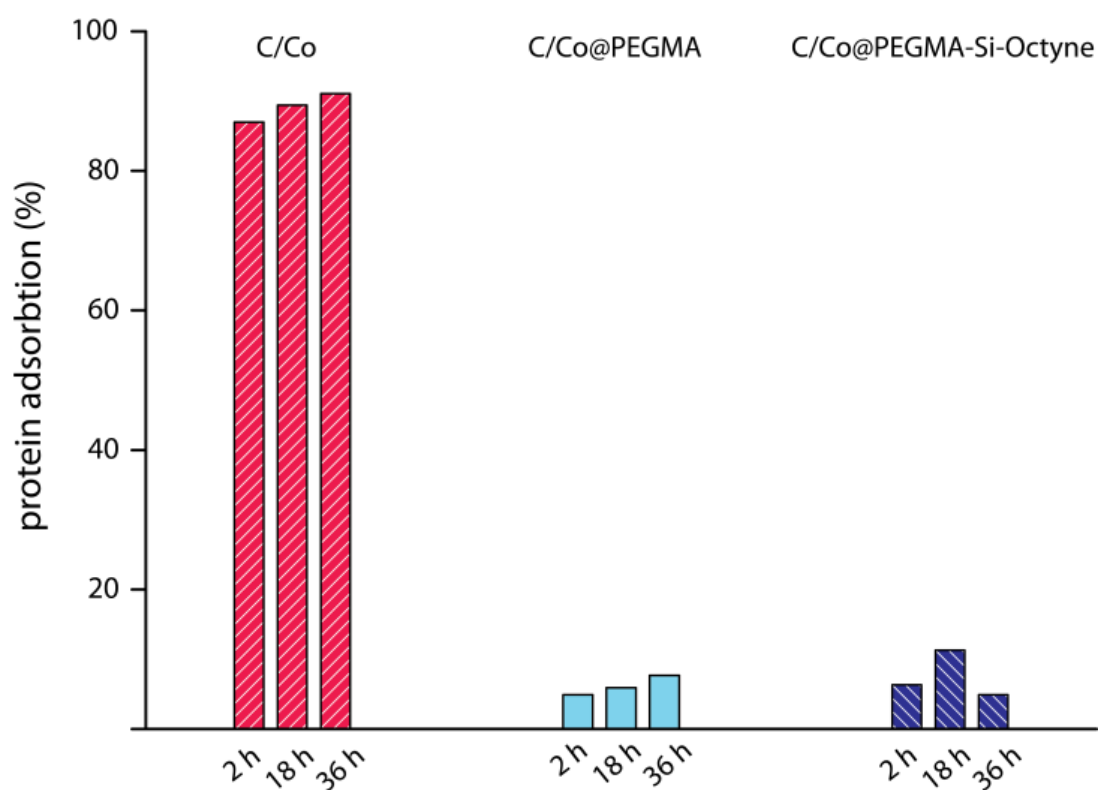
Figure 4-5. *Chart depicting the unspecific protein adsorption. Rhodamine labelled BSA was dissolved in water (0.5 nmol mL^{-1}) and the absorption at 555 nm was measured using naked particles, **2** or **3** (20 mg each).*

The amount of cleaved dye was used to calculate the loading, determined as 0.35 ± 0.05 µmol g^{-1}. The loading was intentionally set lower (by controlling the amount of mono-chlorinated species added to C/Co@PEGMA) than in the case of 1-naphthol (49 ± 0.4 µmol g^{-1}), because many biomolecules are large in diameter (1-6 nm)[159] and therefore make a high loading onto nanoparticles impossible due to size constraints. It should be mentioned that a higher loading could possibly be achieved, but since copper-free click reagents are expensive in large quantities (*e.g.* grams) and the resulting benefit (*i.e.* higher biomolecule loading) is low, this was not pursued further. Furthermore, unspecific protein binding onto the nanoparticles ("fouling") was
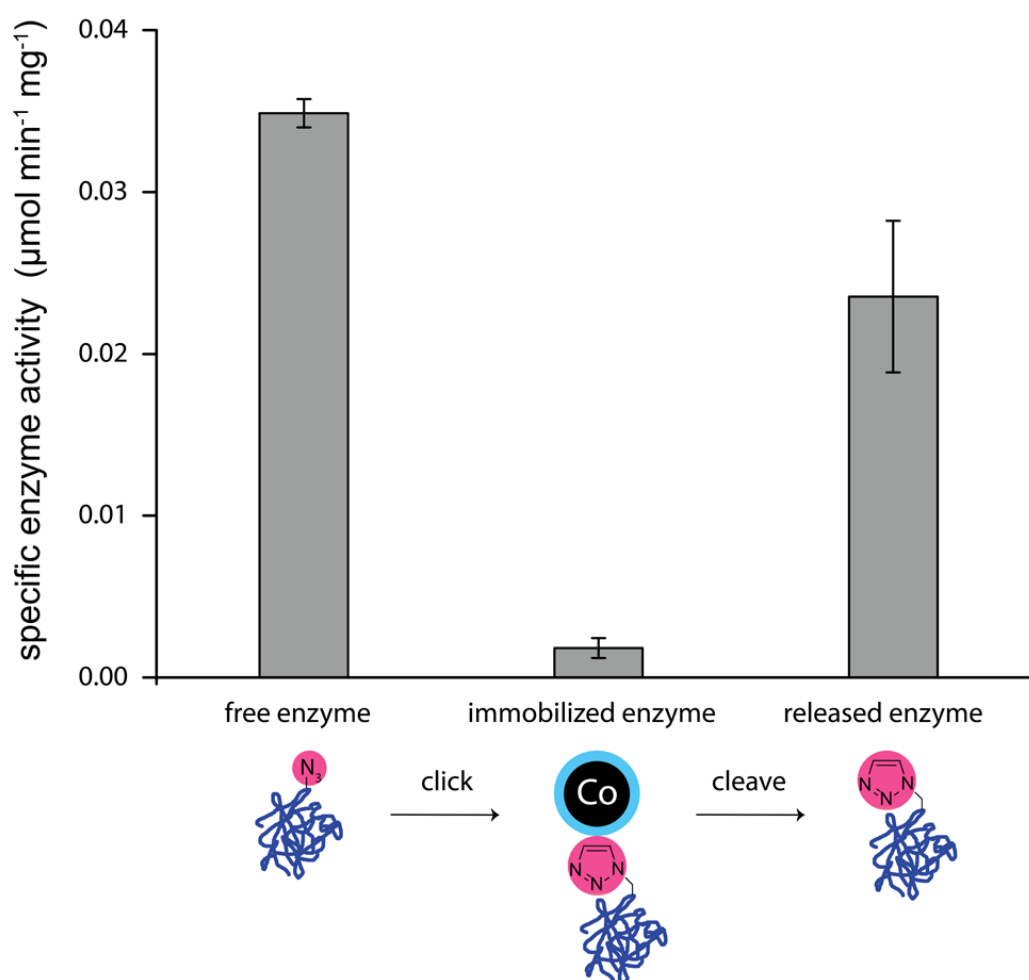
Figure 4-6. *Specific activity of azide-functionalized α-chymotrypsin. Enzymatic assay was performed measuring the formation of nitroaniline with UV spectroscopy at 390 nm, using N-benzoyl-L-tyrosine p-nitroanilide as a substrate. Amount of bound enzyme was determined by elemental analysis.*

investigated, since the aim of this work is to catch and release specific (*i.e.* azide-labelled) compounds. It is crucial that non-labelled proteins do not adhere to the particle surface and that bound proteins can be released effectively. This means that there is no unspecific interaction between the particle and a bound protein. Therefore, rhodamine labelled BSA was dissolved in water (0.5 nmol mL^{-1}) and the absorption at 555 nm was measured at t= 0 h, then after 2, 18, 32 h using naked particles, **2** or **3** (20 mg each, see **Figure 4-5**). While the naked C/Co particles irreversibly adsorbed over 90% of the protein over time, the PEG-functionalized particles **2** and **3** showed much lower unspecific protein adsorption (*i.e.* <5% after 32 h). Since PEG-coating has been known to prevent unspecific protein adsorption, these results are in line with recent literature.[160] To demonstrate applicability in the biological field, the protease enzyme α-chymotrypsin (from bovine pancreas) has been functionalized with an azide group by using a commercially available Azide-PEG4-NHS reagent. The well-studied reaction of NHS-ester with unprotonated, free amine groups of proteins (*e.g.* lysine) proceeded smoothly in basic buffer solution. The activity of the azide-functionalized enzyme was then compared to the immobilized enzyme (*i.e.* bound by click-reaction to the magnetic particle) using a standard enzymatic assay (**Figure 4-6**). As anticipated, the immobilized enzyme exhibited a lower specific activity (*i.e.* <5% of the free enzyme). Compared to other reports of covalent[161, 162] or biospecific[163] immobilization of enzymes on magnetic nanoparticles (15-35%, resp. 106% retained activity) the herein reported retained activity is low. A possible explanation for this drop can be the random orientation of the immobilized enzyme. Also, the covalent linking strategy might negatively influence the enzyme activity.

However, if the clicked enzyme was released by the use of 13 mM BOE, the activity of the released enzyme was substantially increased (*i.e.* to 67%, compared to the free enzyme). It should be noted that the destructive effect of buffered oxide etch on chymotrpysin is marginal (93 ± 3.1% retained activity after 16 h in 13 mM BOE at RT). As mentioned before, the here used dilute F$^-$ solution proved to be harmless to DNA and even RNA.[26, 144-147] Therefore, buffered oxide etch is assumed to be bio-orthogonal and mild, making it a suitable reagent for a wide use in biochemistry. However, there are also limitations to this cleavage system: pH 4 for 16 h can be too harsh for certain proteins, resulting in denaturing. The long time span could be reduced by optimizing the conditions (*e.g.* higher fluoride concentration) if necessary. Furthermore, fluoride can interact with certain metal ions, (*e.g.* calcium, forming CaF_2) forming stable compound and thus deactivating an enzyme by binding the cofactor.

4.4   Conclusion

In summary, a well-dispersed, magnetic and cleavable copper-free click-nano-reagent has been synthesized and characterized. An azide-functionalized dye has been clicked to the magnetic particle and released using 13 mM dilute F⁻ solution. Furthermore, it was shown that also enzymes could be bound and released without a substantial loss of activity, hence proofing the mild nature of the releasing agent. The bioorthogonal approach enables us to work in complex biological systems with many different reactivities.

5   Efficient recycling of polylactic acid nanoparticle templates for the synthesis of hollow silica spheres
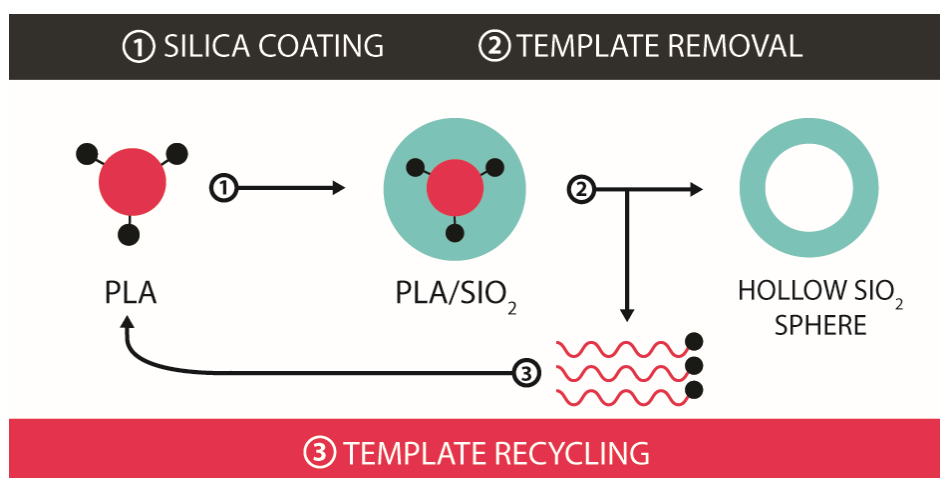
published in parts as:

Elia M. Schneider, Shuto Taniguchi, Yuma Kobayashi, Samuel C. Hess, Ratna Balgis, Takashi Ogi, Kikuo Okuyama, Wendelin J. Stark

Author contribution:
E.M.S., W.J.S. and T.O. elaborated the concept. E.M.S., S.T. and Y.K performed the experiments with support of S.H. E.M.S., R.B., T.O., K. O. and W.J.S. wrote the manuscript with review from all authors.

5.1   Introduction

Hollow nanomaterial research has emerged as a particularly interesting field,[164] motivated by intriguing properties of hollow nanoparticles, such as very low density and high surface area. The large internal void results in a *plethora* of applications, for example electronic capacitors,[165, 166] catalyst supports[167] and drug nanocarriers.[168, 169] Next to hollow particles of carbon[170-174] and zeolite,[175-177] the most prominent material is pure silica, SiO_2. It is immensely popular due to its relatively high chemical inertness, low price, high transparency, high abundance in nature and low toxicity. Two further advantages of silica from a chemist's point of view are the controllable sol-gel synthesis of nanostructures *via* the Stöber[178, 179] or similar processes,[26, 180, 181] and simple chemical functionalization.[46, 182] These properties render silica highly compatible with biological systems. Therefore, silica is generally classified as a safe, bio-compatible material and is a FDA approved additive in many daily-use products (for example nano-silica, E551).[183] Hence, many applications of hollow silica spheres (HSS) and similar structures in biochemistry and pharmaceutical science have been discovered and elucidated, such as gene transfection, *in-vivo* imaging and drug delivery.[184,181, 185, 186] Additionally, many further, non-biochemistry related applications of hollow silica spheres have been explored, such as thermal and electrical insulators,[41] anti-reflection coatings[187-189] and catalyst supports.[190]

Hollow silica spheres are on the verge of being widely used in industry. Therefore, it is expected that in the near future the need of large quantities of hollow silica spheres will rise. Nowadays, the research on the synthesis of hollow silica spheres is quite established on the laboratory scale: the synthesis methods of hollow silica spheres can be divided into two main approaches: soft templating and hard templating.[191] In the soft templating approach, flexible, liquid nano templates (*e.g.* emulsion droplets, vesicles or gas bubbles), formed by surfactants or additives, are used as starting points of the silica formation.[192] In the hard templating method, solid templates, such as polystyrene spheres(PSS),[188] poly(methyl methacrylate) nanoparticles[192] and metal nanoparticles[193] are generally used. An advantage of the method is that the desired size and size distribution of the resulting hollow silica sphere can be controlled by choosing the appropriate size of the hard template.[192] In both approaches, template removal is often done *via* calcination, *i.e.* heating to temperatures above 600 °C.
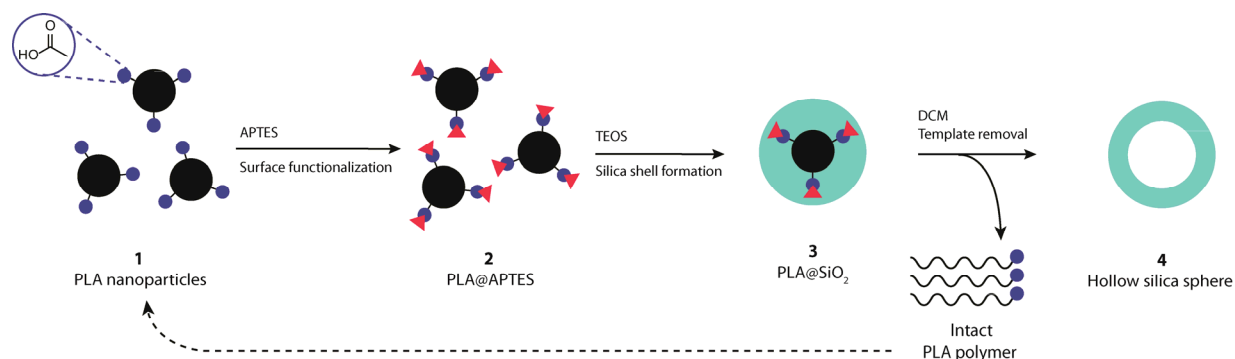
Scheme 5-1. *Illustration of the preparation of hollow silica spheres and subsequent recycling of polylactic acid. The first step includes activation of the carboxylic acid with N-(3-dimethylaminopropyl)-N'-ethylcarbo-diimide hydrochloride (EDC), followed by addition of (3-aminopropyl)triethoxysilane (APTES), resulting in amide bond formation and thus surface functionalization. The second step is a standard base-catalyzed silica formation with TEOS, resulting in a core-shell structure PLA@SiO₂. The third step involves template removal* via *solvent dissolution, yielding hollow silica spheres. The still intact PLA polymers can then be recycled and used as substrate for the PLA nanoparticle synthesis.*

This usually results in irreversible destruction of the template; hence, the method is called "sacrificial template method". Other template removal methods include acid dissolution and solvent extraction. However, in the regard of sustainable chemistry, many of these approaches are not suitable for mass production because they depend heavily on fossil-derived chemicals and demand substantial amounts of energy. In our opinion, the development of a sustainable and cost-effective process for the synthesis of hollow silica spheres should be based on recycling principles, as well as on chemicals which are derived from renewable resources.

Polylactic acid (PLA), a biodegradable polymer synthesized from plant derived products (processed corn or sugar feedstock)[194] has recently attracted a considerable amount of attention, amongst other things because of its use in biodegradable packaging.[195, 196] Thus, many companies have started producing PLA on large scale, resulting in a worldwide production of PLA of about 120000 metric tons in the year 2006.[197, 198] It can be safely assumed that the PLA production has been further increased since making PLA a readily available, relatively inexpensive biodegradable

polymer. The increased attention subsequently led to the development of a variety of PLA nanostructures with applications above all in the field of drug delivery.[199, 200] The synthesis of PLA nanoparticles *via* the nanoprecipitation method[201] proved to be a versatile and scalable process (g to kg scale). The commercial availability of these plant derived nanoparticles as well as the emerging need of large amounts of hollow silica particles persuaded us to investigate the use of PLA nanoparticles as hard template material for a more sustainable synthesis of hollow silica spheres. In contrast to other frequently used templates, such as polystyrene nanoparticles or carbon nanoparticles, PLA nanoparticles can be dissolved in organic solvents such as acetone, dichloromethane (DCM) or chloroform, depending on the racemic mixture and the polymer chain length. Therefore, the PLA nanoparticle template can be removed after silica shell formation and the PLA polymer chains can be recycled *via* solvent evaporation. As mentioned previously, the formation of PLA nanoparticles from PLA polymers can be done *via* nanoprecipitation method and is overall a straightforward synthesis using no surfactants or similar agents.

Herein, we present the first successful (to the best of our knowledge) silica coating of PLA-nanoparticles, resulting in fully coated PLA@SiO$_2$ core-shell nanoparticles (**Scheme 5-1**). Subsequent treatment with solvent at room temperature dissolved the PLA-template and yielded hollow silica spheres. The polymer template material and the solvent could be efficiently recovered from the recycling stream (**Table 5-1**).

Table 5-1. *Comparison of the use of Polystyrene (PSS) and PLA templates for HSS synthesis*

Template	PSS	PLA
Removal method	calcination	solvent dissolution
CO$_2$ emission of removal process (kg CO$_2$ / t HSS)[a]	4829	422
Electricity invested (kJ / g HSS)[b]	3358[41]	1170
Template material recycled (%)	0	85

a. Calculated for the production of 1 t of HSS (see **Table A4-2**) b. Calculated for the production of 1 g of HSS in a laboratory on a small scale (see **Table A4-3**).

5.2 Experimental

The following chemicals were used as received: polylactic acid (PLA, Mw 60000, Sigma Aldrich), polylactic acid nanoparticles (PLA nanoparticles, Mw 17000, 10 mg mL^{-1}, 150 nm, Micromod), (3-aminopropyl)triethoxysilane (APTES, 99%, Sigma-Aldrich), N-(3-dimethylaminopropyl)-N′-ethylcarbo-diimide hydrochloride (EDC, 98%, Sigma-Aldrich), tetraethyl orthosilicate (TEOS, 99.9%, Sigma-Aldrich), 1 M ammonia solution (Kanto Chemical Co. Inc.), dichloromethane (DCM, 99%, Sigma-Aldrich). The ζ-potential and DSL size distribution of the PSL particles were measured using a zetasizer (Zetasizer Nano ZSP, Malvern Instruments Ltd., Malvern, UK). The morphology of the synthesized nanostructures was observed using a field-emission scanning electron microscope (SEM; S-5000, 20 kV, Hitachi High-Tech. Corp., Tokyo, Japan) and transmission electron microscopy (TEM; JEM-2010, 200 kV, JEOL Ltd. Tokyo, Japan). Fourier-transform infrared (FT-IR) spectroscopy was used to investigate the recycling of polylactic acid (Spectrum one, Perkin Elmer Inc., Waltham, MA, USA). The thermal behavior before and after template removal was investigated using thermogravimetric analysis (TG; TGA-50/51 Shimadzu Corp., Kyoto, Japan).

5.2.1 Synthesis of the silica-coated nanoparticles and subsequent template removal

Synthesis of PLA nanoparticles 1

Polylactic acid (60000 Da Mw, D/L mixture, 25 mg, 0.0004 mmol) was dissolved in 2 mL of DCM. 0.1 mL of ethylene glycol was added. 0.7 ml of EtOH and 0.15 ml of H$_2$O were mixed and subsequently added to the polymer solution (inner phase). The resulting dispersion was put into the ultra-sonication bath for 1 min. 5 ml of 70% EtOH were prepared and put into a 20 ml vial equipped with a magnetic stirring bar. Then, the polymer dispersion was added dropwise into the EtOH solution (outer phase) under mild stirring. Stirring was continued in a fume hood for 3 h until the organic solvents had evaporated. The dispersion was then filtered using a paper filter. The resulting dispersion was centrifuged for 10 min at 10000 RPM, the supernatant discarded and the nanoparticles re-dispersed in ultra-pure water *via* ultrasonication. Yield was typically between 40 and 65%. Characterization was done using DLS in order to determine the size of the synthesized nanoparticles.

Synthesis of PLA@APTES **2**

In this experiment, a variation of the Steglich esterification was used. 4 ml ultrapure water was added to a PLA nanoparticle solution (1 ml, 10 mg ml^{-1}) in a 6 ml vial equipped with a magnetic stirrer. Subsequently, EDC was added (10 mg, 0.05 mmol) and the solution stirred at RT for 30 min. Then APTES (250 µl, 1.07 mmol) was added *via* syringe and the dispersion was stirred for 2 h. The dispersion was transferred to an Eppendorf tube and centrifuged (10min, 10000 RPM). The supernatant was removed and 1 ml ultrapure water was added.
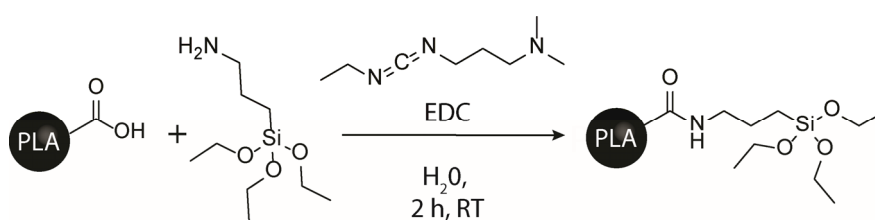
Scheme 5-2. *Surface functionalization* via *modified Steglich esterification. Activation of the carboxylic acid with EDC is followed by amide bond formation with APTES.*

Synthesis of PLA@SiO$_2$ **3**

PLA@APTES **2** solution (10 mg in 5 ml H$_2$O) were diluted with 25 ml H$_2$O in a 50 mL vial and stirred for 10 min (400 RPM). After good dispersion quality was reached (*i.e.* an opaque solution), 1M NH$_3$ (25 µl, 0.025 mmol) was added and the solution stirred for additional 10 min. Subsequently, TEOS (80 µl, 0.35 mmol) was added and silica formation was initiated. The dispersion was stirred for 4 h at room temperature. The silica coated particles were then centrifuged in Eppendorf tubes (1 ml aliquots) for 10 min at 10000 RPM. The supernatant was removed, ultrapure water added (1 ml) and the particles were dispersed using an ultra-sonication bath. Then, the dispersion was centrifuged again in order to wash away residual TEOS and catalyst. After removal of supernatant the particles were dried at RT in a vacuum oven over night.

*Synthesis of hollow silica spheres **4** (template removal)*

Dry PLA@SiO$_2$ **3** particles (1 mg) were dispersed in 1 ml of dichloromethane in a 6 ml vial using an ultra-sonication bath. A magnetic stirrer was added and the dispersion was stirred for 3 h at RT. Subsequently, centrifugation (10 min, 10000 RPM) was used to remove DCM and fresh DCM was added. This was repeated for three times. Finally, the hollow silica spheres were obtained by centrifugation and dried in a vacuum oven at RT. The yield was typically around 65%. Most of the template polymer could be recycled from the DCM template removal solution after DCM evaporation. Alternatively, the DCM/PLA solution could be used to synthesize new PLA nanoparticles.

5.3   Results and discussion

5.3.1   Surface functionalization of PLA nanoparticles

Since a negative surface charge of a nanoparticle can negatively influence the growth of silica on a surface, surface functionalization had to be done. Unfunctionalized PLA nanoparticles did not result in silica core-shell particles (**Figure 5-1**). The surface functionalization of the PLA nanoparticles **1** was done using a modified version of the Steglich esterification.[202, 203] The carboxylic acid end groups of the PLA polymer were activated using a charged and therefore water-soluble carbodiimde, EDC (**Scheme 5-2**).

Table 5-2. *DLS determined nanoparticle size and ζ-potential results for the 4 different species*

Sample	DLS mean size (nm)	ζ-potential (mV)
PLA NPs **1**	250	-8.0
PLA@APTES **2**	335	3.4
PLA@SiO$_2$ **3**	380	-20.5
HSS **4**	355	-24.3

Subsequent addition of the primary amine bearing silane APTES resulted in an amide bond. Surface functionalization was monitored *via* ζ-potential change (**Table 5-2**). The dispersion

stability of APTES-modified PLA nanoparticles PLA@APTES **2** is slightly reduced. It is assumed that the capping of the carboxylic acids and the therefore more positive surface charge led to aggregation. However, the PLA@APTES samples could be stored in the fridge overnight and further processed. Other methods to change the surface charge of the PLA nanoparticles were investigated, such as adsorption of poly-(ethylene imine), polyvinylpyrrolidone and poly(sodium 4-styrenesulfonate). The surface charge of the nanoparticles could be changed, but it was not possible to obtain a highly positive charge (**Table A4-1**). Additionally, silica coating experiments with these species were not successful (**Figure 5-1**).

a) PVP surface modification b) PEI surface modification c) Non-modified PLA

d) No catalyst e) Acetic acid as catalyst
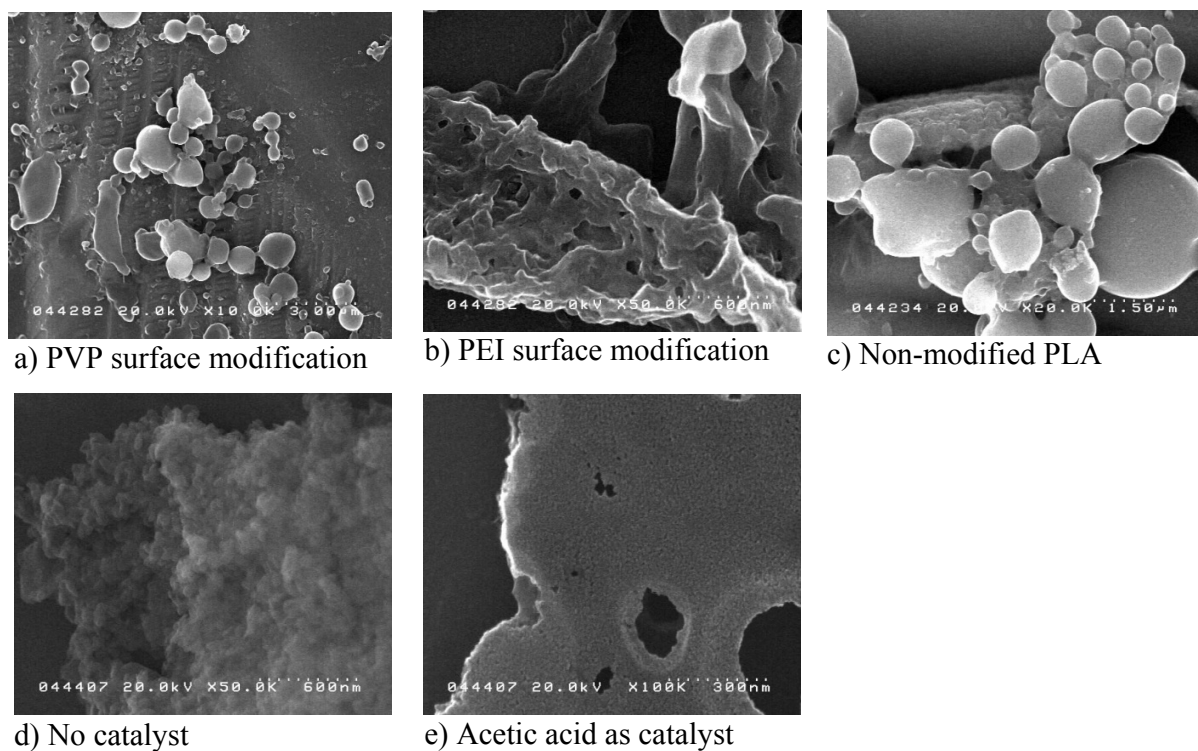
Figure 5-1. *SEM micrographs of unsuccessful attempts to synthesize PLA/silica core shell particles. Reaction conditions: 2 mg PLA@APTES, 16 μl TEOS, 6 ml H_2O, 5 μl catalyst (1 M), 4 h at RT unless otherwise stated.*

5.3.2 Silica shell formation on the modified PLA nanoparticles

In order to obtain silica-coated nanoparticles, it is important to control the reaction kinetics (*i.e.* the rate of hydrolysis). If hydrolysis of TEOS occurs too fast, dense silica particles grow as a result of rapid homogeneous nucleation and subsequent nanoparticle growth. The reaction rate can be controlled by changing the TEOS concentration, amount and nature of the catalyst, reaction temperature and reaction time. The ideal conditions for the synthesis of PLA/silica core-shell particles **3** included a short reaction time (4 h) and room temperature using a low amount of NH$_3$ as a catalyst (**Figure 5-2**). Before arriving at these ideal conditions, the following problems had to be analyzed and solved. In the first attempts, reactions were done at 40 °C, which mostly resulted in either large silica aggregates or small, dense silica nanoparticles.
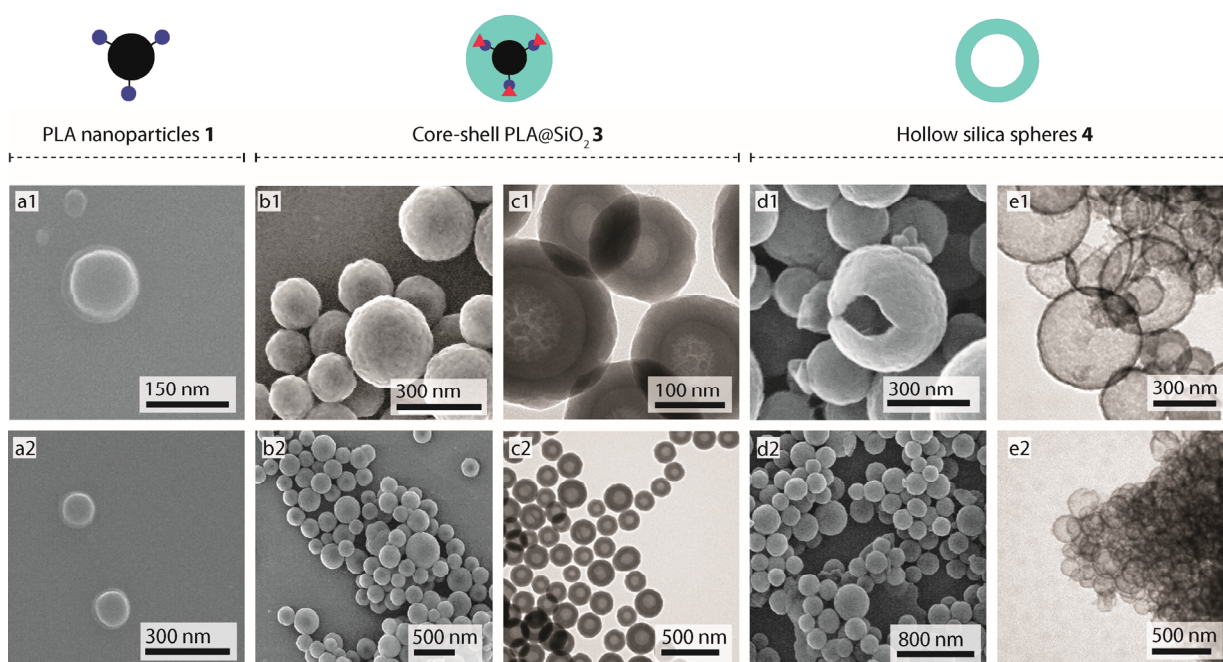
Figure 5-2. Scanning (SEM, a,b,d) and transmission (TEM, c,e) electron microscopy images of the synthesized nanoparticles and hollow spheres with high (1) and low magnification (2). a1 and a2: unfunctionalized PLA template *1*. b1, b2, c1 and c2: PLA@SiO$_2$ *3* synthesized using the standard procedure described in the experimental part. d1, d2, e1 and e2: hollow silica spheres *4*.
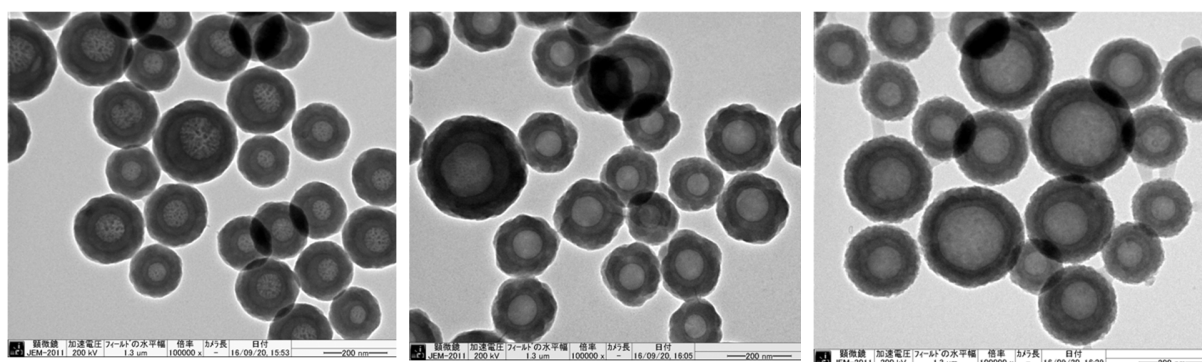
Standard conditions	Catalyst concentration x 5	TEOS concentration x 3

Figure 5-3. *TEM micrographs of PLA@SiO₂* ***3*** *for different concentration of NH₃ catalyst and TEOS.*

Therefore, we switched to RT in order to slow down the rate of hydrolysis. One intrinsic difficulty of this system is that the PLA nanoparticles **1** as well as PLA@APTES **2** exhibit a strong pH-dependent dispersion stability in water. Especially at highly basic pH values, the nanoparticles formed aggregates within hours. Therefore, large amount of basic or acidic catalyst are not favorable in this case. NH₃ and acetic acid were tested as catalysts, as well as a reaction without any catalyst. Notably, only the addition of NH₃ resulted in silica shell formation (**Figure 5-2**), while acetic acid and catalyst free conditions did not result in spherical particles (**Figure 5-1**). The low starting amount of catalyst (*i.e.* 25 µl 1 M NH₃ solution for 10 mg of PLA@APTES) as well as the TEOS concentration proved to be fitting. PLA@SiO₂ **3** core-shell particles were obtained with an average diameter of 189 ± 25 nm (TEM micrograph derived). The size of the particles corresponds to the size (and size distribution) of the PLA nanoparticle template (150 nm). The average shell thickness was determined to be 38 ± 3 nm *via* TEM micrograph analysis. Higher amounts of catalyst as well as higher TEOS concentration increased shell thickness (**Figure 5-3**), indicating a slightly faster reaction rate.[45]

5.3.3 Template removal procedure for the synthesis of hollow silica spheres

In order to obtain hollow silica spheres, the template has to be removed. PLA contains one chiral center per monomer unit and can therefore consist of a number of different compositions and exhibits various conformations (racemic / enantiomerically pure, syndiotactic, isotactic, atactic) which all greatly influence the solubility in different solvents.[204] For example enantiomerically

pure poly-lactic acid polymers have a higher degree of crystallinity and are therefore much more difficult to dissolve. Additionally, the molecular weight is also an important factor for solubility (*i.e.* high Mw polymers are hard to dissolve). In our case, the polylactic acid used was soluble in dichloromethane or chloroform only. Consequently, we investigated different template removal conditions using DCM as a solvent. PLA@SiO$_2$ **3** in DCM at RT overnight resulted in hollow spheres, but mixed with core-shell particles.

Thus, template removal at 40 °C was investigated, but this also resulted in mixed core-shell/hollow sphere material (**Figure A4-1**). Furthermore, a pH 12 mixture with DCM at RT for 18 h was tested, but the resulting spheres were half-broken or destroyed (**Figure A4-1**). The same experiment with pH 1 resulted in hollow spheres, but mixed with small silica aggregates (≈5 nm). If the template removal in pure DCM was elongated to 60 hours, only hollow spheres remained. In order to shorten this long template removal procedure, we investigated an approach which included exchanging the DCM solution after 3 h. If the DCM solution was exchanged twice, hollow silica spheres were
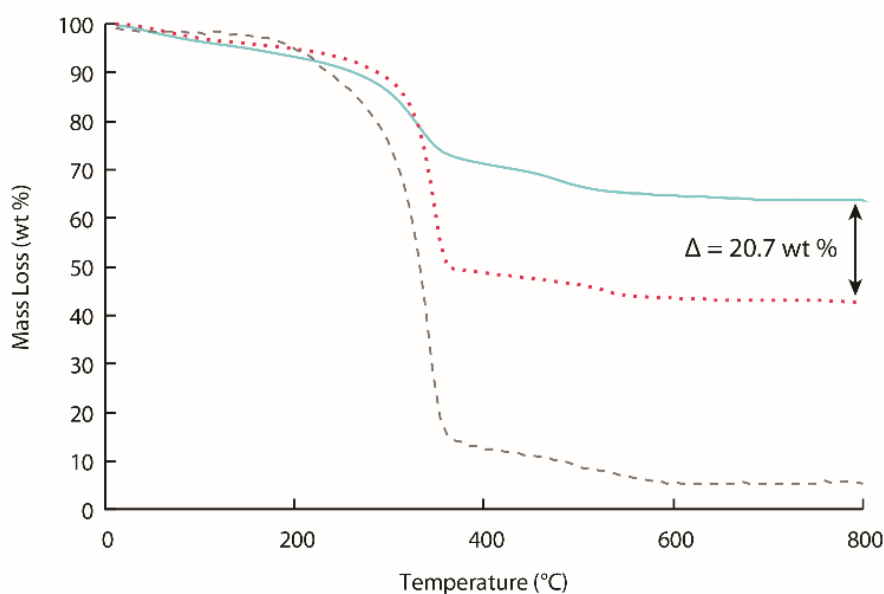
Figure 5-4. *Thermogravimetric analysis of the different nanoparticle samples. Solid cyan line: HSS **4**, dotted magenta line: PLA@SiO$_2$ **3**, dashed grey line: PLA@APTES **2**. The difference between **3** and **4** is the amount of PLA that could be removed* via *solvent dissolution.*
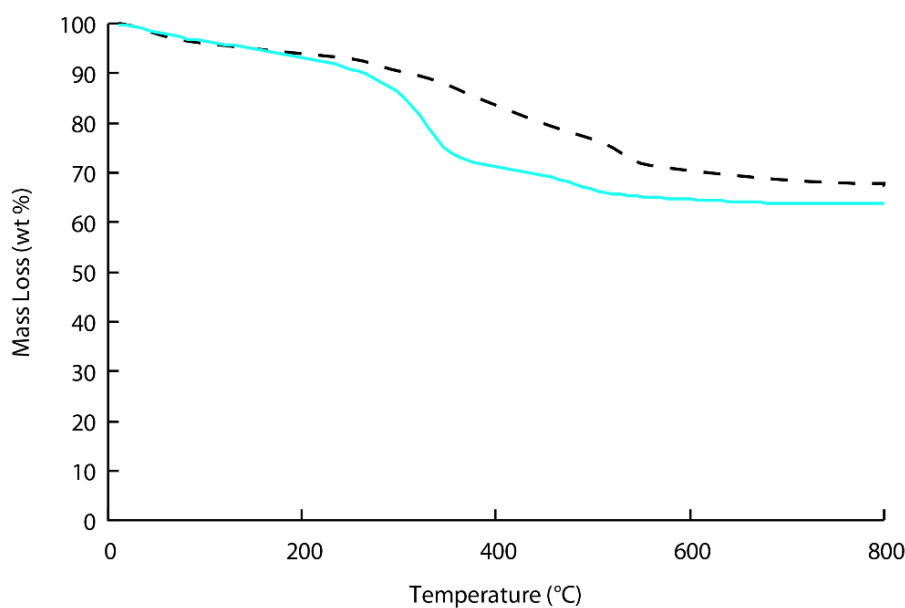
Figure 5-5. *Thermogravimetric analysis of the dense silica particles and HSS **4**. Solid cyan line: HSS **4**, dashed black line: dense SiO$_2$. Dense silica particles were synthesized using the same educts (TEOS), temperatures and catalysts as for the silica coating of PLA nanoparticles.*

obtained after 18 h at room temperature (e1 and e2, **Figure 5-2**). Interestingly, the shell thickness of the HSS (16 ± 1 nm) changed considerably compared to the core-shell nanoparticles (38 ± 3 nm). A possible explanation for this finding is that without the template core the silica shell is less stabilized by a supporting structure and, therefore, shrinks into a more stable, denser structure.

Thermogravimetric analysis of PLA nanoparticles **1** and the core-shell sample PLA@SiO$_2$ **3** were done (**Figure 5-4**). For the PLA@APTES nanoparticle sample, a sharp drop to 5 wt% around 340 °C can be observed. This is in line with literature reports on thermogravimetric analysis of PLA nanocomposites.[205] In the case of PLA@SiO$_2$ **3**, the main drop is in the same temperature range, indicating the burning of PLA. The drop from 100 wt% to 43 wt% is indicating that about 57% of the total mass of PLA@SiO$_2$ **3** is some sort of organic material. Interestingly, also the HSS **4** still contained a certain amount of organic material (36 wt%). First, we assumed that the template removal process was not complete.
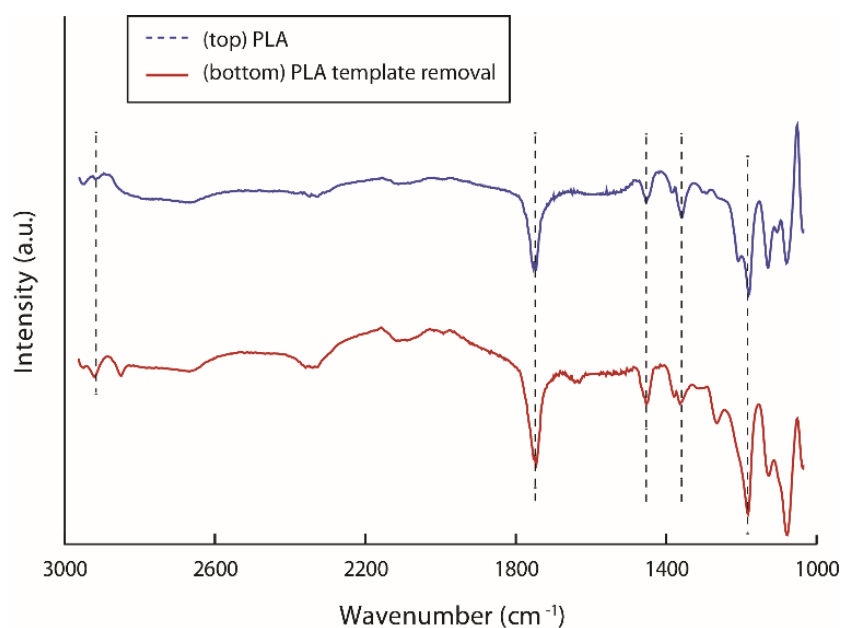
Figure 5-6. *FT-IR spectroscopy of PLA (Mw 60k) and the PLA that was removed* via *DCM solvent extraction. Assignment of the important peaks from left to right (dotted lines): 2912-2947 cm^{-1} CH$_3$ symmetric and asymmetric stretching modes, 1745 cm^{-1} C=O stretching vibration modes, 1452 cm^{-1} & 1357 cm^{-1} asymmetric and symmetric CH$_3$ deformation modes, 1178 cm^{-1} COC stretching vibration modes and CH$_3$ rocking modes.*

However, after synthesizing dense silica particles with the same method and analyzing them with thermogravimetric analysis (**Figure 5-5**), it could be shown that almost all of the residual organic material (33 wt%) came from the silica precursor (*i.e* is not PLA). With these results, a recovery efficiency of 85% of PLA was calculated.

It should be noted that, compared to the most common template removal process (calcination), this process does not involve high temperatures and, thus, no sintering or agglomeration (necking) of HSS occurs. This greatly simplifies further processing (*i.e*. mostly for dispersions in polymers). Furthermore, since calcination is not necessary, there are no heat-related CO_2 emissions in the template removal process (**Table 5-1**).
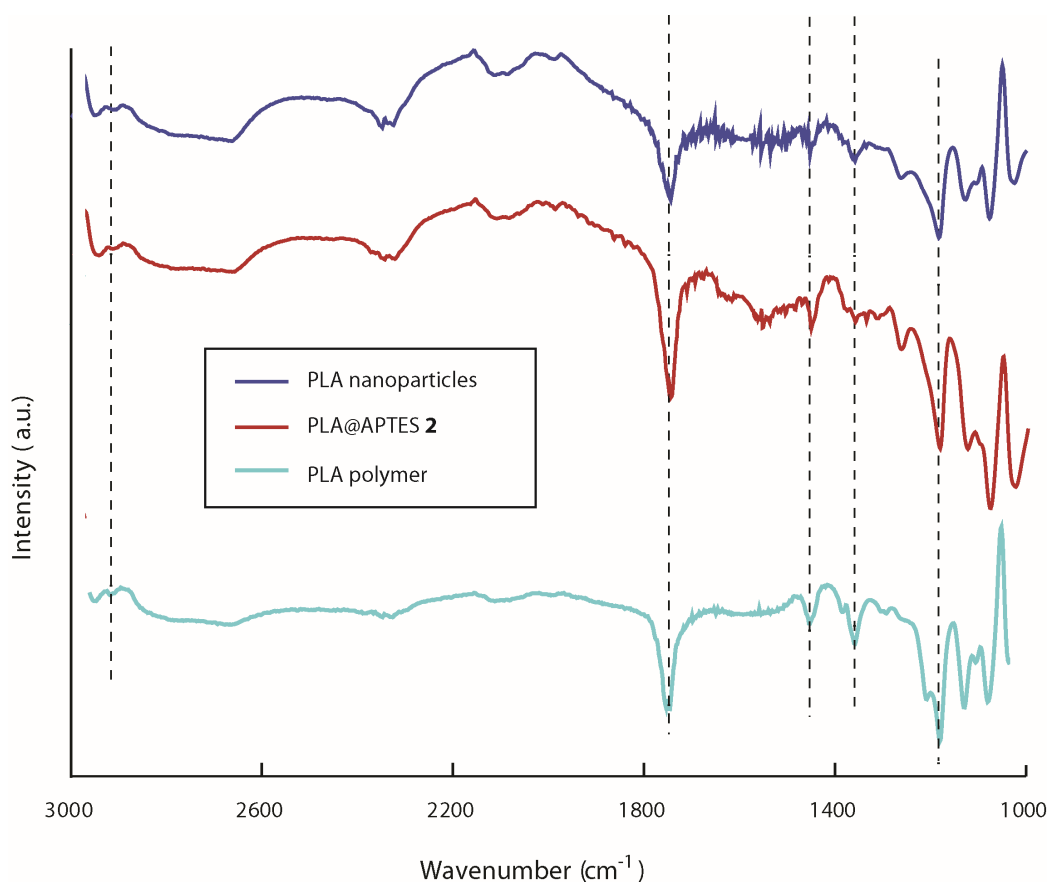
Figure 5-7*. Fourier transform infrared spectroscopy of PLA nanoparticles **1**, PLA@APTES **2** and PLA polymer. The functionalization of PLA nanoparticles with APTES cannot be detected, indicating a low amount of surface functionalization.*

5.3.4 PLA polymer template recycling

After template removal and solvent evaporation, the integrity of PLA polymer was tested with FT-IR (**Figure 5-6**). Compared to the starting material (PLA polymer Mw 60000), the material from the dissolved template exhibits mainly the same peaks. Notable are the peaks at 1745 cm^{-1} (C=O stretching vibration modes), 1452 cm^{-1} (asymmetric CH$_3$ deformation modes) and 1178 cm^{-1} (COC stretching vibration modes and CH$_3$ rocking modes).[206] Therefore, it was assumed that the PLA polymer was not destroyed in the dissolving process. It should be noted that the dissolving process also takes places at RT in order to avoid polymer degradation. The recycled PLA chains were then used to re-synthesize PLA nanoparticles, resulting in nanoparticles of similar size (DLS size = 285 nm, compared to starting PLA nanoparticles DLS size = 250 nm,

Figure A4-2). An advantage of this method is that the template removal solution can be directly used to synthesize the PLA nanoparticles again, since the nanoprecipitation process starts with dissolving PLA polymer in DCM. This is a favorable feature from both an economic and ecologic point of view, since no distillation, separation or drying steps are required. This reduces the amount of solvent needed and also minimizes the necessary process steps.

Since we covalently functionalized the template with APTES, one might have expected differently sized nanoparticles. However, the obtained nanoparticles were similar to the nanoparticles synthesized with unfunctionalized PLA (FT-IR, **Figure 5-7**). It should be noted that this kind of surface functionalization only functionalizes a very small partition of all the PLA polymers. The direct use of APTES-functionalized PLA chains for nanoparticle formation (in order to avoid the surface modification step) is part of ongoing research.

5.4   Conclusion

A novel, more sustainable process for the synthesis of hollow silica spheres has been developed. The process involved surface functionalization of polylactic acid nanoparticles with (3-amino-propyl)-triethoxysilane, in order to change the surface charge of the particles and to provide silica nucleation seeds. Subsequent silica coating of the template was done using tetraethyl orthosilicate and NH_3 as a catalyst. Homogeneous coated core-shell particles were obtained after 4 hours with a mean shell thickness of 38 ± 3 nm. Variation of catalyst amount and silica source concentration reliably afforded hollow spheres with a different shell thickness. Template removal procedure was done overnight *via* dissolution of the polymer nanoparticle-core with solvent. Thus, hollow silica spheres were obtained. The resulting solution containing removed polylactic acid template was analyzed and it could be shown that the template material was still intact and that it was possible to regenerate PLA nanoparticles with similar size to the starting material.

6   General conclusions and outlook

6.1   Conclusions

This work presents different approaches towards the goal of a more sustainable chemical industry using organic-inorganic hybrid functional materials. Although the term *sustainable* is difficult to define thoroughly from the perspective of chemistry, with the green technology factors in mind, we can identify the problems that need to be tackled in chemical industry.

Separation is definitely one of them, and has a vast optimization potential. A lot of research in sustainable process engineering is pointing towards membranes, but in the present case, the problem was tackled using a magnetic, inorganic nano-support functionalized with an organic base-catalyst. Using this reagent, solvent and time could be saved during catalysis. Additionally, the isolated yield was higher compared to the homogeneous catalysis, because column chromatography could be avoided. However, in order to apply this approach in a real industrial process, more applied knowledge in the handling of magnetic nanoparticles on larger scales has to be obtained.

Magnetic separation in biological systems can also increase the efficiency and sustainability of synthesis, especially since small formulation and low yields are common. In this work, the separation and release of the active enzyme also showed that mild cleavage methods, that do not destroy the tertiary structure of biomolecules, are possible and can be applied by bio-chemists without much training. Buffered oxide etch, essentially diluted and buffered hydrogen fluoride, can be handled without great precautions, in contrary to concentrated hydrofluoric acid. An argument against this separation method is that it has to be reactivated before reuse, which can be difficult for people without organic synthesis training.

Also, less complicated materials can be used to enhance the sustainability of chemical processes by optimizing the separation step. This was done by using a simple and inexpensive catalyst, namely bulk copper powder. After successful catalysis, the micro-sized catalyst could be filtered off, using commercially available filters. However, to remove leached copper-ion species, aluminum oxide had to be used in order to obtain pure isolated product.

Aside from separation, the sustainability of a whole process also depends on the rational use of raw materials. Therefore, a process based on recycling principles has been developed for the synthesis of hollow silica spheres. By using polylactic acid, a bio-derived polymer, as a template, an additional green technology factor could be implanted, namely the use of green basic chemicals.

6.2   Outlook

The implementation of green technology concepts into industry is an important and ongoing process. Yet, there are many problems that have to be overcome before the chemical industry in the whole world will depend solely on green processes. However, sooner or later this is bound to happen, since non-renewable resources will become scarce and thus quite expensive. It is imperative that, at that point in future, the sustainable technologies as well as the infrastructure should already be developed.

Therefore, research exploring more sustainable separation methods is growing massively. These efforts will eventually create sustainable solutions that will also make sense from an economical perspective, for as long as we are operating in a free market, economic factors will always be essential. Nevertheless, elaborate magnetic separation has a good perspective in this viewpoint since it also decreases the overall process cost by reducing synthesis time substantially. The main obstacles will be the missing infrastructure and experience in handling magnetic reagents. However, this is a problem of many new technologies and can be overcome if an effort is made. The same is true when new, more sustainable processes, such as the recycling of PLA for hollow silica productions, are entering the market. An important task of scientists in this field is to make the research accessible and applicable in order to facilitate the translation from pure university knowledge to industrial application.

Appendix

A.1   Supplementary data for chapter 2
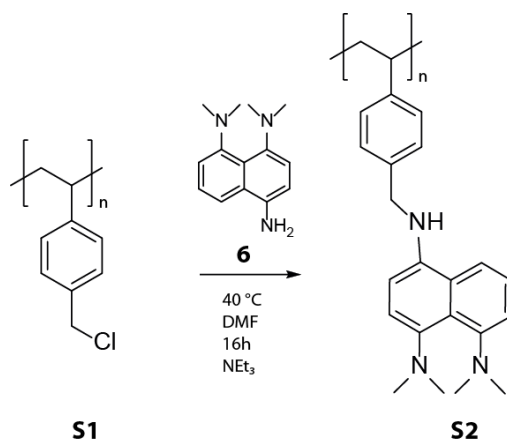
Scheme A1-1. *Preparation of PS@DMAN **S2** starting from commercially available Merrifield-Resin **S1**.*
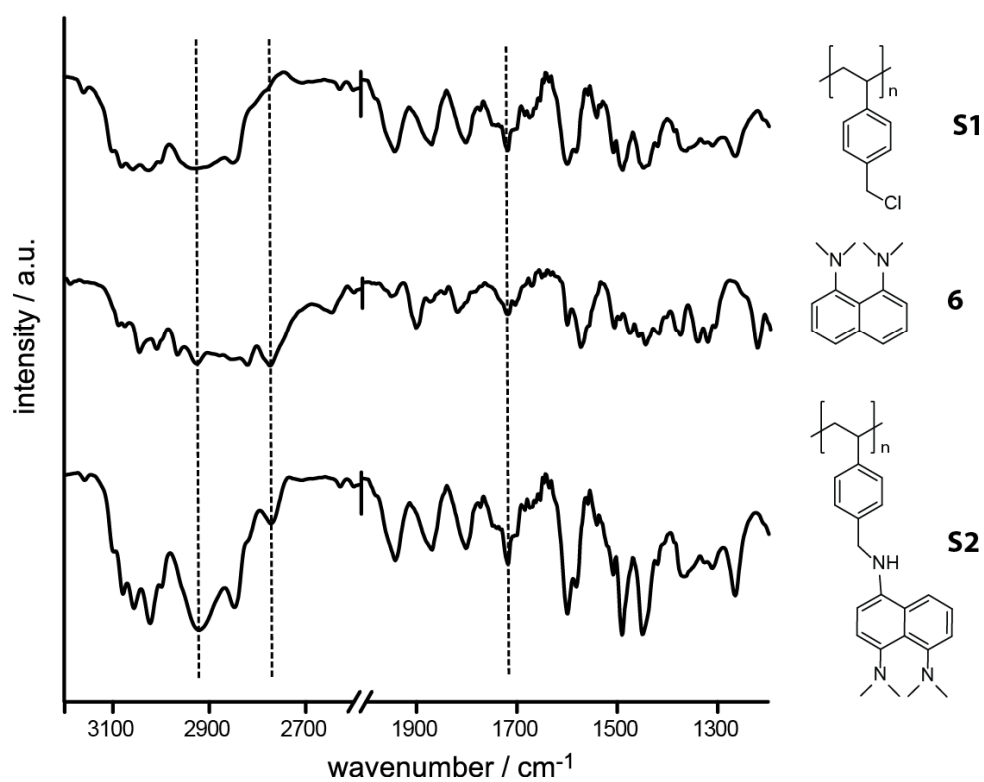
Figure A1-1. *IR Spectra of polystyrene-bound DMAN **S2**.*

A.2   Supplementary data for chapter 3
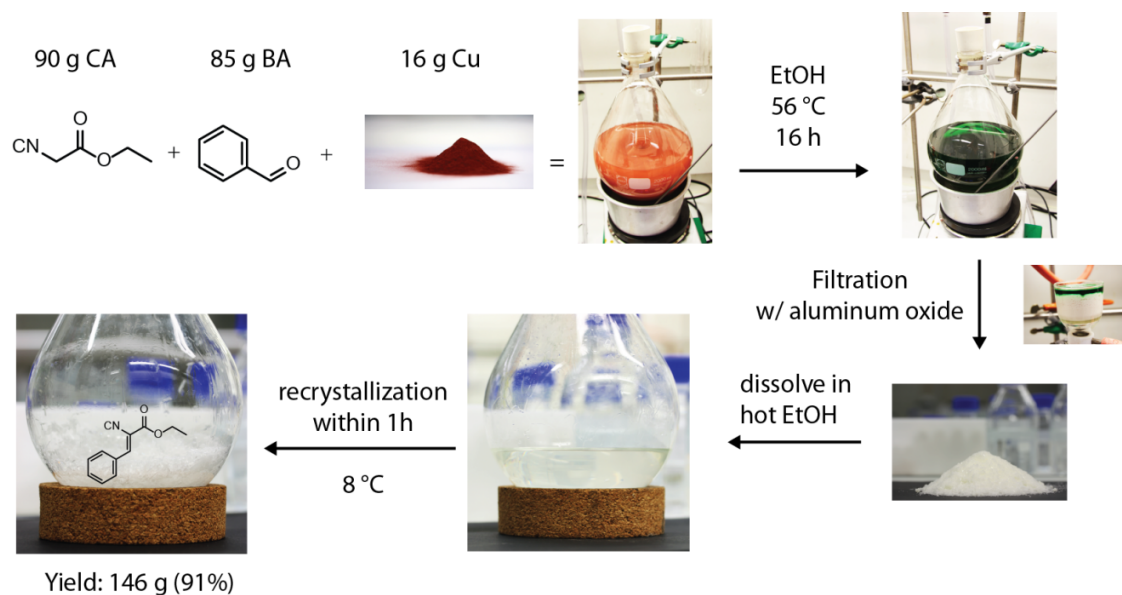
Figure A2-1. Scale up experiment: Knoevenagel condensation of benzaldehyde (81.2 mL, 0.8 mol) and ethyl cyanoacetate (84.8 mL, 0.8 mol) in 1000 mL EtOH with 16 g copper catalyst. Yield after recrystallization: 146 g (91 %).
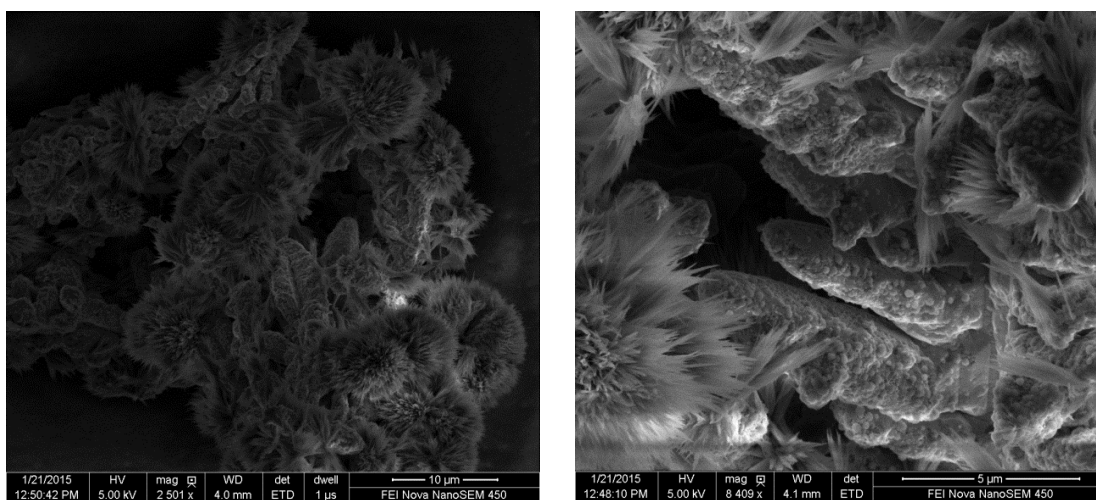
Figure A2-2. Cu(0) powder after catalysis in cold ethanol: product crystal formation visible on copper surface.
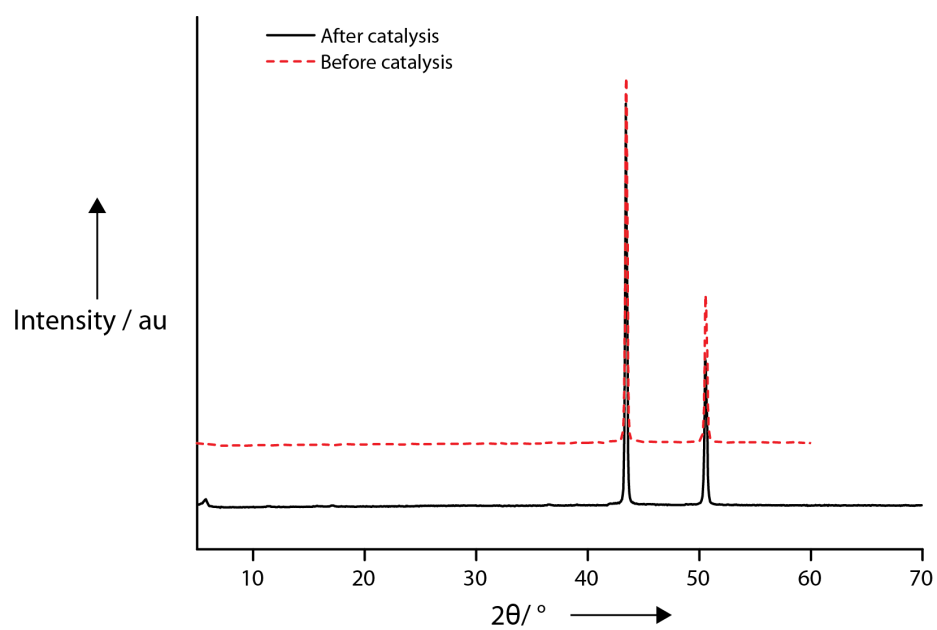
Figure A2-3. XRD measurement of the Cu powder used in the scale up experiment before (red, dashed line) and after (black, solid line) catalysis.

A.3   Supplementary data for chapter 4
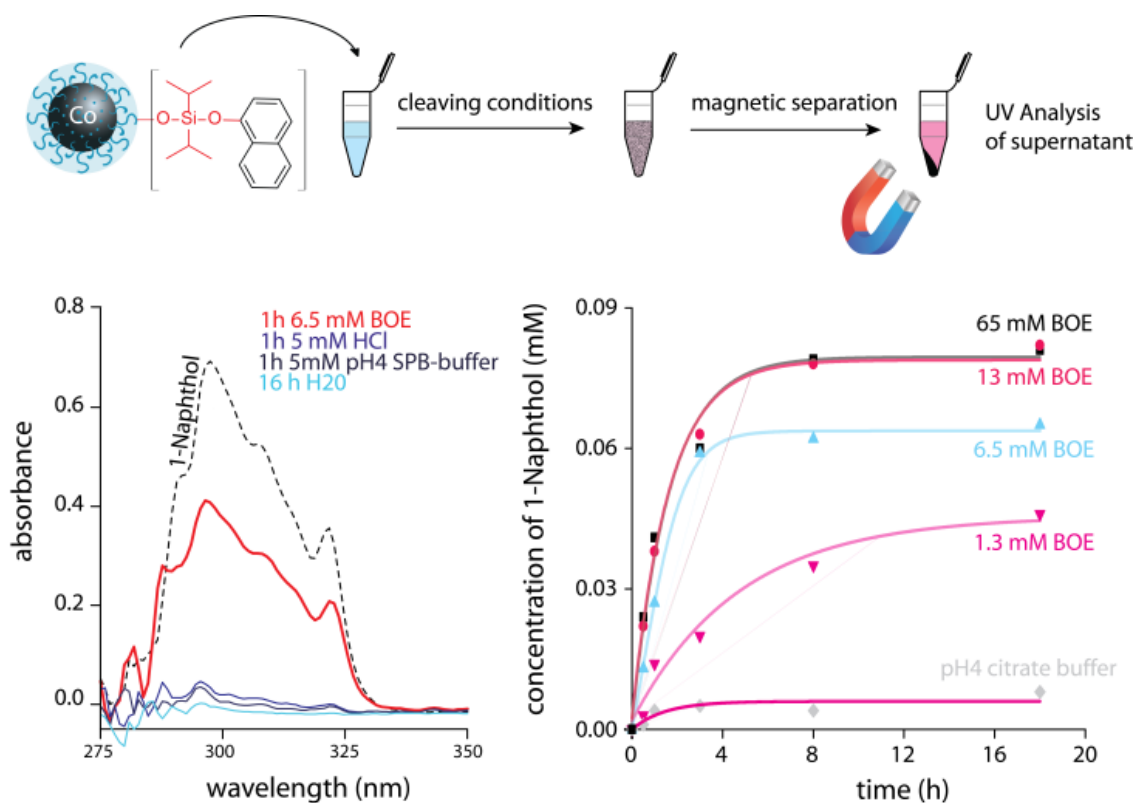
Figure A3-1. *Deprotection analysis using different buffers and concentrations of buffered oxide etch. Conditions: 1 mL of solvent (buffer, water or BOE) and 10-20 mg of 1-naphthol functionalized magnetic particles.*
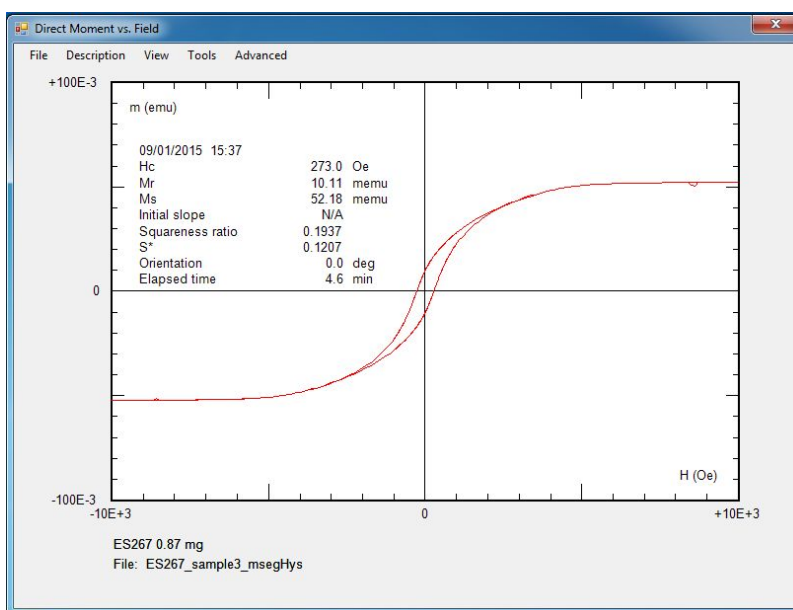
Figure A3-2. *VSM measurement of C/Co@PEGMA-Si-Octyne 3*.
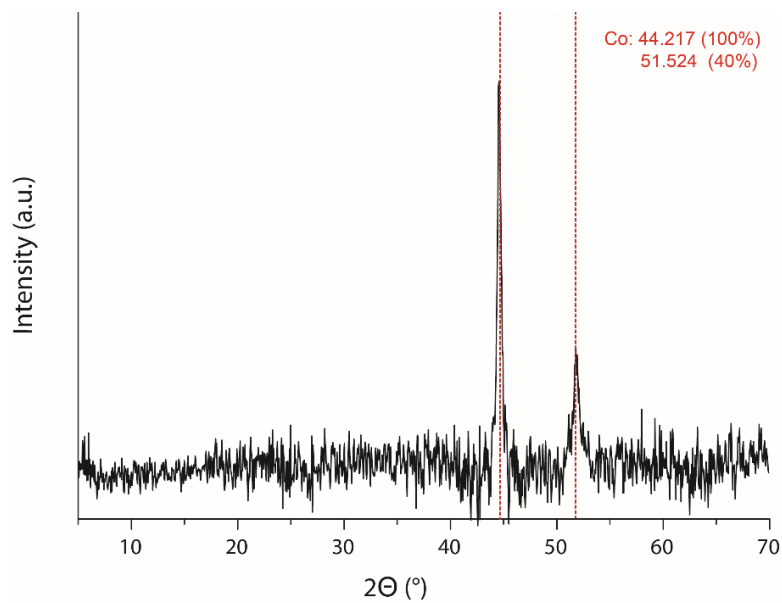
Figure A3-3. XRD measurement of C/Co@PEGMA-Si-Octyne **3**.

A.4   Supplementary data for chapter 5

a) DCM 18 h with 2 times exchange of solvent

b) NH$_3$ 5 h followed by 18 h DCM

c) DCM : pH 12 H$_2$O 1 :1 for 18 h

d) DCM : pH 1 H$_2$O 1 :1 for 18 h

e) 60 h DCM

f. DCM at 40 °C 18 h
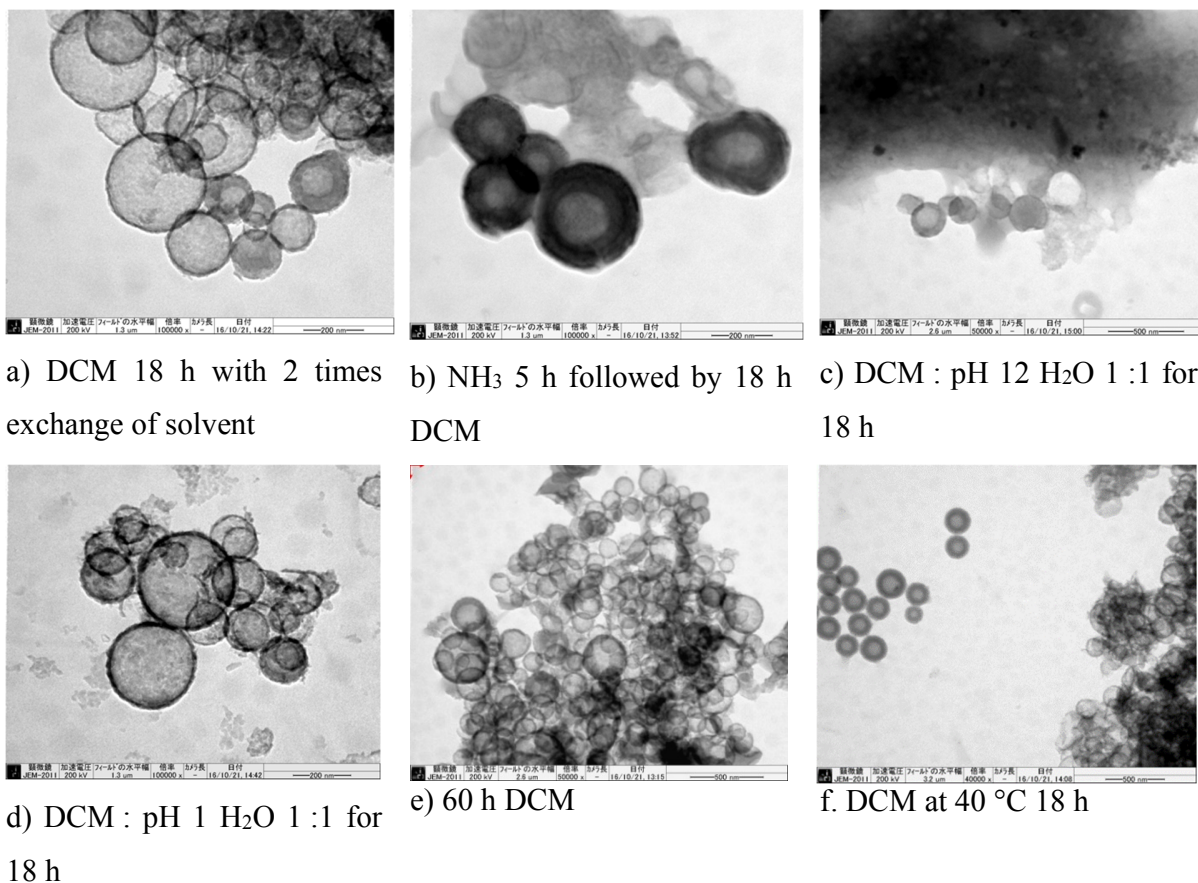
Figure A4-1. *TEM micrographs of hollow silica spheres after different template removal conditions.*

Table A4-1. *Zeta-potential of PLA nanoparticles after adsorption of different polymers (40 mg / g, 2 h stirring, in 0.15 M NaCl)*

Nanoparticle	Surface modification agent	ζ-potential (mV)
PLA NPs **1**	Polyvinylpyrrolidone Mw 360k	-0.55
PLA NPs **1**	Poly(ethyleneimine) Mw 60k linear	0.96
PLA NPs **1**	Poly(ethyleneimine) Mw 60k branched	1.41
PLA NPs **1**	Poly(sodium 4-styrenesulfonate) Mw 1000k	-16.6

Table A4-2. *Comparison of the CO_2 emission in the template removal process for PSS and PLA hard template synthesis of 1 t of HSS*

Process	PSS	PLA
CO_2 (kg)	4829	422[a]
Moles of CO_2 (mol)	109733	9583
Moles of C (mol)	109733	9583
Amount of C (kg)	1318	115
Carbon percentage (%)	92	50
Percentage that gets burned to CO_2 (%)	100	15
Amount of template necessary (kg)	1429	1538
Yield of reaction	70	65

a.) Conservative assumption that all of the lost PLA (*i.e.* not recycled, 15%) will eventually be converted to CO_2.

Table A4-3. *Comparison of the invested electricity for PSS and PLA hard template synthesis of 1 g HSS*

Process step	PSS (kWh)[a]	PLA (kWh)[b]	PSS (h)	PLA (h)
Nanoparticle synthesis	0.285	0.006	1	1
Surface modification	0	0.012	0	2
Synthesis	0.018	0.024	3	4
Template removal	0.58	0.108	2	18
Centrifugation[c]	0.05	0.175		
Total process	0.933	0.325		

a.) PSS process values were taken from literature.[41]   b.) The values are only approximately accurate and based on the aforementioned literature values.   c.) Centrifugation process is the sum of all centrifugations needed for the total process
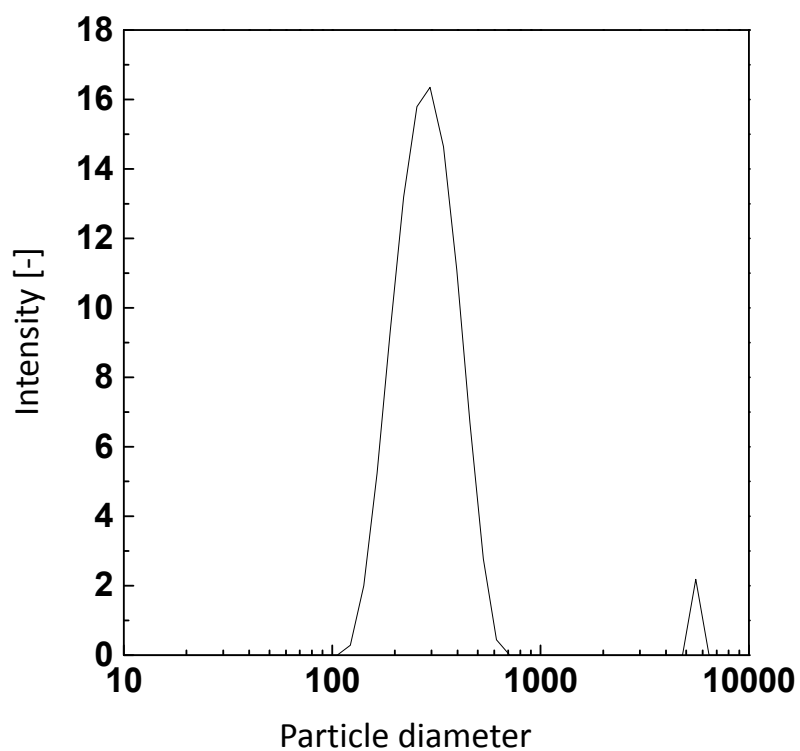
Figure A4-2. *DLS measurement of the regenerated PLA nanoparticles. These particles exhibited similar aggregation behavior and the dispersion had a similar size distribution as the starting PLA nanoparticles. Peak is at 285 nm.*

References

1. Koltuniewicz, A. B., *Sustainable Process Engineering: Prospects and Opportunities*. De Gruyter: **2014**.

2. Livi-Bacci, M., *A Concise History of World Population*. Wiley: **2012**.

3. Unesco, *Knowledge for sustainable development: an insight into the encyclopedia of life support systems*. EOLSS Publishers/UNESCO: **2002**.

4. Umwelt, E. K. G., *Industrial Pollution, European Solutions: Clean Technologies: LIFE and the Directive on Integrated Pollution Prevention and Control (IPPC Directive)*. Office for Official Publ. of the Europ. Communities: **2004**.

5. Gallucci, F.; van Sint Annaland, M., *Process Intensification for Sustainable Energy Conversion*. Wiley: **2015**.

6. Sanders, D. F.; Smith, Z. P.; Guo, R.; Robeson, L. M.; McGrath, J. E.; Paul, D. R.; Freeman, B. D., Energy-efficient polymeric gas separation membranes for a sustainable future: A review. *Polymer* **2013,** *54* (18), 4729-4761.

7. Hess, S. C.; Grass, R. N.; Stark, W. J., MOF Channels within Porous Polymer Film: Flexible, Self-Supporting ZIF-8 Poly(ether sulfone) Composite Membrane. *Chem. Mater.* **2016,** *28* (21), 7638-7644.

8. Centi, G.; Perathoner, S., Methods and Tools of Sustainable Industrial Chemistry: Catalysis. In *Sustainable Industrial Chemistry*, Wiley-VCH Verlag GmbH & Co. KGaA: **2009**; pp 73-198.

9. Astruc, D.; Lu, F.; Aranzaes, J. R., Nanoparticles as Recyclable Catalysts: The Frontier between Homogeneous and Heterogeneous Catalysis. *Angew. Chem. Int. Ed.* **2005,** *44* (48), 7852-7872.

10. Ruiz-hitzky, E., Genie Cristallin Dans Les Solides Organo-Mineraux. *Mol. Cryst. Liq. Cryst. Inc. Nonlinear Opt.* **1988,** *161* (1), 433-452.

11. Ruiz-Hitzky, E.; Aranda, P.; Darder, M.; Ogawa, M., Hybrid and biohybrid silicate based materials: molecular vs. block-assembling bottom-up processes. *Chem. Soc. Rev.* **2011,** *40* (2), 801-828.

12. Laberty-Robert, C.; Valle, K.; Pereira, F.; Sanchez, C., Design and properties of functional hybrid organic-inorganic membranes for fuel cells. *Chem. Soc. Rev.* **2011,** *40* (2), 961-1005.

13. Lebeau, B.; Innocenzi, P., Hybrid materials for optics and photonics. *Chem. Soc. Rev.* **2011,** *40* (2), 886-906.

14. Sanchez, C.; Belleville, P.; Popall, M.; Nicole, L., Applications of advanced hybrid organic-inorganic nanomaterials: from laboratory to market. *Chem. Soc. Rev.* **2011,** *40* (2), 696-753.

15. Judeinstein, P.; Sanchez, C., Hybrid organic-inorganic materials: a land of multidisciplinarity. *J. Mater. Chem.* **1996,** *6* (4), 511-525.

16. Quinkert, G.; Egert, E.; Griesinger, C., *Aspects of Organic Chemistry: Structure*. Verlag Helvetica Chimica Acta: **1996**.

17. Bettelheim, F. A.; Brown, W. H.; Campbell, M. K.; Farrell, S. O., *Introduction to General, Organic and Biochemistry*. Cengage Learning: **2009**.

18. Gomez-Romero, P., Hybrid Organic–Inorganic Materials—In Search of Synergic Activity. *Adv. Mater.* **2001,** *13* (3), 163-174.

19. Gomez-Romero, P.; Sanchez, C., *Functional Hybrid Materials*. Wiley: **2006**.

20. Livage, J.; Henry, M.; Sanchez, C., Sol-gel chemistry of transition metal oxides. *Prog. Solid State Ch.* **1988,** *18* (4), 259-341.

21. Georgakilas, V.; Otyepka, M.; Bourlinos, A. B.; Chandra, V.; Kim, N.; Kemp, K. C.; Hobza, P.; Zboril, R.; Kim, K. S., Functionalization of Graphene: Covalent and Non-Covalent Approaches, Derivatives and Applications. *Chem. Rev.* **2012,** *112* (11), 6156-6214.

22. Koehler, F. M.; Luechinger, N. A.; Ziegler, D.; Athanassiou, E. K.; Grass, R. N.; Rossi, A.; Hierold, C.; Stemmer, A.; Stark, W. J., Permanent Pattern-Resolved Adjustment of the Surface Potential of Graphene-Like Carbon through Chemical Functionalization. *Angew. Chem. Int. Edit.* **2009,** *48* (1), 224-227.

23. Matyjaszewski, K.; Dong, H.; Jakubowski, W.; Pietrasik, J.; Kusumo, A., Grafting from surfaces for "Everyone": ARGET ATRP in the presence of air. *Langmuir* **2007,** *23* (8), 4528-4531.

24. Wang, J.-S.; Matyjaszewski, K., Controlled/"living" radical polymerization. atom transfer radical polymerization in the presence of transition-metal complexes. *J. Am. Chem. Soc.* **1995,** *117* (20), 5614-5615.

25. Zeltner, M.; Grass, R. N.; Schaetz, A.; Bubenhofer, S. B.; Luechinger, N. A.; Stark, W. J., Stable dispersions of ferromagnetic carbon-coated metal nanoparticles: preparation via surface initiated atom transfer radical polymerization. *J. Mater. Chem.* **2012,** *22* (24), 12064-12071.

26. Paunescu, D.; Puddu, M.; Soellner, J. O. B.; Stoessel, P. R.; Grass, R. N., Reversible DNA encapsulation in silica to produce ROS-resistant and heat-resistant synthetic DNA 'fossils'. *Nat. Protocols* **2013,** *8* (12), 2440-2448.

27. Rahman, I. A.; Padavettan, V., Synthesis of silica nanoparticles by sol-gel: size-dependent properties, surface modification, and applications in silica-polymer nanocomposites; a review. *J. Nanomaterials* **2012,** *2012*, 8-8.

28. Jal, P. K.; Patel, S.; Mishra, B. K., Chemical modification of silica surface by immobilization of functional groups for extractive concentration of metal ions. *Talanta* **2004,** *62* (5), 1005-1028.

29. Sandoval, J. E.; Pesek, J. J., Synthesis and characterization of a hydride-modified porous silica material as an intermediate in the preparation of chemically bonded chromatographic stationary phases. *Anal. Chem.* **1989,** *61* (18), 2067-2075.

30. Schmidt, H.; Seiferling, B., Chemistry And Applications Of Inorganic-Organic Polymers (Organically Modified Silicates). *MRS Proc.* **1986,** *73*.

31. McDaniel, M. P., Surface halides of silica. 1. Chloride. *J. Phys. Chem.-US.* **1981,** *85* (5), 532-537.

32. Vericat, C.; Vela, M. E.; Benitez, G.; Carro, P.; Salvarezza, R. C., Self-assembled monolayers of thiols and dithiols on gold: new challenges for a well-known system. *Chem. Soc. Rev.* **2010,** *39* (5), 1805-1834.

33. Hakkinen, H., The gold-sulfur interface at the nanoscale. *Nat. Chem.* **2012,** *4* (6), 443-455.

34. Neouze, M.-A.; Schubert, U., Surface Modification and Functionalization of Metal and Metal Oxide Nanoparticles by Organic Ligands. *Monatsh. Chem.* **2008,** *139* (3), 183-195.

35. Sperling, R. A.; Parak, W. J., Surface modification, functionalization and bioconjugation of colloidal inorganic nanoparticles. *Philos. T. Roy. Soc. A* **2010,** *368* (1915), 1333-1383.

36. Zareie, H. M.; Boyer, C.; Bulmus, V.; Nateghi, E.; Davis, T. P., Temperature-Responsive Self-Assembled Monolayers of Oligo(ethylene glycol): Control of Biomolecular Recognition. *ACS Nano* **2008,** *2* (4), 757-765.

37. Smith, G. V.; Notheisz, F., *Heterogeneous Catalysis in Organic Chemistry*. Elsevier Science: **1999**.

38. Amatore, C.; Jutand, A., Anionic Pd(0) and Pd(II) Intermediates in Palladium-Catalyzed Heck and Cross-Coupling Reactions. *Accounts Chem. Res.* **2000,** *33* (5), 314-321.

39. Miyaura, N.; Suzuki, A., Palladium-Catalyzed Cross-Coupling Reactions of Organoboron Compounds. *Chem. Rev.* **1995,** *95* (7), 2457-2483.

40. Brinker, C. J.; Scherer, G. W., *Sol-Gel Science: The Physics and Chemistry of Sol-Gel Processing*. Elsevier Science: **2013**.

41. Gao, T.; Jelle, B. P.; Sandberg, L. I. C.; Gustavsen, A., Monodisperse Hollow Silica Nanospheres for Nano Insulation Materials: Synthesis, Characterization, and Life Cycle Assessment. *ACS Appl. Mater. Interfaces* **2013,** *5* (3), 761-767.

42. Huo, Q.; Feng, J.; Schüth, F.; Stucky, G. D., Preparation of Hard Mesoporous Silica Spheres. *Chem. Mater.* **1997,** *9* (1), 14-17.

43. Lu, B.; An, S.; Song, D.; Su, F.; Yang, X.; Guo, Y., Design of organosulfonic acid functionalized organosilica hollow nanospheres for efficient conversion of furfural alcohol to ethyl levulinate. *Green Chem.* **2015,** *17* (3), 1767-1778.

44. Morikawa, A.; Iyoku, Y.; Kakimoto, M.-A.; Imai, Y., Feature article. Preparation of new polyimide-silica hybrid materials via the sol-gel process. *J. Mater. Chem.* **1992,** *2* (7), 679-689.

45. Nandiyanto, A. B. D.; Akane, Y.; Ogi, T.; Okuyama, K., Mesopore-Free Hollow Silica Particles with Controllable Diameter and Shell Thickness via Additive-Free Synthesis. *Langmuir* **2012,** *28* (23), 8616-8624.

46. Paunescu, D.; Fuhrer, R.; Grass, R. N., Protection and Deprotection of DNA—High-Temperature Stability of Nucleic Acid Barcodes for Polymer Labeling. *Angew. Chem. Int. Edit.* **2013,** *52* (15), 4269-4272.

47. Monge-Marcet, A.; Pleixats, R.; Cattoën, X.; Wong Chi Man, M., Sol–gel immobilized Hoveyda–Grubbs complex through the NHC ligand: A recyclable metathesis catalyst. *J. Mol. Catal. A-Chem* **2012,** *357*, 59-66.

48. Giakisikli, G.; Anthemidis, A. N., Magnetic materials as sorbents for metal/metalloid preconcentration and/or separation. A review. *Anal. Chim. Acta* **2013,** *789*, 1-16.

49. Wittmann, S.; Schätz, A.; Grass, R. N.; Stark, W. J.; Reiser, O., A Recyclable Nanoparticle-Supported Palladium Catalyst for the Hydroxycarbonylation of Aryl Halides in Water. *Angew. Chem. Int. Ed.* **2010,** *49* (10), 1867-1870.

50. Schneider, E. M.; Raso, R. A.; Hofer, C. J.; Zeltner, M.; Stettler, R. D.; Hess, S. C.; Grass, R. N.; Stark, W. J., Magnetic Superbasic Proton Sponges Are Readily Removed and Permit Direct Product Isolation. *J. Org. Chem.* **2014,** *79* (22), 10908-10915.

51. Lu, A. H.; Salabas, E. L.; Schuth, F., Magnetic nanoparticles: Synthesis, protection, functionalization, and application. *Angew. Chem. Int. Ed.* **2007,** *46* (8), 1222-1244.

52. Grass, R. N.; Athanassiou, E. K.; Stark, W. J., Covalently functionalized cobalt nanoparticles as a platform for magnetic separations in organic synthesis. *Angew. Chem. Int. Ed.* **2007,** *46* (26), 4909-4912.

53. Alder, R. W.; Bryce, M. R.; Goode, N. C.; Miller, N.; Owen, J., Preparation of a range of NNN[prime or minute]N[prime or minute]-tetrasubstituted 1,8-diaminonaphthalenes. *J. Chem. Soc. Perk. T. 1* **1981,** (0), 2840-2847.

54. Ishikawa, T., General Aspects of Organosuperbases. In *Superbases for Organic Synthesis*, John Wiley & Sons, Ltd: 2009; pp 1-7.

55. Gwaltney, S. L.; Sakata, S. T.; Shea, K. J., Bridged to Fused Ring Interchange. Methodology for the Construction of Fused Cycloheptanes and Cyclooctanes. Total Syntheses of Ledol, Ledene, and Compressanolide. *J. Org. Chem.* **1996,** *61* (21), 7438-7451.

56. Ireland, R. E.; Liu, L. B.; Roper, T. D.; Gleason, J. L., Total synthesis of FK-506 .2. Completion of the synthesis. *Tetrahedron* **1997,** *53* (39), 13257-13284.

57. Nielsen, M.; Jacobsen, C. B.; Jørgensen, K. A., Asymmetric Organocatalytic Electrophilic Phosphination. *Angew. Chem. Int. Ed.* **2011,** *50* (14), 3211-3214.

58. Baruwati, B.; Guin, D.; Manorama, S. V., Pd on surface-modified NiFe2O4 nanoparticles: A magnetically recoverable catalyst for Suzuki and Heck reactions. *Org. Lett.* **2007,** *9* (26), 5377-5380.

59. Corma, A.; Iborra, S.; Rodriguez, I.; Sanchez, F., Immobilized proton sponge on inorganic carriers. *J. Catal.* **2002,** *211* (1), 208-215.

60. Gianotti, E.; Diaz, U.; Velty, A.; Corma, A., Strong Organic Bases as Building Blocks of Mesoporous Hybrid Catalysts for C-C Forming Bond Reactions. *Eur. J. Inorg. Chem.* **2012,** (32), 5175-5185.

61. Gao, J. H.; Gu, H. W.; Xu, B., Multifunctional Magnetic Nanoparticles: Design, Synthesis, and Biomedical Applications. *Accounts Chem. Res.* **2009,** *42* (8), 1097-1107.

62. Xu, Z. P.; Zeng, Q. H.; Lu, G. Q.; Yu, A. B., Inorganic nanoparticles as carriers for efficient cellular delivery. *Chem. Eng. Sci.* **2006,** *61* (3), 1027-1040.

63. Pankhurst, Q. A.; Connolly, J.; Jones, S. K.; Dobson, J., Applications of magnetic nanoparticles in biomedicine. *J. Phys. D. Appl. Phys.* **2003,** *36* (13), 167-181.

64. Huh, Y.-M.; Jun, Y.-w.; Song, H.-T.; Kim, S.; Choi, J.-s.; Lee, J.-H.; Yoon, S.; Kim, K.-S.; Shin, J.-S.; Suh, J.-S.; Cheon, J., In Vivo Magnetic Resonance Detection of Cancer by Using Multifunctional Magnetic Nanocrystals. *J. Am. Chem. Soc.* **2005,** *127* (35), 12387-12391.

65. Schätz, A.; Grass, R. N.; Kainz, Q.; Stark, W. J.; Reiser, O., Cu(II)−Azabis(oxazoline) Complexes Immobilized on Magnetic Co/C Nanoparticles: Kinetic Resolution of 1,2-Diphenylethane-1,2-diol under Batch and Continuous-Flow Conditions. *Chem. Mater.* **2009,** *22* (2), 305-310.

66. Schaetz, A.; Zeltner, M.; Michl, T. D.; Rossier, M.; Fuhrer, R.; Stark, W. J., Magnetic Silyl Scaffold Enables Efficient Recycling of Protecting Groups. *Chem.-Eur. J.* **2011,** *17* (38), 10565-10572.

67.   Gleeson, O.; Tekoriute, R.; Gun'ko, Y. K.; Connon, S. J., The First Magnetic Nanoparticle-Supported Chiral DMAP Analogue: Highly Enantioselective Acylation and Excellent Recyclability. *Chem.-Eur. J.* **2009,** *15* (23), 5669-5673.

68.   Keller, M.; Collière, V.; Reiser, O.; Caminade, A.-M.; Majoral, J.-P.; Ouali, A., Pyrene-Tagged Dendritic Catalysts Noncovalently Grafted onto Magnetic Co/C Nanoparticles: An Efficient and Recyclable System for Drug Synthesis. *Angew. Chem. Int. Ed.* **2013,** *52* (13), 3626-3629.

69.   Polshettiwar, V.; Baruwati, B.; Varma, R. S., Magnetic nanoparticle-supported glutathione: a conceptually sustainable organocatalyst. *Chem. Commun.* **2009,** (14), 1837-1839.

70.   Riente, P.; Yadav, J.; Pericas, M. A., A Click Strategy for the Immobilization of MacMillan Organocatalysts onto Polymers and Magnetic Nanoparticles. *Org. Lett.* **2012,** *14* (14), 3668-3671.

71.   Schätz, A.; Reiser, O.; Stark, W. J., Nanoparticles as Semi-Heterogeneous Catalyst Supports. *Chem.-Eur. J.* **2010,** *16* (30), 8950-8967.

72.   Stevens, P. D.; Fan, J.; Gardimalla, H. M. R.; Yen, M.; Gao, Y., Superparamagnetic Nanoparticle-Supported Catalysis of Suzuki Cross-Coupling Reactions. *Org. Lett.* **2005,** *7* (11), 2085-2088.

73.   Stevens, P. D.; Li, G. F.; Fan, J. D.; Yen, M.; Gao, Y., Recycling of homogeneous Pd catalysts using superparamagnetic nanoparticles as novel soluble supports for Suzuki, Heck, and Sonogashira cross-coupling reactions. *Chem. Commun.* **2005,** (35), 4435-4437.

74.   Zeltner, M.; Schaetz, A.; Hefti, M. L.; Stark, W. J., Magnetothermally responsive C/Co@PNIPAM-nanoparticles enable preparation of self-separating phase-switching palladium catalysts. *J. Mater. Chem.* **2011,** *21* (9), 2991-2996.

75.   Cantillo, D.; Moghaddam, M. M.; Kappe, C. O., Hydrazine-mediated Reduction of Nitro and Azide Functionalities Catalyzed by Highly Active and Reusable Magnetic Iron Oxide Nanocrystals. *J. Org. Chem.* **2013,** *78* (9), 4530-4542.

76.   Zheng, Y.; Stevens, P. D.; Gao, Y., Magnetic Nanoparticles as an Orthogonal Support of Polymer Resins: Applications to Solid-Phase Suzuki Cross-Coupling Reactions. *J. Org. Chem.* **2005,** *71* (2), 537-542.

77.   Kainz, Q. M.; Linhardt, R.; Grass, R. N.; Vile, G.; Perez-Ramirez, J.; Stark, W. J.; Reiser, O., Palladium Nanoparticles Supported on Magnetic CarbonCoated Cobalt Nanobeads: Highly Active and Recyclable Catalysts for Alkene Hydrogenation. *Adv. Funct. Mater.* **2014,** *24* (14), 2020-2027.

78.   Linhardt, R.; Kainz, Q. M.; Grass, R. N.; Stark, W. J.; Reiser, O., Palladium nanoparticles supported on ionic liquid modified, magnetic nanobeads - recyclable, high-capacity catalysts for alkene hydrogenation. *RSC Adv.* **2014,** *4* (17), 8541-8549.

79. Ozeryanskii, V. A.; Pozharskii, A. F., peri-naphthylenediamines .22. Synthesis of 1,4,5-tris(dimethylamino)naphthalene and other "proton sponge" 4-amino derivatives. *Russ. Chem. Bull.* **1997,** *46* (8), 1437-1440.

80. Schumacher, C. M.; Herrmann, I. K.; Bubenhofer, S. B.; Gschwind, S.; Hirt, A.-M.; Beck-Schimmer, B.; Guenther, D.; Stark, W. J., Quantitative Recovery of Magnetic Nanoparticles from Flowing Blood: Trace Analysis and the Role of Magnetization. *Adv. Funct. Mater.* **2013,** *23* (39), 4888-4896.

81. Rodriguez, I.; Iborra, S.; Corma, A.; Rey, F.; Jorda, J. L., MCM-41-Quaternary organic tetraalkylammonium hydroxide composites as strong and stable Bronsted base catalysts. *Chem. Commun.* **1999,** (7), 593-594.

82. Schumacher, C. M.; Grass, R. N.; Rossier, M.; Athanassiou, E. K.; Stark, W. J., Physical Defect Formation in Few Layer Graphene-like Carbon on Metals: Influence of Temperature, Acidity, and Chemical Functionalization. *Langmuir* **2012,** *28* (9), 4565-4572.

83. Machado, B. F.; Serp, P., Graphene-based materials for catalysis. *Cat. Sci. Tec.* **2012,** *2* (1), 54-75.

84. Schaetz, A.; Zeltner, M.; Stark, W. J., Carbon Modifications and Surfaces for Catalytic Organic Transformations. *ACS Catal.* **2012,** *2* (6), 1267-1284.

85. Gomes, A.; Couto, D.; Alves, A.; Dias, I.; Freitas, M.; Porto, G.; Duarte, J. A.; Fernandes, E., Trihydroxyflavones with antioxidant and anti-inflammatory efficacy. *BioFactors* **2012,** *38* (5), 378-386.

86. Cushnie, T. P. T.; Lamb, A. J., Antimicrobial activity of flavonoids. *Int. J. Antimicrob. Ag.* **2005,** *26* (5), 343-356.

87. Woo, H. D.; Kim, J., Dietary Flavonoid Intake and Smoking-Related Cancer Risk: A Meta-Analysis. *PLoS ONE* **2013,** *8* (9), e75604.

88. Novak, M.; Loudon, G. M., The pKa of acetophenone in aqueous solution. *J. Org. Chem.* **1977,** *42* (14), 2494-2498.

89. Climent, M. J.; Corma, A.; Iborra, S.; Primo, J., Base Catalysis for Fine Chemicals Production: Claisen-Schmidt Condensation on Zeolites and Hydrotalcites for the Production of Chalcones and Flavanones of Pharmaceutical Interest. *J. Catal.* **1995,** *151* (1), 60-66.

90. Karaoğlu, E.; Baykal, A.; Şenel, M.; Sözeri, H.; Toprak, M. S., Synthesis and characterization of Piperidine-4-carboxylic acid functionalized Fe3O4 nanoparticles as a magnetic catalyst for Knoevenagel reaction. *Mater. Res. Bull.* **2012,** *47* (9), 2480-2486.

91. Luo, S.; Zheng, X.; Xu, H.; Mi, X.; Zhang, L.; Cheng, J.-P., Magnetic nanoparticle-supported Morita-Baylis-Hillan catalysts. *Adv. Synth. Catal.* **2007,** *349* (16), 2431-2434.

92. Zhang, Y.; Zhao, Y.; Xia, C., Basic ionic liquids supported on hydroxyapatite-encapsulated gamma-Fe2O3 nanocrystallites: An efficient magnetic and recyclable heterogeneous catalyst for aqueous Knoevenagel condensation. *J. Mol. Catal. A-Chem* **2009,** *306* (1-2), 107-112.

93. Goya, G. F.; Berquó, T. S.; Fonseca, F. C.; Morales, M. P., Static and dynamic magnetic properties of spherical magnetite nanoparticles. *J. Appl. Phys.* **2003,** *94* (5), 3520-3528.

94. Phan, N. T. S.; Jones, C. W., Highly accessible catalytic sites on recyclable organosilane-functionalized magnetic nanoparticles: An alternative to functionalized porous silica catalysts. *J. Mol. Catal. A-Chem* **2006,** *253* (1-2), 123-131.

95. Rondinone, A. J.; Samia, A. C. S.; Zhang, Z. J., Superparamagnetic relaxation and magnetic anisotropy energy distribution in CoFe2O4 spinel ferrite nanocrystallites. *J. Phys. Chem. B* **1999,** *103* (33), 6876-6880.

96. Mori, K.; Kanai, S.; Hara, T.; Mizugaki, T.; Ebitani, K.; Jitsukawa, K.; Kaneda, K., Development of ruthenium-hydroxyapatite-encapsulated superparamagnetic gamma-Fe2O3 nanocrystallites as an efficient oxidation catalyst by molecular oxygen. *Chem. Mater.* **2007,** *19* (6), 1249-1256.

97. Rossier, M.; Schreier, M.; Krebs, U.; Aeschlimann, B.; Fuhrer, R.; Zeltner, M.; Grass, R. N.; Günther, D.; Stark, W. J., Scaling up magnetic filtration and extraction to the ton per hour scale using carbon coated metal nanoparticles. *Sep. Purif. Technol.* **2012,** *96* (0), 68-74.

98. Corma, A.; Garcia, H., Silica-Bound Homogenous Catalysts as Recoverable and Reusable Catalysts in Organic Synthesis. *Adv. Synth. Catal.* **2006,** *348* (12-13), 1391-1412.

99. Han, Y.-J.; Stucky, G. D.; Butler, A., Mesoporous Silicate Sequestration and Release of Proteins. *J. Am. Chem. Soc.* **1999,** *121* (42), 9897-9898.

100. Nakamura, E.; Mori, S., Wherefore art thou copper? Structures and reaction mechanisms of organocuprate clusters in organic chemistry. *Angew. Chem. Int. Edit.* **2000,** *39* (21), 3750-3771.

101. Johnson, J. S.; Evans, D. A., Chiral bis(oxazoline) copper(II) complexes: Versatile catalysts for enantioselective cycloaddition, aldol, Michael, and carbonyl ene reactions. *Accounts Chem. Res.* **2000,** *33* (6), 325-335.

102. Evans, D. A.; Barnes, D. M.; Johnson, J. S.; Lectka, R.; von Matt, P.; Miller, S. J.; Murry, J. A.; Norcross, R. D.; Shaughnessy, E. A.; Campos, K. R., Bis(oxazoline) and bis(oxazolinyl)pyridine copper complexes as enantioselective Diels-Alder catalysts: Reaction scope and synthetic applications. *J. Am. Chem. Soc.* **1999,** *121* (33), 7582-7594.

103. Cristau, H. J.; Cellier, P. P.; Spindler, J. F.; Taillefer, M., Highly efficient and mild copper-catalyzed N- and C-arylations with aryl bromides and iodides. *Chem. Eur. J.* **2004,** *10* (22), 5607-5622.

104. Alexakis, A.; Benhaim, C., Enantioselective copper-catalysed conjugate addition. *Eur. J. Org. Chem.* **2002,** (19), 3221-3236.

105. Daugulis, O.; Do, H.-Q.; Shabashov, D., Palladium- and Copper-Catalyzed Arylation of Carbon-Hydrogen Bonds. *Accounts Chem. Res.* **2009,** *42* (8), 1074-1086.

106. Beletskaya, I. P.; Cheprakov, A. V., Copper in cross-coupling reactions: The post-Ullmann chemistry. *Coordin. Chem. Rev.* **2004,** *248* (21–24), 2337-2364.

107. Fanta, P. E., The Ullmann Synthesis of Biaryls. *Chem. Rev.* **1946,** *38* (1), 139-196.

108. Chan, D. M. T.; Monaco, K. L.; Wang, R. P.; Winters, M. P., New N- and O-arylations with phenylboronic acids and cupric acetate. *Tetrahedron Lett.* **1998,** *39* (19), 2933-2936.

109. Lam, P. Y. S.; Clark, C. G.; Saubern, S.; Adams, J.; Winters, M. P.; Chan, D. M. T.; Combs, A., New aryl/heteroaryl C-N bond cross-coupling reactions via arylboronic acid cupric acetate arylation. *Tetrahedron Lett.* **1998,** *39* (19), 2941-2944.

110. Kolb, H. C.; Finn, M. G.; Sharpless, K. B., Click Chemistry: Diverse Chemical Function from a Few Good Reactions. *Angew. Chem. Int. Ed.* **2001,** *40* (11), 2004-2021.

111. Nicolaou, K. C.; Bulger, P. G.; Sarlah, D., Palladium-catalyzed cross-coupling reactions in total synthesis. *Angew. Chem. Int. Edit.* **2005,** *44* (29), 4442-4489.

112. Bratlie, K. M.; Lee, H.; Komvopoulos, K.; Yang, P.; Somorjai, G. A., Platinum nanoparticle shape effects on benzene hydrogenation selectivity. *Nano Lett.* **2007,** *7* (10), 3097-3101.

113. Bond, G. C.; Thompson, D. T., Catalysis by gold. *Catal. Rev.* **1999,** *41* (3-4), 319-388.

114. Madivada, L. R.; Anumala, R. R.; Gilla, G.; Alla, S.; Charagondla, K.; Kagga, M.; Bhattacharya, A.; Bandichhor, R., An Improved Process for Pioglitazone and Its Pharmaceutically Acceptable Salt. *Org. Process. Res. Dev.* **2009,** *13* (6), 1190-1194.

115. Martinez, C. A.; Hu, S.; Dumond, Y.; Tao, J.; Kelleher, P.; Tully, L., Development of a chemoenzymatic manufacturing process for pregabalin. *Org. Process. Res. Dev.* **2008,** *12* (3), 392-398.

116. Walker, S. D.; Borths, C. J.; DiVirgilio, E.; Huang, L.; Liu, P.; Morrison, H.; Sugi, K.; Tanaka, M.; Woo, J. C. S.; Faul, M. M., Development of a Scalable Synthesis of a GPR40 Receptor Agonist. *Org. Process. Res. Dev.* **2011,** *15* (3), 570-580.

117. Knoevenagel, E., Condensation von Malonsäure mit aromatischen Aldehyden durch Ammoniak und Amine. *Ber. Dtsch. Chem. Ges.* **1898,** *31* (3), 2596-2619.

118. Tietze, L. F.; Beifuss, U., 1.11 - The Knoevenagel Reaction. In *Comprehensive Organic Synthesis*, Fleming, B. M. T., Ed. Pergamon: Oxford, 1991; pp 341-394.

119. Corma, A.; Fornes, V.; Martín-Aranda, R. M.; Garcia, H.; Primo, J., Zeolites as Base Catalysts - Condensation of Aldehydes with Derivatives of Malonic Esters. *Appl. Catal.* **1990,** *59* (2), 237-248.

120. Corma, A.; Martín-Aranda, R. M., Alkaline-substituted Sepiolites as a New Type of Strong Base Catalyst. *J. Catal.* **1991,** *130* (1), 130-137.

121. Ranu, B. C.; Jana, R., Ionic Liquid as Catalyst and Reaction Medium – A Simple, Efficient and Green Procedure for Knoevenagel Condensation of Aliphatic and Aromatic Carbonyl Compounds Using a Task-Specific Basic Ionic Liquid. *Eur. J. Org. Chem.* **2006,** *2006* (16), 3767-3770.

122. Su, C.; Chen, Z.-C.; Zheng, Q.-G., Organic Reactions in Ionic Liquids: Knoevenagel Condensation Catalyzed by Ethylenediammonium Diacetate. *Synthesis* **2003,** *2003* (04), 0555-0559.

123. Schneider, E. M.; Raso, R. A.; Hofer, C. J.; Zeltner, M.; Stealer, R. D.; Hess, S. C.; Grass, R. N.; Stark, W. J., Magnetic Superbasic Proton Sponges Are Readily Removed and Permit Direct Product Isolation. *J. Org. Chem.* **2014,** *79* (22), 10908-10915.

124. Mase, N.; Horibe, T., Organocatalytic Knoevenagel Condensations by Means of Carbamic Acid Ammonium Salts. *Org. Lett.* **2013,** *15* (8), 1854-1857.

125. Sonawane, Y. A.; Phadtare, S. B.; Borse, B. N.; Jagtap, A. R.; Shankarling, G. S., Synthesis of Diphenylamine-Based Novel Fluorescent Styryl Colorants by Knoevenagel Condensation Using a Conventional Method, Biocatalyst, and Deep Eutectic Solvent. *Org. Lett.* **2010,** *12* (7), 1456-1459.

126. Koehler, F. M.; Rossier, M.; Waelle, M.; Athanassiou, E. K.; Limbach, L. K.; Grass, R. N.; Guenther, D.; Stark, W. J., Magnetic EDTA: coupling heavy metal chelators to metal nanomagnets for rapid removal of cadmium, lead and copper from contaminated water. *Chem. Commun.* **2009,** (32), 4862-4864.

127. Rajasekhar Pullabhotla, V. S. R.; Rahman, A.; Jonnalagadda, S. B., Selective catalytic Knoevenagel condensation by Ni–SiO2 supported heterogeneous catalysts: An environmentally benign approach. *Catal. Commun.* **2009,** *10* (4), 365-369.

128. Komiya, S.; Sone, T.; Usui, Y.; Hirano, M.; Fukuoka, A., Condensation reactions of benzaldehyde catalysed by gold alkoxides. *Gold Bull.* **1996,** *29* (4), 131-136.

129. Kränzlin, N.; Ellenbroek, S.; Durán-Martín, D.; Niederberger, M., Liquid-Phase Deposition of Freestanding Copper Foils and Supported Copper Thin Films and Their Structuring into Conducting Line Patterns. *Angew. Chem. Int. Edit.* **2012,** *51* (19), 4743-4746.

130. Kränzlin, N.; Niederberger, M., Wet-Chemical Preparation of Copper Foam Monoliths with Tunable Densities and Complex Macroscopic Shapes. *Adv. Mater.* **2013,** *25* (39), 5599-5604.

131. Sletten, E. M.; Bertozzi, C. R., From Mechanism to Mouse: A Tale of Two Bioorthogonal Reactions. *Accounts Chem. Res.* **2011,** *44* (9), 666-676.

132. Neef, A. B.; Schultz, C., Selective Fluorescence Labeling of Lipids in Living Cells. *Angew. Chem. Int. Ed.* **2009,** *48* (8), 1498-1500.

133. Plass, T.; Milles, S.; Koehler, C.; Schultz, C.; Lemke, E. A., Genetically Encoded Copper-Free Click Chemistry. *Angew. Chem. Int. Ed.* **2011,** *50* (17), 3878-3881.

134. Sletten, E. M.; Bertozzi, C. R., Bioorthogonal Chemistry: Fishing for Selectivity in a Sea of Functionality. *Angew. Chem. Int. Ed.* **2009,** *48* (38), 6974-6998.

135. Saxon, E.; Bertozzi, C. R., Cell surface engineering by a modified Staudinger reaction. *Science* **2000,** *287* (5460), 2007-2010.

136. Lorenzen, K.; Duijn, E. V., Native Mass Spectrometry as a Tool in Structural Biology. In *Current Protocols in Protein Science*, John Wiley & Sons, Inc.: 2001.

137. Zhang, X.; Zhang, Y., Applications of Azide-Based Bioorthogonal Click Chemistry in Glycobiology. *Molecules* **2013,** *18* (6), 7145-7159.

138. Zhang, H.; Tang, X.; Munske, G. R.; Tolic, N.; Anderson, G. A.; Bruce, J. E., Identification of Protein-Protein Interactions and Topologies in Living Cells with Chemical Cross-linking and Mass Spectrometry. *Mol. Cell Proteomics* **2009,** *8* (3), 409-420.

139. Sibbersen, C.; Lykke, L.; Gregersen, N.; Jorgensen, K. A.; Johannsen, M., A cleavable azide resin for direct click chemistry mediated enrichment of alkyne-labeled proteins. *Chem. Commun.* **2014,** *50* (81), 12098-12100.

140. Wang, S.; Xie, W.; Zhang, X.; Zou, X.; Zhang, Y., Disulfide- and terminal alkyne-functionalized magnetic silica particles for enrichment of azido glycopeptides. *Chem. Commun.* **2012,** *48* (47), 5907-5909.

141. Corey, E. J.; Snider, B. B., Total Synthesis of (+/-)-Fumagillin. *J. Am. Chem. Soc.* **1972,** *94* (7), 2549-2550.

142. Danishefsky, S. J.; McClure, K. F.; Randolph, J. T.; Ruggeri, R. B., A Strategy for the Solid-Phase Synthesis of Oligosaccharides. *Science* **1993,** *260* (5112), 1307-1309.

143. Sakakiba.S; Shimonis.Y; Kishida, Y.; Okada, M.; Sugihara, H., Use of Anhydrous Hydrogen Fluoride in Peptide Synthesis .I. Behavior of Various Protective Groups in Anhydrous Hydrogen Fluoride. *B. Chem. Soc. Jpn.* **1967,** *40* (9), 2164-2167.

144. Grass, R. N.; Heckel, R.; Puddu, M.; Paunescu, D.; Stark, W. J., Robust Chemical Preservation of Digital Information on DNA in Silica with Error-Correcting Codes. *Angew. Chem. Int. Ed.* **2015,** *54* (8), 2552-2555.

145. Paunescu, D.; Fuhrer, R.; Grass, R. N., Cover Picture: Protection and Deprotection of DNA—High-Temperature Stability of Nucleic Acid Barcodes for Polymer Labeling (Angew. Chem. Int. Ed. 15/2013). *Angew. Chem. Int. Ed.* **2013,** *52* (15), 4041-4041.

146. Puddu, M.; Paunescu, D.; Stark, W. J.; Grass, R. N., Magnetically Recoverable, Thermostable, Hydrophobic DNA/Silica Encapsulates and Their Application as Invisible Oil Tags. *ACS Nano* **2014,** *8* (3), 2677-2685.

147. Puddu, M.; Stark, W. J.; Grass, R. N., Silica Microcapsules for Long-Term, Robust, and Reliable Room Temperature RNA Preservation. *Adv. Healthcare Mater.* **2015,** *4* (9), 1332-1338.

148. Link, A. J.; Vink, M. K. S.; Tirrell, D. A., Presentation and Detection of Azide Functionality in Bacterial Cell Surface Proteins. *J. Am. Chem. Soc.* **2004,** *126* (34), 10598-10602.

149. Agard, N. J.; Prescher, J. A.; Bertozzi, C. R., A strain-promoted 3+2 azide-alkyne cycloaddition for covalent modification of biomolecules in living systems. *J. Am. Chem. Soc.* **2004,** *126* (46), 15046-15047.

150. Baskin, J. M.; Prescher, J. A.; Laughlin, S. T.; Agard, N. J.; Chang, P. V.; Miller, I. A.; Lo, A.; Codelli, J. A.; Bertozzi, C. R., Copper-free click chemistry for dynamic in vivo imaging. *Proc. Natl. Acad. Sci. USA* **2007,** *104* (43), 16793-16797.

151. Dommerholt, J.; Schmidt, S.; Temming, R.; Hendriks, L. J. A.; Rutjes, F. P. J. T.; van Hest, J. C. M.; Lefeber, D. J.; Friedl, P.; van Delft, F. L., Readily Accessible Bicyclononynes for Bioorthogonal Labeling and Three-Dimensional Imaging of Living Cells. *Angew. Chem. Int. Ed.* **2010,** *49* (49), 9422-9425.

152. McKay, C. S.; Moran, J.; Pezacki, J. P., Nitrones as dipoles for rapid strain-promoted 1,3-dipolar cycloadditions with cyclooctynes. *Chem. Commun.* **2010,** *46* (6), 931-933.

153. Stark, W. J., Nanoparticles in Biological Systems. *Angew. Chem. Int. Ed.* **2011,** *50* (6), 1242-1258.

154. Zlateski, V.; Fuhrer, R.; Koehler, F. M.; Wharry, S.; Zeltner, M.; Stark, W. J.; Moody, T. S.; Grass, R. N., Efficient Magnetic Recycling of Covalently Attached Enzymes on Carbon-Coated Metallic Nanomagnets. *Bioconjugate Chem.* **2014,** *25* (4), 677-684.

155. Hofer, C. J.; Zlateski, V.; Stoessel, P. R.; Paunescu, D.; Schneider, E. M.; Grass, R. N.; Zeltner, M.; Stark, W. J., Stable dispersions of azide functionalized ferromagnetic metal nanoparticles. *Chem. Commun.* **2015,** *51* (10), 1826-1829.

156. Edmondson, S.; Osborne, V. L.; Huck, W. T. S., Polymer brushes via surface-initiated polymerizations. *Chem. Soc. Rev.* **2004,** *33* (1), 14-22.

157. Kato, M.; Kamigaito, M.; Sawamoto, M.; Higashimura, T., Polymerization of Methyl Methacrylate with the Carbon Tetrachloride/Dichlorotris-(triphenylphosphine)ruthenium(II)/Methylaluminum Bis(2,6-di-tert-butylphenoxide) Initiating System: Possibility of Living Radical Polymerization. *Macromolecules* **1995,** *28* (5), 1721-1723.

158. Twetman, S.; Axelsson, S.; Dahlgren, H.; Holm, A. K.; Kallestal, C.; Lagerlof, F.; Lingstrom, P.; Mejare, I.; Nordenram, G.; Norlund, A.; Petersson, L. G.; Soder, B., Caries-preventive effect of fluoride toothpaste: a systematic review. *Acta Odontol. Scand.* **2003,** *61* (6), 347-355.

159. Erickson, H. P., Size and Shape of Protein Molecules at the Nanometer Level Determined by Sedimentation, Gel Filtration, and Electron Microscopy. *Biol. Proced. Online* **2009,** *11*, 32-51.

160. Banerjee, I.; Pangule, R. C.; Kane, R. S., Antifouling Coatings: Recent Developments in the Design of Surfaces That Prevent Fouling by Proteins, Bacteria, and Marine Organisms. *Adv. Mater.* **2011,** *23* (6), 690-718.

161. Lee, J.; Lee, Y.; Youn, J. K.; Na, H. B.; Yu, T.; Kim, H.; Lee, S.-M.; Koo, Y.-M.; Kwak, J. H.; Park, H. G.; Chang, H. N.; Hwang, M.; Park, J.-G.; Kim, J.; Hyeon, T., Simple Synthesis of Functionalized Superparamagnetic Magnetite/Silica Core/Shell Nanoparticles and their Application as Magnetically Separable High-Performance Biocatalysts. *Small* **2008,** *4* (1), 143-152.

162. Park, H. J.; McConnell, J. T.; Boddohi, S.; Kipper, M. J.; Johnson, P. A., Synthesis and characterization of enzyme–magnetic nanoparticle complexes: effect of size on activity and recovery. *Colloid. Surface B* **2011,** *83* (2), 198-203.

163. Garcia, J.; Zhang, Y.; Taylor, H.; Cespedes, O.; Webb, M. E.; Zhou, D., Multilayer enzyme-coupled magnetic nanoparticles as efficient, reusable biocatalysts and biosensors. *Nanoscale* **2011,** *3* (9), 3721-3730.

164. Caruso, F., Hollow Capsule Processing through Colloidal Templating and Self-Assembly. *Chem. Eur. J.* **2000,** *6* (3), 413-419.

165. Ghosh Chaudhuri, R.; Paria, S., Core/Shell Nanoparticles: Classes, Properties, Synthesis Mechanisms, Characterization, and Applications. *Chem. Rev.* **2012,** *112* (4), 2373-2433.

166. Ogi, T.; Nandiyanto, A. B. D.; Okuyama, K., Nanostructuring strategies in functional fine-particle synthesis towards resource and energy saving applications. *Adv. Powder Technol.* **2014,** *25* (1), 3-17.

167. Guan, Z. H.; Hu, J. L.; Gu, Y. L.; Zhang, H. J.; Li, G. X.; Li, T., PdCl2(py)(2) encaged in monodispersed zeolitic hollow spheres: a highly efficient and reusable catalyst for Suzuki-Miyaura cross-coupling reaction in aqueous media. *Green Chem.* **2012,** *14* (7), 1964-1970.

168. Chen, Y.; Chen, H.; Guo, L.; He, Q.; Chen, F.; Zhou, J.; Feng, J.; Shi, J., Hollow/Rattle-Type Mesoporous Nanostructures by a Structural Difference-Based Selective Etching Strategy. *ACS Nano* **2010,** *4* (1), 529-539.

169. Liu, J.; Liu, F.; Gao, K.; Wu, J.; Xue, D., Recent developments in the chemical synthesis of inorganic porous capsules. *J. Mater. Chem.* **2009,** *19* (34), 6073-6084.

170. Arif, A. F.; Kobayashi, Y.; Balgis, R.; Ogi, T.; Iwasaki, H.; Okuyama, K., Rapid microwave-assisted synthesis of nitrogen-functionalized hollow carbon spheres with high monodispersity. *Carbon* **2016,** *107*, 11-19.

171. Balgis, R.; Ogi, T.; Wang, W.-N.; Anilkumar, G. M.; Sago, S.; Okuyama, K., Aerosol Synthesis of Self-Organized Nanostructured Hollow and Porous Carbon Particles Using a Dual Polymer System. *Langmuir* **2014,** *30* (38), 11257-11262.

172. Hofer, C. J.; Grass, R. N.; Zeltner, M.; Mora, C. A.; Krumeich, F.; Stark, W. J., Hollow Carbon Nanobubbles: Synthesis, Chemical Functionalization, and Container-Type Behavior in Water. *Angew. Chem. Int. Edit.* **2016,** *55* (30), 8761-8765.

173. Feng, S.; Li, W.; Shi, Q.; Li, Y.; Chen, J.; Ling, Y.; Asiri, A. M.; Zhao, D., Synthesis of nitrogen-doped hollow carbon nanospheres for CO2 capture. *Chem. Commun.* **2014,** *50* (3), 329-331.

174. Mezzavilla, S.; Baldizzone, C.; Mayrhofer, K. J. J.; Schüth, F., General Method for the Synthesis of Hollow Mesoporous Carbon Spheres with Tunable Textural Properties. *ACS Appl. Mater. Interfaces* **2015,** *7* (23), 12914-12922.

175. Wang, X. D.; Yang, W. L.; Tang, Y.; Wang, Y. J.; Fu, S. K.; Gao, Z., Fabrication of hollow zeolite spheres. *Chem. Commun.* **2000,** (21), 2161-2162.

176. Dong, A. G.; Wang, Y. J.; Tang, Y.; Ren, N.; Zhang, Y. H.; Gao, Z., Hollow zeolite capsules: A novel approach for fabrication and guest encapsulation. *Chem. Mater.* **2002,** *14* (8), 3217-3219.

177. Groen, J. C.; Bach, T.; Ziese, U.; Donk, A.; de Jong, K. P.; Moulijn, J. A.; Perez-Ramirez, J., Creation of hollow zeolite architectures by controlled desilication of Al-zoned ZSM-5 crystals. *J. Am. Chem. Soc* **2005,** *127* (31), 10792-10793.

178. Stöber, W.; Fink, A.; Bohn, E., Controlled growth of monodisperse silica spheres in the micron size range. *J. Colloid. Interf. Sci.* **1968,** *26* (1), 62-69.

179. Wang, X.-D.; Shen, Z.-X.; Sang, T.; Cheng, X.-B.; Li, M.-F.; Chen, L.-Y.; Wang, Z.-S., Preparation of spherical silica particles by Stöber process with high concentration of tetra-ethyl-orthosilicate. *J. Colloid. Interf. Sci.* **2010,** *341* (1), 23-29.

180. Pileni, M.-P., The role of soft colloidal templates in controlling the size and shape of inorganic nanocrystals. *Nat. Mater.* **2003,** *2* (3), 145-150.

181. Yang, Y.; Coradin, T., A green route to silica nanoparticles with tunable size and structure. *Green Chem.* **2008,** *10* (2), 183-190.

182. Zlateski, V.; Keller, T. C.; Perez-Ramirez, J.; Grass, R. N., Immobilizing and de-immobilizing enzymes on mesoporous silica. *RSC Adv.* **2015,** *5* (106), 87706-87712.

183. Athinarayanan, J.; Periasamy, V. S.; Alsaif, M. A.; Al-Warthan, A. A.; Alshatwi, A. A., Presence of nanosilica (E551) in commercial food products: TNF-mediated oxidative stress and altered cell cycle progression in human lung fibroblast cells. *Cell Biol. Toxicol.* **2014,** *30* (2), 89-100.

184. Hu, H.; Zhou, H.; Du, J.; Wang, Z.; An, L.; Yang, H.; Li, F.; Wu, H.; Yang, S., Biocompatiable hollow silica microspheres as novel ultrasound contrast agents for in vivo imaging. *J. Mater. Chem.* **2011,** *21* (18), 6576-6583.

185. Manzano, M.; Vallet-Regi, M., New developments in ordered mesoporous materials for drug delivery. *J. Mater. Chem.* **2010,** *20* (27), 5593-5604.

186. Yang, J.; Lee, J.; Kang, J.; Lee, K.; Suh, J.-S.; Yoon, H.-G.; Huh, Y.-M.; Haam, S., Hollow Silica Nanocontainers as Drug Delivery Vehicles. *Langmuir* **2008,** *24* (7), 3417-3421.

187. Du, Y.; Luna, L. E.; Tan, W. S.; Rubner, M. F.; Cohen, R. E., Hollow Silica Nanoparticles in UV−Visible Antireflection Coatings for Poly(methyl methacrylate) Substrates. *ACS Nano* **2010,** *4* (7), 4308-4316.

188. Ernawati, L.; Ogi, T.; Balgis, R.; Okuyama, K.; Stucki, M.; Hess, S. C.; Stark, W. J., Hollow Silica as an Optically Transparent and Thermally Insulating Polymer Additive. *Langmuir* **2016,** *32* (1), 338-345.

189. Zhang, X.; Lan, P.; Lu, Y.; Li, J.; Xu, H.; Zhang, J.; Lee, Y.; Rhee, J. Y.; Choy, K.-L.; Song, W., Multifunctional Antireflection Coatings Based on Novel Hollow Silica–Silica Nanocomposites. *ACS Appl. Mater. Interfaces* **2014,** *6* (3), 1415-1423.

190. Sharma, R. K.; Sharma, S.; Dutta, S.; Zboril, R.; Gawande, M. B., Silica-nanosphere-based organic-inorganic hybrid nanomaterials: synthesis, functionalization and applications in catalysis. *Green Chem.* **2015,** *17* (6), 3207-3230.

191. Li, Y. S.; Shi, J. L., Hollow-Structured Mesoporous Materials: Chemical Synthesis, Functionalization and Applications. *Adv. Mater.* **2014,** *26* (20), 3176-3205.

192. Wu, S.-H.; Mou, C.-Y.; Lin, H.-P., Synthesis of mesoporous silica nanoparticles. *Chem. Soc. Rev.* **2013,** *42* (9), 3862-3875.

193. Zhao, W.; Lang, M.; Li, Y.; Li, L.; Shi, J., Fabrication of uniform hollow mesoporous silica spheres and ellipsoids of tunable size through a facile hard-templating route. *J. Mater. Chem.* **2009,** *19* (18), 2778-2783.

194. Williams, C. K.; Hillmyer, M. A., Polymers from Renewable Resources: A Perspective for a Special Issue of Polymer Reviews. *Polym. Rev.* **2008,** *48* (1), 1-10.

195. Auras, R.; Harte, B.; Selke, S., An Overview of Polylactides as Packaging Materials. *Macromol. Biosci.* **2004,** *4* (9), 835-864.

196. Jamshidian, M.; Tehrany, E. A.; Imran, M.; Jacquot, M.; Desobry, S., Poly-Lactic Acid: Production, Applications, Nanocomposites, and Release Studies. *Compr. Rev. Food. Sci. Food. Saf.* **2010,** *9* (5), 552-571.

197. Madhavan Nampoothiri, K.; Nair, N. R.; John, R. P., An overview of the recent developments in polylactide (PLA) research. *Bioresource Technol.* **2010,** *101* (22), 8493-8501.

198. Datta, R.; Henry, M., Lactic acid: recent advances in products, processes and technologies — a review. *J. Chem. Technol. Biot.* **2006,** *81* (7), 1119-1129.

199. Kumari, A.; Yadav, S. K.; Yadav, S. C., Biodegradable polymeric nanoparticles based drug delivery systems. *Colloid. Surface B* **2010,** *75* (1), 1-18.

200. Lassalle, V.; Ferreira, M. L., PLA Nano- and Microparticles for Drug Delivery: An Overview of the Methods of Preparation. *Macromol. Biosci.* **2007,** *7* (6), 767-783.

201. Hyvönen, S.; Peltonen, L.; Karjalainen, M.; Hirvonen, J., Effect of nanoprecipitation on the physicochemical properties of low molecular weight poly(l-lactic acid) nanoparticles loaded with salbutamol sulphate and beclomethasone dipropionate. *Int. J. Pharm.* **2005,** *295* (1–2), 269-281.

202. Neises, B.; Steglich, W., Simple Method for the Esterification of Carboxylic Acids. *Angew. Chem. Int. Edit.* **1978,** *17* (7), 522-524.

203. Sheehan, J. C.; Hess, G. P., A New Method of Forming Peptide Bonds. *J. Am. Chem. Soc* **1955,** *77* (4), 1067-1068.

204. Södergård, A.; Stolt, M., Properties of lactic acid based polymers and their correlation with composition. *Prog. Polym. Sci.* **2002,** *27* (6), 1123-1163.

205. Fukushima, K.; Tabuani, D.; Dottori, M.; Armentano, I.; Kenny, J. M.; Camino, G., Effect of temperature and nanoparticle type on hydrolytic degradation of poly(lactic acid) nanocomposites. *Polym. Degrad. Stabil.* **2011,** *96* (12), 2120-2129.

206. Kister, G.; Cassanas, G.; Vert, M., Effects of morphology, conformation and configuration on the IR and Raman spectra of various poly(lactic acid)s. *Polymer* **1998,** *39* (2), 267-273.

Curriculum Vitae

Elia Michael Schneider

ETH Zurich
Institute for Chemical and Bioengineering
Department of Chemistry and Applied Biosciences
Functional Materials Laboratory – HCI E113
Vladimir-Prelog-Weg 1
8093 Zurich
Switzerland
Phone: +41 44 633 62 57
Email: elia.schneider@chem.ethz.ch

Private Address
Elia Schneider
Rathausbogen 7
8200 Schaffhausen
Switzerland

Date and place of birth: July 14th 1988, Bellinzona, Switzerland.
Citizen of Switzerland
Languages: German (native), English (fluent), Spanish (fluent), French (basic)

Education

02/2014 – current **PhD studies** in Chemical and Bioengineering at the Functional Materials Laboratory under the supervision of Prof. Wendelin Stark, at the Institute of Chemical and Bioengineering, D-CHAB, **ETH Zurich** (CH), Zürich.

Dissertation: *Organic Chemistry on Functional Materials for Sustainable Process Engineering*, Prof. Wendelin Stark, ETH Zurich.

08/2016 – 11/2016 Research stay at the Thermal-Fluid Engineering Laboratory headed by Prof. Takashi Ogi, **Hiroshima University** (Japan) with the strategic program "JSPS Postdoctoral Fellowship for Overseas Researchers".

Project: *Recycling of Polylactic Acid Nanoparticle Templates for the Synthesis of Hollow Silica Spheres.*

09/2011 - 08/2013 **Master studies** in Chemistry at D-CHAB, **ETH Zurich** (CH), Zürich.

Master thesis: *Linking Superbases and Carbon-Coated Cobalt-Nanoparticles* under the supervision of Prof. Wendelin Stark, Institute of Chemical and Bioengineering, ETH Zurich.

Research project I: *Synthesis of Ferrocenyl-Tethered Ruthenium-Arene Complexes and their Application in Asymmetric Transfer Hydrogenation*, under the supervision of Prof. Antonio Togni, Laboratory of Inorganic Chemistry, ETH Zurich.

Research project II: *Designed Enzyme Synthesis and Evaluation of Activity in the Intramolecular Rauhut-Currier Reaction*, under the supervision of Prof. Donald Hilvert, Laboratory of Organic Chemistry, ETH Zurich.

09/2008 – 08/2011 **Bachelor studies** in Chemistry at D-CHAB, **ETH Zurich** (CH), Zürich.

08/2007 High school diploma (Swiss Matura), Kantonsschule Schaffhausen, Schaffhausen (CH)

Refereed journal articles

7. <u>E. M. Schneider</u>, S. Taniguchi, Y. Kobayashi, S. C. Hess, R. Balgis, T. Ogi, K. Okuyama, W. J. Stark, Efficient recycling of polylactic acid nanoparticle templates for the synthesis of hollow silica spheres, *ACS Sustain. Chem. Eng.*, Just Accepted Manuscript.

6. A. Zwyssig, <u>E. M. Schneider</u>, M. Zeltner, B. Rebmann, V. Zlateski, R. N. Grass, W. J. Stark, Protein reduction and dialysis-free work-up through phosphines immobilized on a magnetic support: TCEP-functionalized carbon-coated cobalt nanoparticles, *Chem. Eur. J.*, Just Accepted Manuscript.

5. S.C. Hess, F.A. Permatasari, H. Fukazawa, <u>E. M. Schneider</u>, R. Balgis, T. Ogi, K. Okuyama and W. J. Stark, Direct synthesis of carbon quantum dots in aqueous polymer solution: one-pot reaction and preparation of transparent UV-blocking films, *J. Mater. Chem. A*, 2017, **5**, 5187.

4. <u>E. M.Schneider</u>, M. Zeltner, V. Zlateski, R. N. Grass and W.J. Stark, Click and release: fluoride cleavable linker for mild biorthogonal separation *Chem. Commun.*, 2016, **52**, 938.

3. <u>E M. Schneider</u>, M. Zeltner, N. Kränzlin, R. N. Grass, W. J. Stark, Base-free Knoevenagel condensation catalyzed by copper metal surfaces, *Chem. Commun.*, 2015, **51**, 10695.

2. C. J. Hofer, V. Zlateski, P. Stoessel, D. Paunescu, <u>E. M. Schneider</u>, M. Zeltner, R. N. Grass and W. J. Stark, Stable dispersions of azide functionalized ferromagnetic metal nanoparticles, *Chem. Commun.*, 2015, **51**, 1826.

1. <u>E. M. Schneider</u>, R. A. Raso, C. J. Hofer, M. Zeltner, R. D. Stettler, S. C. Hess, R. N. Grass and W. J. Stark, Magnetic superbasic proton sponges are readily removed and permit direct product isolation, *J. Org. Chem.*, 2014, **79**, 10908.

Teaching experience

03/2014 – 12/2015   Process Control I for chemical engineers. Main teaching assistant. Helped to write problem sets and conducted exams. Designed new experiments for the practical course. Led weekly tutorial classes. Institute for Chemical and Bioengineering, ETH Zurich.

02/2012 – 09/2012   Chemistry I for mechanical engineers. Teaching assistant. Helped to write problem sets and exams. Led weekly tutorial classes. Institute for Chemical and Bioengineering, ETH Zurich.

Honors and awards

08/2016   FY2016 JSPS Postdoctoral Fellowship for Overseas Researchers (Strategic Program) by the Japan Society for the Promotion of Science (JSPS)

06/2016   Chemistry Travel Award from the Swiss Chemical Society (SCS)

Conference presentations, invited seminars and proceedings

8.   E. M. Schneider, M. Zeltner, R. Grass, W. Stark, Click and Release: Fluoride Cleavable Linker for Mild Biorthogonal Separation, oral presentation, AIChE annual meeting in San Francisco, USA. November, 18, 2016.

7.   E. M. Schneider, R. A. Raso, R. Grass, W. Stark, Magnetic Superbasic Proton Sponges: a Simple Way to Direct Product Isolation, oral presentation, AIChE annual meeting in San Francisco, USA. November, 17, 2016.

6.   E. M. Schneider, M. Zeltner, R. Grass, W. Stark, Base-free Knoevenagel Condensation Catalyzed by Copper Metal Surfaces, poster, AIChE annual meeting in San Francisco, USA. November, 16, 2016.

5.   E. M. Schneider, S. C. Hess, Click and Release: Fluoride Cleavable Linker for Mild Biorthogonal Separation, invited seminar talk, Tamotsu group, Ehime University, Matsuyama, Japan. October, 24, 2016.

4.   E. M. Schneider, S. C. Hess, Magnetic Reagents: Synthesis and Applications, invited seminar talk, Maeda group, RIKEN, Tokyo, Japan. October, 16, 2016.

3.   E. M. Schneider, S. C. Hess, Magnetic Reagents: Synthesis and Applications, invited seminar talk, Yamaguchi group, Tokyo Institute of Technology, Tokyo, Japan. October, 15, 2016.

2.   E. M. Schneider, R. A. Raso, R. Grass, W. Stark, Magnetic Superbasic Proton Sponges: a Simple Way to Direct Product Isolation, oral presentation, 250th ACS National Meeting in Boston, USA. August, 16, 2015.

1   E. M. Schneider, R. A. Raso, R. Grass, W. Stark, Superbasic Carbon-Coated Nanoparticles and their Application in Catalysis, oral presentation, Material and Processes Graduate Symposium in Zurich, Switzerland. June, 3, 2015.

Student supervision

5. Shuto Taniguchi, (Bachelor project, 8/2016 – 12/2016) Recycling of Polylactic Acid Nanoparticle Templates for the Synthesis of Hollow Silica Spheres.

4. Yuma Kobayashi, (Semester project, 8/2016 – 12/2016) N-rich Hollow Carbon Spheres from Hexamethoxymethyl Melamine for Low Energy CO_2 Adsorption.

3. Adrian Zwyssig, (Master project, 3/2016 - 07/2016) Covalent Immobilization of Tris(2-carboxyethyl)phosphine on Magnetic Particles for the Reduction of Disulfide Bonds in Biomolecules.

2. Adrian Zwyssig, (Semester project, 10/2015 - 02/2016) Towards the Total Synthesis of a Pharmaceutical on Magnetic Nanoparticles.

1. David Stadler, (Semester project, 01/2015 - 06/2015), Cleavable Linkers for Analysis of SI-ATRP Grafted Polymers on Magnetic Particles.